Sensor and Simulation Note
Note 574

18 February 2016

Conformal Impulse Receive Antennas

D. V. Giri
Pro-Tech, 11-C Orchard Court, Alamo, CA 94057
Dept. of ECE, University of New Mexico, Albuquerque, NM

M.D. Abdalla and M.C. Skipper
ASR Corporation, Albuquerque, NM

and

Y. Rahmat-Samii
Department of Electrical Engineering, University of California, Los Angeles, CA

ABSTRACT

In this note, we describe the design, fabrication, and demonstration of a wideband and conformal receiving antenna array. The array consists of 4 bow-tie antennas with metallic extensions. We know that low-profile electrical antennas such as the bow tie arrays work well by themselves, but they have serious performance degradations when placed near a metallic surface such as the skin of an aircraft. This has been the challenge in this work. We have succeeded in this endeavor by placing an Electromagnetic Band Gap (EBG) structure between the antenna array and the metallic back plane and have achieved reasonably good performance. The antenna is determined to be operational when S11 is less than -10dB or when the VSWR is less than 2. The antenna is not operational over any significant frequency range when the antenna is placed over a conductive ground plane. When the antenna is placed over the EBG structure, however, it exhibited good performance over a very wide frequency range, up to 500 MHz without "wings" and 800MHz with "wings." With additional work, this concept can be scaled to precise frequency bands of interest.

Acknowledgement

This work was sponsored under an SBIR Phase II award to Pro-Tech, by AFRL/ RDH 3550 Aberdeen Avenue, Kirtland AFB NM, 87117-5776 - Contract: FA9451-05-C-0015;

Pro-Tech's subcontractors for this effort are: 1) Northrop Grumman Corporation (NGC), in El Segundo, CA and 2) ASR Corporation, Albuquerque, NM. NGC has designed and fabricated a section of a generic UAV aircraft skin, which has been used in testing the performance of our conformal antenna array. ASR personnel focused on the measurement aspect of the conformal antenna. Their support is acknowledged with gratitude. Dr. Yahya Rahmat-Samii, of University of California, Los Angeles assisted with the design of an Electromagnetic Band Gap (EBG) Structure, and also participated in this effort as a consultant and has contributed significantly via valuable discussions.

This has been a collaborative effort and the constant guidance and support from Mr. William Prather and Tyrone Tran of AFRL/DEHP is gratefully acknowledged, along with the assistance from Ms. Deb McGrath and Rita Pidcoe of Det 8 AFRL/PKDP.

1. Executive Summary

Prior to this work, we had designed, built and tested a prototype 2 x 2 array of bow-tie antennas [1]. The antennas are configured in a series-parallel configuration so that the net impedance is approximately (Z_0 / 8) ~ 47 Ohms. Starting with a 50 Ohm connector/cable, we split this into 2 x 100 Ohm cables and then convert each 100 Ohm line into two 200 Ohm strip lines. Each of these 200 Ohm strip line then connects to one of the four antenna elements. The performance of the array is monitored by measuring TDR and S11 (return loss). From the measured S11, we also derive the VSWR. The isolated conformal array testing indicated a very broad bandwidth of operation (transmit or receive modes). It was also established that the isolated array can be made to perform in the desired bandwidth of 200 MHz to 2 GHz. The prototype array was built on a rigid substrate of nylon material.

Low-profile conformal electrical antennas have a serious problem when they are placed near a metallic surface. We placed the prototype conformal array near perfect conducting ground planes, and saw that the performance is completely degraded and there is no bandwidth to speak of. We then analyzed, designed and fabricated an Electromagnetic Band Gap (EBG) structure to be placed between the antenna array and the metallic back plane.

The prototype conformal array was fabricated on a ***rigid structure*** that does not allow the antenna to be contoured to the surface shape. An updated conformal array has been fabricated using ***flexible material*** allowing installation of the array on the skin. A section of the composite and curved aircraft skin was fabricated by Northrop Grumman Corporation in El Segundo, CA for this research effort.

The measurements demonstrate that the conformal array performs significantly better when placed over the EBG structure. The antenna is determined to be operational when S11 is less than -10 db or when the VSWR is less than 2. The antenna is not operational over any significant frequency range when it is placed over or near a conductive ground plane. When the antenna is placed over the EBG structure, good performance is obtained over a significant frequency range. The bandwidth is found to be 500 MHz for the antenna over the EBG without wings and 800 MHz for the antenna with wings.

The updated conformal array performed well when attached to the sample aircraft skin, built by Northrop Grumman Corporation. The bandwidth for the antenna on a non-conductive structure is almost 3 GHz with the low end extending to 200 MHz. When a metal conductor is placed behind the antenna, there is no bandwidth to speak of. The bandwidth is improved significantly (637 MHz to 1.425 GHz), when the conductive plane is replaced with the EBG structure.

2.1 Background

Conformal arrays are of great importance in a variety of applications. The ability of the antenna array to "conform" to the surface of a host platform is of great benefit primarily because of its compactness and non-obtrusiveness (reducing drag) and thus decreasing operational costs, implying that, for example, airborne platforms, such as fixed wing aircraft, including UAVs and helicopters can maintain their designed aerodynamic characteristics while hosting an array antenna. Thus, conformal aperture arrays enable installation on airborne and space platforms as part of load bearing structure without modifying the outer mold line of the platform. They also allow wider field of view than conventional antennas and reduce size and weight requirements. The conformal antenna arrays have great potential to be utilized in systems for radar, electronic countermeasures, electronic support measures, communications, and intelligence collection. Moreover, in recent years there were many efforts to apply conformal antennas and arrays on a surface of inflatable structures - the Goddard Space Flight Center's Spartan 207/Inflatable Antenna Experiment (IAE) in 1996, utilizing conformal reflector antenna on the surface of 14-m structure. NASA estimates that large inflatable antennas will have the following advantage over current technology (advantages increase with size): (1) lower cost by 1 to 2 orders of magnitude, (2) lower stored volume 1 to 2 orders of magnitude and (3) lower mass by factors of 2 to 8 – all this being directly applicable to conformal antennas/arrays, which is an obvious if not the only choice for the inflatable antennas [2].

While today the fabrication and operation of conformal arrays in the conventional narrow-band CW or pulsed electromagnetic systems, including the radars, is a common practice, where such arrays are being built and operated on a variety of both civilian and military airborne platforms, to our knowledge, currently no conformal arrays in a transient (an impulse) regime exist. We believe that there are two primary reasons for that:

1. Implementation of radar systems in a transient regime is a relatively new phenomenon.
2. Design, fabrication and integration of an antenna array in the transient regime involves multitude of subtle elements, and while significant process has been made recently, there still are issues not fully understood.

In this effort, we considered two small-scale conformal arrays capable of operating in an impulse regime. The first array will be one-dimensional (1-D) linear array consisting of 4 radiating elements, and the second array will be two-dimensional (2-D) also consisting of 4 elements. A flat (non conformal) radiator layout for both small-scale arrays is shown in Figure 1, where each radiator has a flat bi-conical shape plates to be fed at the nodes (small dark circles).

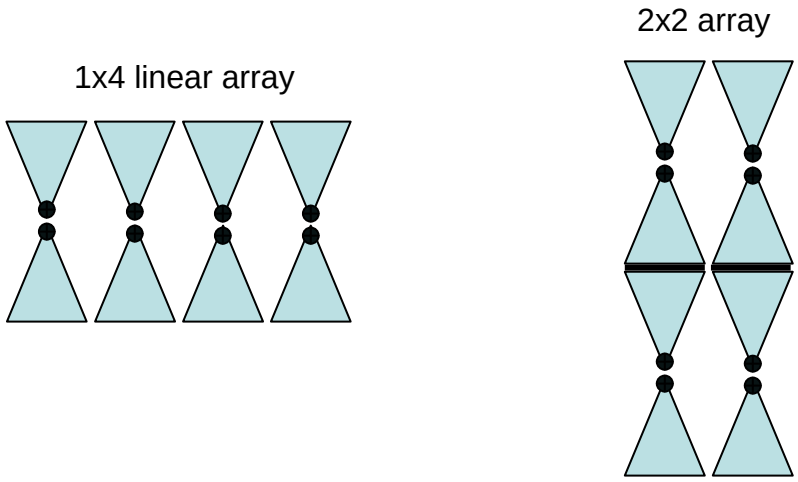

Figure 1. Radiating element layout in a 4-element 1-D and 2-D flat planar antenna arrays utilizing a "bow-tie", planar bi-cones (bi-triangular shape) flat radiators

Figure 2 presents schematic diagram for power distribution as applied to the above 2×2 array configuration, which utilizes a corporate feed in both transmit mode (left) and receive mode (right). In the transmit mode, a voltage source $V(t)$ of impedance Z (the choice of Z can be 50 Ohms, 100 Ohms or whatever turns out to be the best for the element antenna impedance) generates a signal that reaches all four radiating elements via 4 sets of cables. The cable of impedance Z splits into 2 cables of impedance $2Z$ connected in parallel which then connects to sets of cables in series, each of which having impedance Z. Thus, there is match (impedance) from the source to the antenna radiating elements.

In the receive mode, the same cable of impedance 50Ohm is connected to a digitizer or analog oscilloscope, labeled as Recording Instrumentation (RI). If $Z \neq 50$ Ohm, then we will need impedance matching to the measuring scope which is typically 50 Ohm. We now discuss the transition from 3D case to 2D case, obtained by going to the limit $l \rightarrow 0$ (see Figure 3).

Let us discuss briefly the impulse array's single element, consisting of a "bow-tie" or planar, flat plate bicone radiating element shown in Figure 4. ABCD is the unit cell which repeats itself in both x- and y-directions.

With reference to Figure 3, at early times (or high frequencies), the impedance seen by the source is the characteristic impedance of the TEM mode $Z_{early\ time} = Z_o\ f_{gh}(b'/a')$ where Z_o is the characteristic impedance of free space. Again, with reference to Figure 3, (b'/a') can be larger, equal to or smaller than (b/a). It is not essential, but mechanically convenient to impose the condition that (b'/a') = (b/a) in Figure 3. If we impose this condition, it results in triangular or ***planar plates*** which are mechanically convenient. As time goes on, spherical TEM mode gets launched in both directions. The late time (or low frequency) impedance can be written as $Z_{late-time} = (1/2)Z_o(b/a)$. The factor of (1/2) accounts for the presence of waves in both forward

and backward directions. It is now desirable to require the same early and late time impedances leading to $(1/2)(b/a) = f_{gh}(b'/a')$ so as to minimize reflections back to the source.

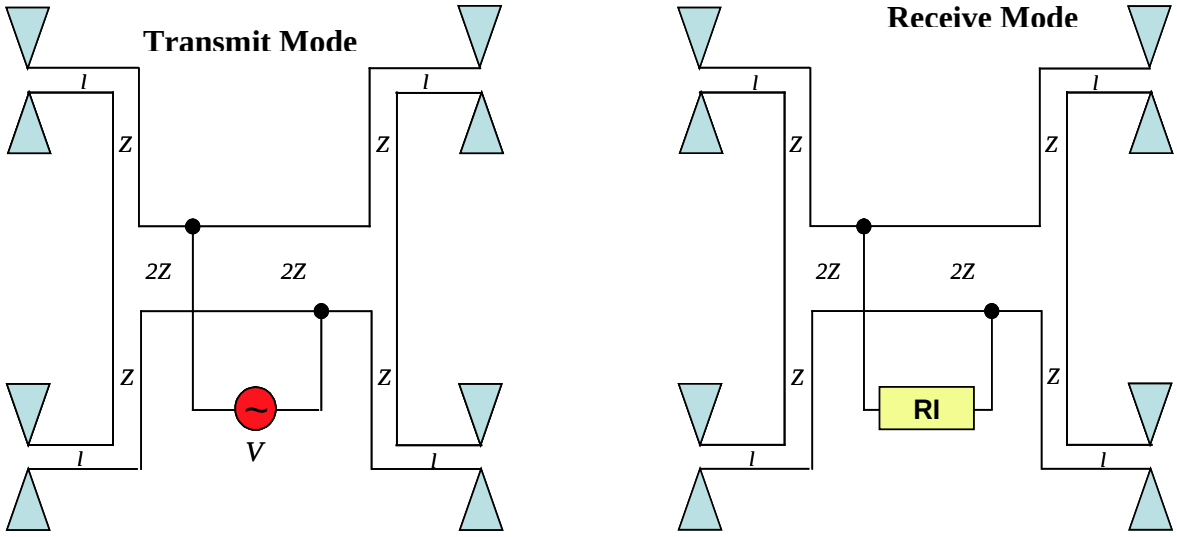

Figure 2. Schematic diagram showing power distribution in transmit and receive modes for a 2×2 array configuration using a corporate feed

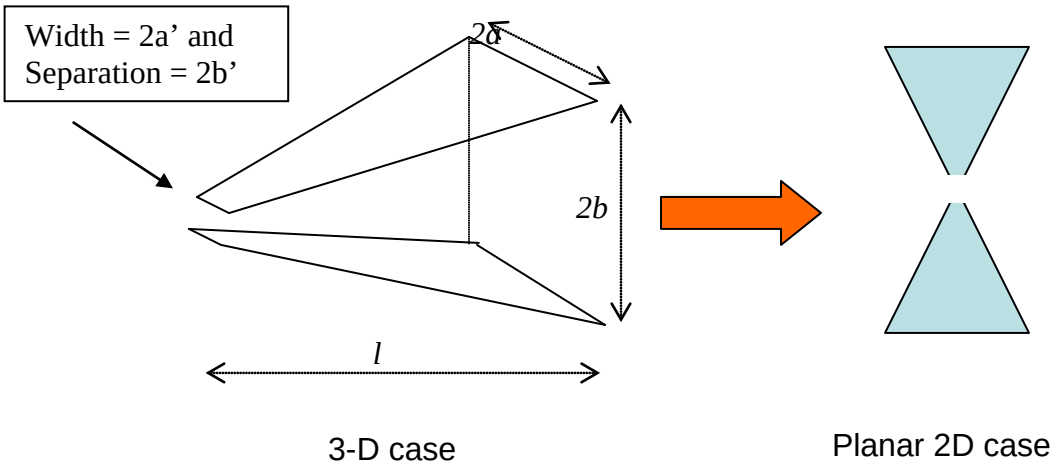

Figure 3. Transition of the radiating element from a 3-D case to a 2-D planar case

These impedance calculations are carried out in Appendix –A of [3] for the general case of (b'/a') smaller than, equal to and larger than (b/a). From the 3D case of Figure 3, we can go to the 2D case of Figure 4, by inserting the length $\ell = 0$. Table 1 presents the list of key parameters associated with the radiating element, which show the relationship between its geometrical parameters, *a, b, a', b', θ* and the normalized effective rate of rise-time, $T_{n1} = ct_1/\sqrt{A}$ of the radiated field (assuming a zero rise time step function input) for planar bicones ($l/\sqrt{A} = 0$), in a

symmetric configuration, for a range of realistic geometric parameters. Parameters *l* and *A=4ab* represent the elementary cell depth and area respectively (see Figures 3 and 4).

The parameter t_1 above is the effective rise time [3] of the radiated field which can be related to the electric field at the center of the aperture in Figure 3. A is the physical area of the aperture in Figure 3, A = aperture area = 4 ab and c = speed of light in air. In the ***planar plate*** case of Figure 4, (b'/a) = (b/a) for all angles.

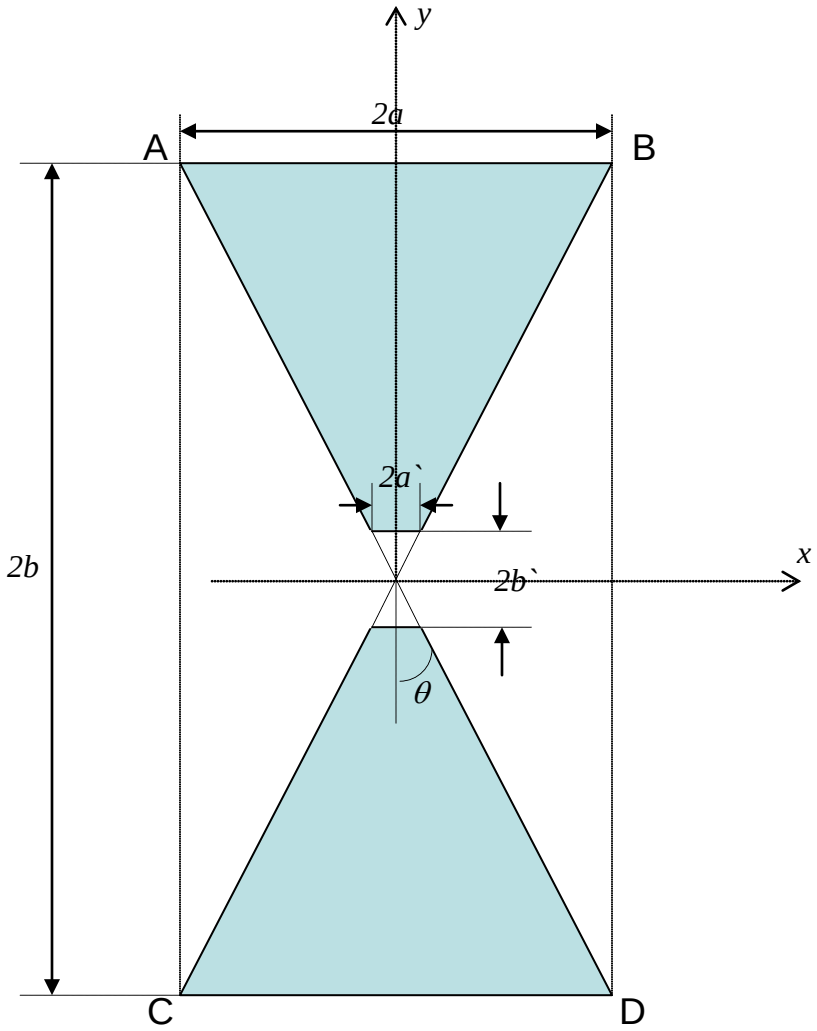

Figure 4. Details of a single radiating element configuration

In Table 1, the planar case represented by Figure 4 is when (b'/a') = ((b/a), the other entries in Table 1 are for the cases where the plates are non-planar.

TABLE 1. Normalized effective rate of rise for planar bicones ($l/\sqrt{A}$ =0), in a symmetric configuration

$\frac{b}{a}$	$f_{gh}(b'/a') = \frac{1}{2}\frac{b}{a}$	$\frac{2\theta}{\pi}$	θ	$\frac{b'}{a'}$	$\frac{ct_1}{a}$	$T_{n1}(sym-planar) = \frac{ct_1}{\sqrt{A}}$
0.000	0.000	1.000	$0.500\,\pi$	0.000	1.000	∞
0.500	0.250	0.890	$0.445\,\pi$	0.175	1.008	0.713
0.877	0.438	0.590	$0.295\,\pi$	0.751	1.115	0.595
1.000*	**0.500**	**0.500**	$\mathbf{0.250\,\pi}$	**1.000**	**1.180**	**0.590**
1.500	0.750	0.235	$0.118\,\pi$	2.585	1.562	0.638
2.000	1.000	0.110	$0.055\,\pi$	5.730	2.014	0.712
3.520	1.760	0.010	$0.005\,\pi$	63.657	3.527	0.940

*** Planar-plate case where the two plates are in the same plane and (b'/a') = (b/a)**

2.2 Illustrative Example of a Bow-Tie Antenna

Assuming *b/a = 2b/2a* = 1, and consequently *b'/a' = 2b'/2a'* = 1 which yields $\theta = 0.25\,\pi =$ 45º (see Table 1). It follows from the same table that

$$ct_1/\sqrt{A} = 0.59 \tag{1}$$

which yields

$$t_1 = \frac{0.59\times\sqrt{A}}{c} = \frac{0.59\times\sqrt{4ab}}{c} \tag{2}$$

In the case of 2×2 array, and *a*=*b*=5 cm we have (see Table 1) $ct_1/a = 1.18$ and $ct_1/\sqrt{A} = 0.59$ yielding the same value for parameter t_1:

$$\begin{aligned} t_1 &= \frac{1.18a}{c} = \frac{1.18\times 5cm}{3\times 10^{10}\,cm/\sec} \sim 200\,ps \\ t_1 &= \frac{0.59\sqrt{4ab}}{c} = \frac{0.59\sqrt{4\times 5cm\times 5cm}}{3\times 10^{10}\,cm/\sec} \sim 200\,ps \end{aligned} \tag{3}$$

Thus, if we excite the radiating element with a zero-rise time step function, we will get a radiated pulse that has a rise time of 200 ps. Figure 5 shows the notional graphs of the input step function and the waveform of the resulting radiated field.

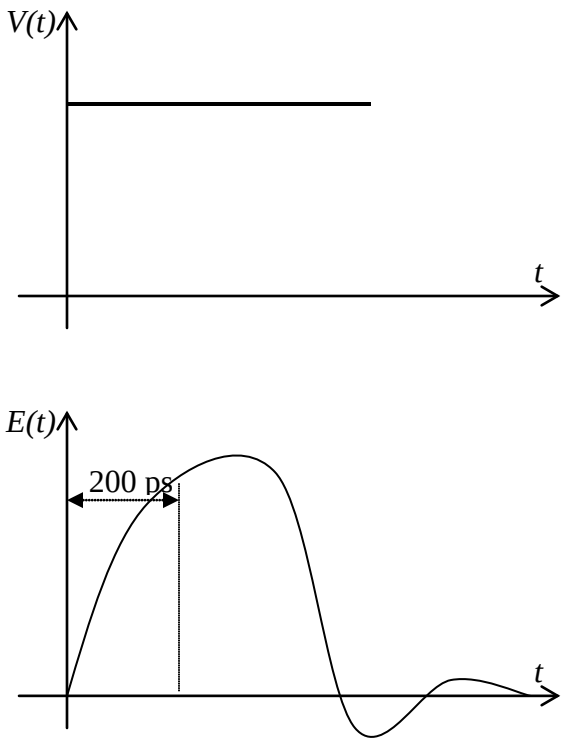

Figure 5. Input voltage (top) and the resulting radiated field (bottom)

For a transient pulse with a 10-90% risetime of t_1, the break frequency (the highest significant frequency may be somewhat more than the break frequency) is given by

$$\Delta f = \frac{\ell n(9)}{2\pi}\frac{1}{t_1} \cong \frac{0.35}{t_1} \tag{4}$$

It follows that 200 ps rise time corresponds to Δf > 1.75 GHz bandwidth

As to the low-frequency end of the bandwidth, for the same 2x2 array, whose overall dimensions correspond to $4a \times 4b$ = 20cm×20cm, with the characteristic dimension being the diagonal l_c:

$$l_c = 4a\sqrt{2} = 20cm \times 1.41 \sim 28.2cm. \tag{5}$$

Since the antenna stops radiating and receiving when antenna characteristic dimension becomes $\lambda/2$ (half of the wavelength), it follows that this low-frequency threshold can be obtained from the following relationships:

$$\frac{\lambda}{2} = l_c \tag{6}$$

which, in turn yields λ ~ 60 cm corresponding to approximately 500 MHz - also close to the lower bound of 200MHz-2GHz range for antenna bandwidth requirements specified in the

current SBIR solicitation. To achieve 200 MHz we need to employ larger array by employing more radiating elements, e.g. utilizing 3×3 array instead of 2×2 array.

2.3 The Bow-Tie Array

Based on the design considerations of the previous section, we have fabricated a 2 x 2array of bow-tie antenna. This array is shown in Figure 6.

(a) **(b)**

Figure 6. The 2 x 2 Bow-tie array (a) without and (b) with the "wings" attached

The antenna utilizes a nylon substrate initially and later, a composite surface fabricated by Northrop Grumman Corporation, especially for this effort. The results indicate that the theoretical basis for the antenna is correct and that some simple improvements can be done to substantially improve the performance. The antenna is driven by a single 50 ohm source. The 50 Ohm source drives two 100 Ohm coaxial cables connected in parallel with each 100 Ohm cable driving two parallel 200 Ohm strip line cables. The four strip line cables drive each of the four antenna elements. Ferrite cores are placed on the outer conductor of the 100 Ohm cables to provide isolation between the individual elements of the array. The array was evaluated in the time and frequency domain. The array was then modified to improve the low frequency response and the measurements were repeated.

2.4 Fabrication of the Prototype Array

A four element (2x2) prototype conformal antenna has been fabricated. The array elements measure 10 cm x 10 cm (width x height) and were formed using 0.2 mm thick copper tape placed on a 6.35 mm thick nylon plate. A Prodyn Technologies SB-10D (Serial Number 29) summing block is used to interface the two 100 Ohm feed cables to the 50 Ohm feed cable. The two 100 Ohm feed cables interface with four 200 Ohm strip transmission lines that are machined into the nylon substrate of the array. Three Ferrite cores were placed on each 100 Ohm cable to provide isolation between the two arrays. The interface between the 100 Ohm cable and the two 200 Ohm cables is shown in Figure 7. The length of the center conductor required to connect to the 200 Ohm line introduced a significant parasitic inductance that was partially compensated for by placing a small amount of epoxy (dielectric constant of 5.1) at the feed point.

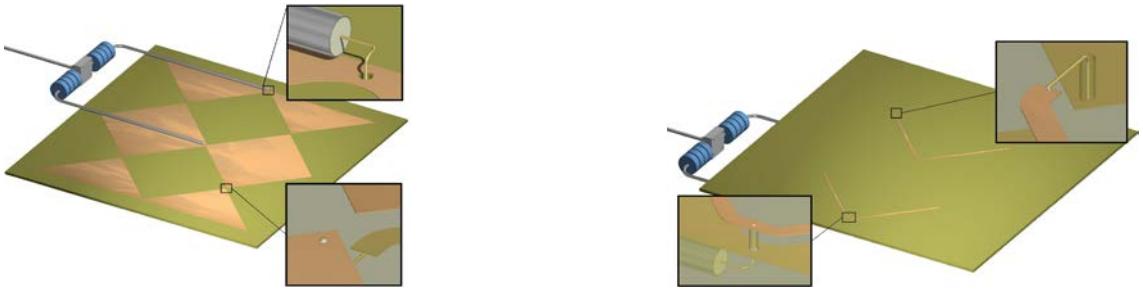

Figure 7. Coaxial 100 Ohm – 200 Ohm Strip transition

Top (left) and bottom (right) views

The array was evaluated in the time domain using a TDR and in the frequency domain with a network analyzer. A Tektronix 11801A sampling oscilloscope with an SD-24 TDR head was using to make the TDR measurements of the array, seen in Figure 8. A Hewlett Packard 8753 frequency domain network analyzer is used to measure S11 (Figure 9). The SWR for the array is obtained from the S11 measurement, as seen in Figure 10.

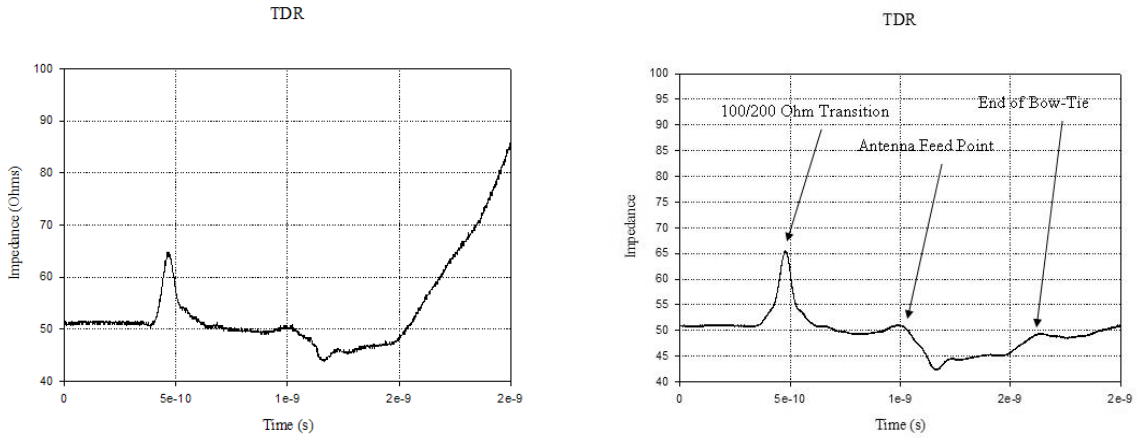

(a) Without the "wings" or metallic extensions (b) With "wings" or metallic extensions

Figure 8. TDR measurement of the isolated conformal array on nylon substrate

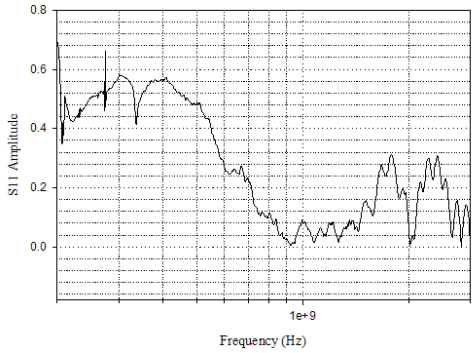

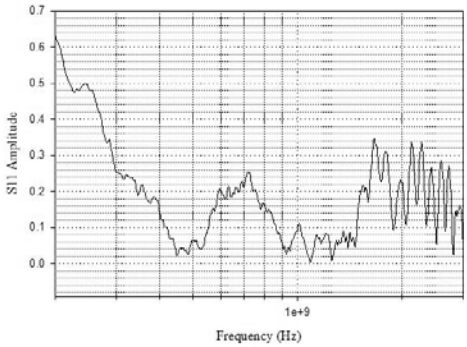

(a) Without the "wings" or metallic extensions (b) With "wings" or metallic extensions

Figure 9. S11 measurement of the isolated conformal array on nylon substrate

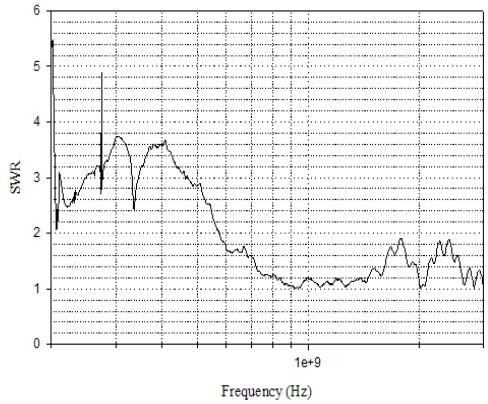

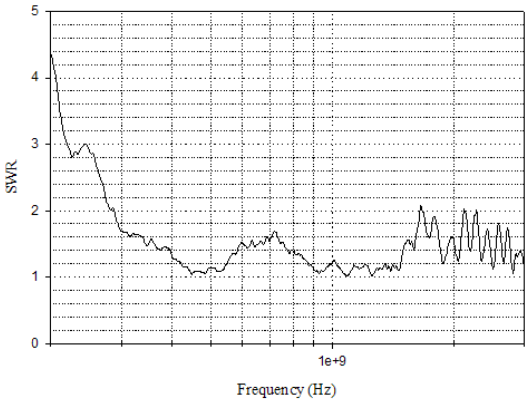

(a) Without the "wings" or metallic extensions (b) With "wings" or metallic extensions

Figure 10. VSWR measurement of the isolated conformal array on nylon substrate

The VSWR is computed from the measured S11 using the following expression.

$$VSWR = (1 + |S11|) / (1-|S11|) \quad (7)$$

For example, if one sets the criterion that the VSWR <2 is acceptable for the array performance, the bandwidth is seen to be 500 MHz to 3 GHz (without the wings) and 200 MHz to 3 GHz with the wings.

This measurement demonstrates the effect of attaching the wings – the lowering of the lower frequency limit or expanding the antenna bandwidth to lower frequencies, as expected. The array dimensions get larger and the array works better at lower frequencies.

Lower frequency limit → antenna size (need more elements)
Upper frequency limit → governed by unit cell dimensions (need smaller individual elements)

Recall that the results displayed in Figures 8, 9 and 10 is for the isolated conformal array on a nylon substrate.

The problem occurs when such an array is brought near a metallic surface, such as the metallic or composite skin of an aircraft.

In addition to the above measurements of TDR, S11 and VSWR, we have also made extensive radiation pattern measurements, which were performed by AntCom, now Allwave Corporation.

- The radiation patterns of the 2 x 2 array **without** the extension have been measured at 500 MHz, 700 MHz, 900 MHz, 1 GHz, 1.1 GHz, 1.3 GHz, 1.5 GHz and 2 GHz.

- The radiation patterns of the 2 x 2 array **with** the extension have been measured at 300 MHz, 500 MHz, 700 MHz, 900 MHz, 1 GHz, 1.3 GHz, 1.5 GHz and 2 GHz.

To demonstrate the bandwidth improvement obtained with the addition of the metallic extensions, we include here the radiation pattern of the array with the extensions at a frequency of 300 MHz in Figure 11 and at 50 MHz in Figure 12.

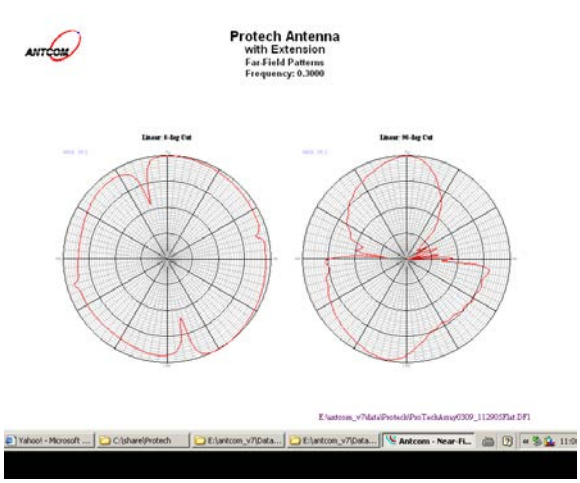

Figure 11. Radiation Pattern at 300 MHz 2 x 2 array with extension

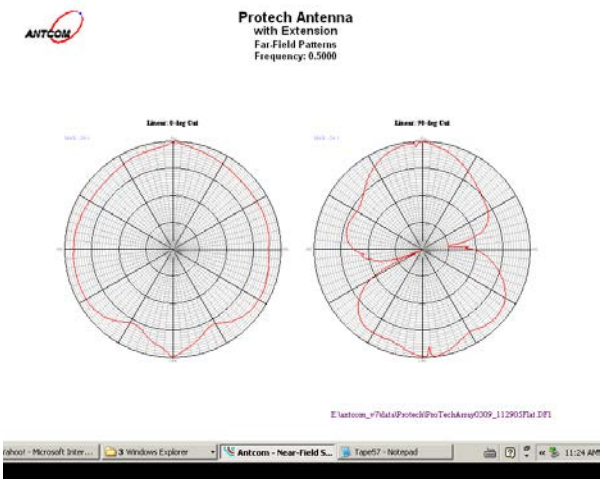

Figures 12. Radiation Pattern at 500 MHz 2 x 2 array with extension

One can see from Figures 11 and 12, that the array antenna begins to have the expected radiation pattern some where between 300 and 500 MHz.

The measured gain and directivity of this 2 x 2 array with and without the metallic extension are listed in Table 2.

In the next section we describe the degradation in antenna performance as it is brought close to a metallic ground plane.

TABLE 2. Gain Measurements of the isolated 2 x2 conformal array on a nylon substrate

Gain Measurement					
No	Frequency (GHz)	Without Extension		With Extension	
		Directivity (dB)	Gain (dB)	Directivity (dB)	Gain (dB)
1	0.3	N/A	N/A	3.3	1.8
2	0.4	N/A	N/A	5.6	4.0
3	0.5	5.0	3.8	6.2	4.5
4	0.6	4.2	3.4	4.4	3.5
5	0.7	4.5	3.6	5.2	3.6
6	0.8	3.3	2.6	2.9	1.2
7	0.9	4.6	2.6	3.6	3.1
8	1.1	4.4	2.9	5.0	3.1
9	1.3	9.1	8.3	8.1	6.8
10	1.5	8.3	7.0	7.8	7.3
11	1.7	7.0	5.1	7.1	4.5
12	1.9	7.5	5.8	9.1	7.4

3.0 Conformal Array Performance near a Metallic Surface

If the conformal array described in the previous section is brought near a metallic surface, one would expect significant performance degradation. Basically the metal surface has the effect of “shorting” the antenna. This has been a serious challenge for this type of low-profile electrical antennas to be placed conformably on or near aircraft skins. We have determined this performance degradation by placing our array on a metallic surface, as seen in Figure 13 and repeating the TDR (Figure 14), S11 (Figure 15) and VSWR (Figure 16).

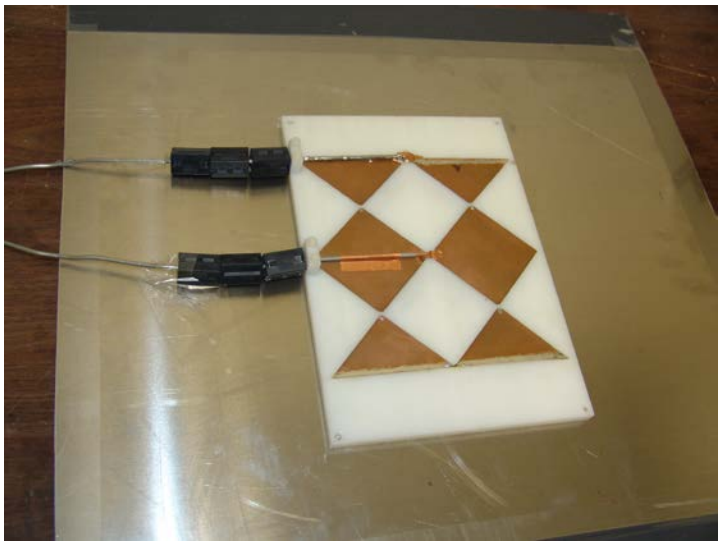

Figure 13. Photo of conformal antenna array placed on a conductive ground plane

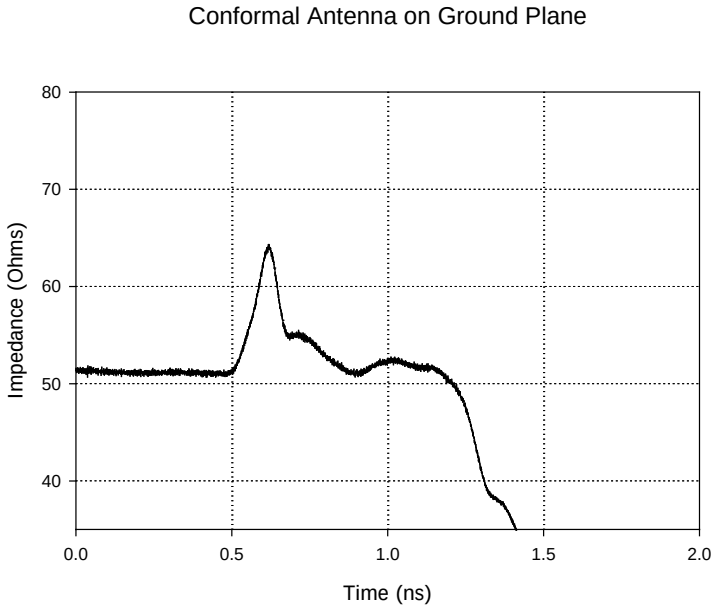

Figure 14. TDR measurement of conformal antenna placed on conductive ground plane

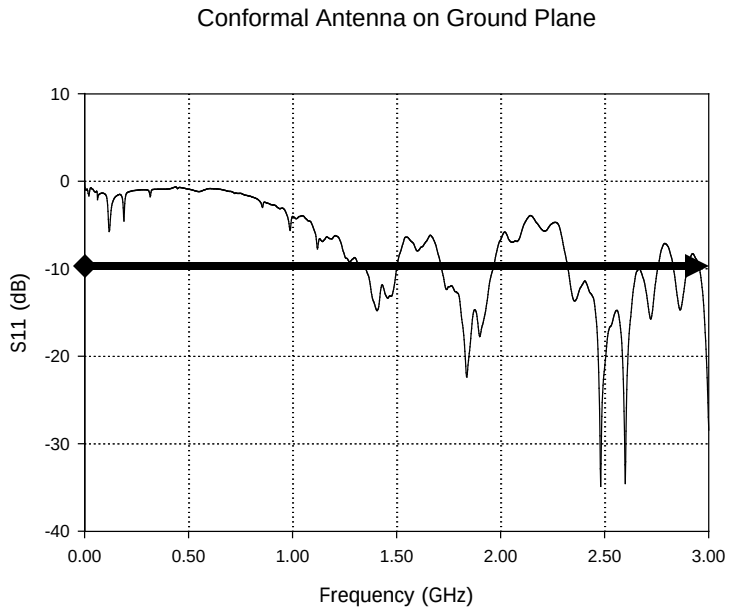

Figure 15. S11 measurement of conformal antenna placed on conductive ground plane

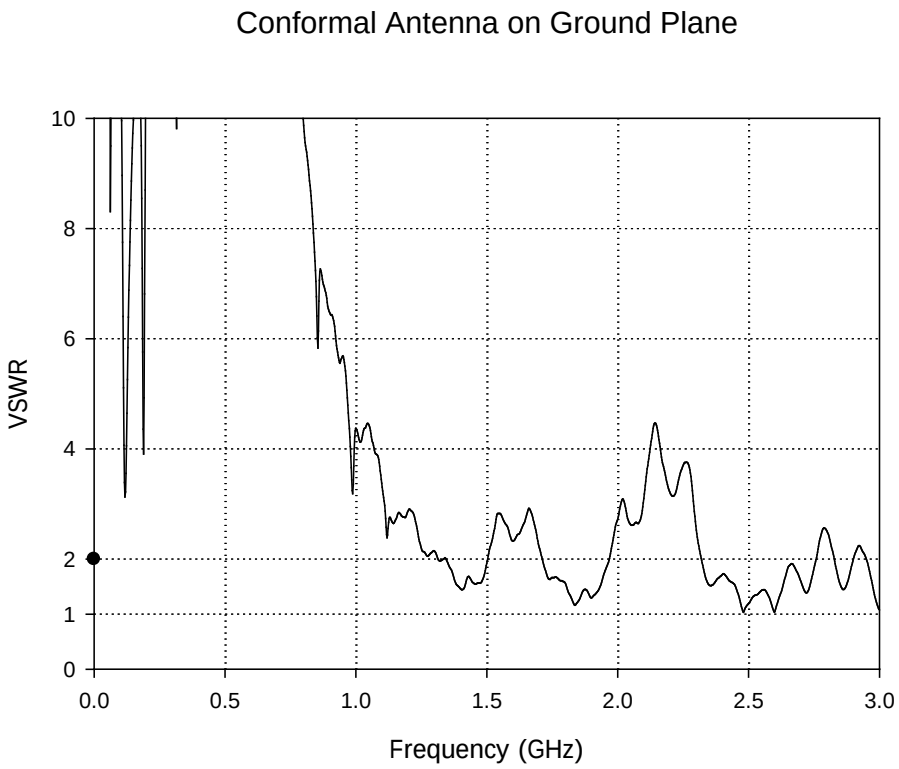

Figure 16. SWR measurement (calculated from S11) of conformal antenna placed on conductive ground plane

We set a criterion that S11 should be less than -10 dB to define an operational bandwidth. This is an industry-wide accepted norm. If we employ this criterion for Figure 15, it is obvious that when the conformal array on the nylon substrate is placed on a metallic surface, *there is no bandwidth to speak of.* This conclusion can also be reached by a cursory examination of the VSWR measurement as well.

At this point, we have established:

- *That the conformal 2 x 2 array of bow ties certainly provides the desired receive bandwidth, when it is isolated or by itself; a bandwidth of 200 MHz to 2 GHz is easily achievable with this approach. We have proved the concept with a slightly narrower bandwidth. But extending the bandwidth by using a few more antenna elements is quite straightforward.*

- *The antenna performance is seriously degraded when the array is brought near a metallic surface. There is no bandwidth to speak of, basically.*

- *Yet another complication is the fact that the aircraft surface is curved and not totally flat.*

- *Initially, we had anticipated that the conformal array would be placed on the aircraft wing surface, which is fairly flat. However, Northrop Grumman Corporation indicated that placing conformal antennas on the wing surface is not feasible and a logical place would be on the under-surface of the fuselage, which is clearly a curved surface. Northrop Grumman has actually fabricated a section of a generic- curved composite material illustrated in Figure 17. We have experimented with this curved surface, by placing the conformal antenna on top and metallic surfaces on the bottom. .*

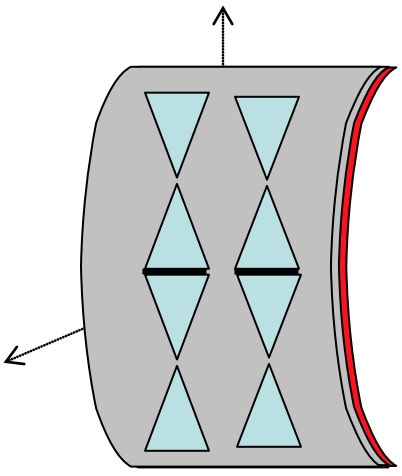

Figure 17. Conformal array antenna on a curved composite substrate which may be backed by a metallic surface

In an attempt to circumvent the adverse effects of the metallic back plane, we have investigated the use of electromagnetic band gap (EBG) structures to be introduced between the conformal array and the metallic surface to improve the antenna performance when it is located near the metallic surface.

The design of the EBG structure is the subject of the next section.

4.0 Electromagnetic Band Gap Structures

The basic geometry of the EBG structure we have considered here is shown in Figure 18. Square shaped metallic patches are distributed in a 2 dimensional array. The patches are of size w x w. There is a uniform gap g between the patches. The height of the dielectric substrate is h and there are vias or metallic pins of circular cross section.

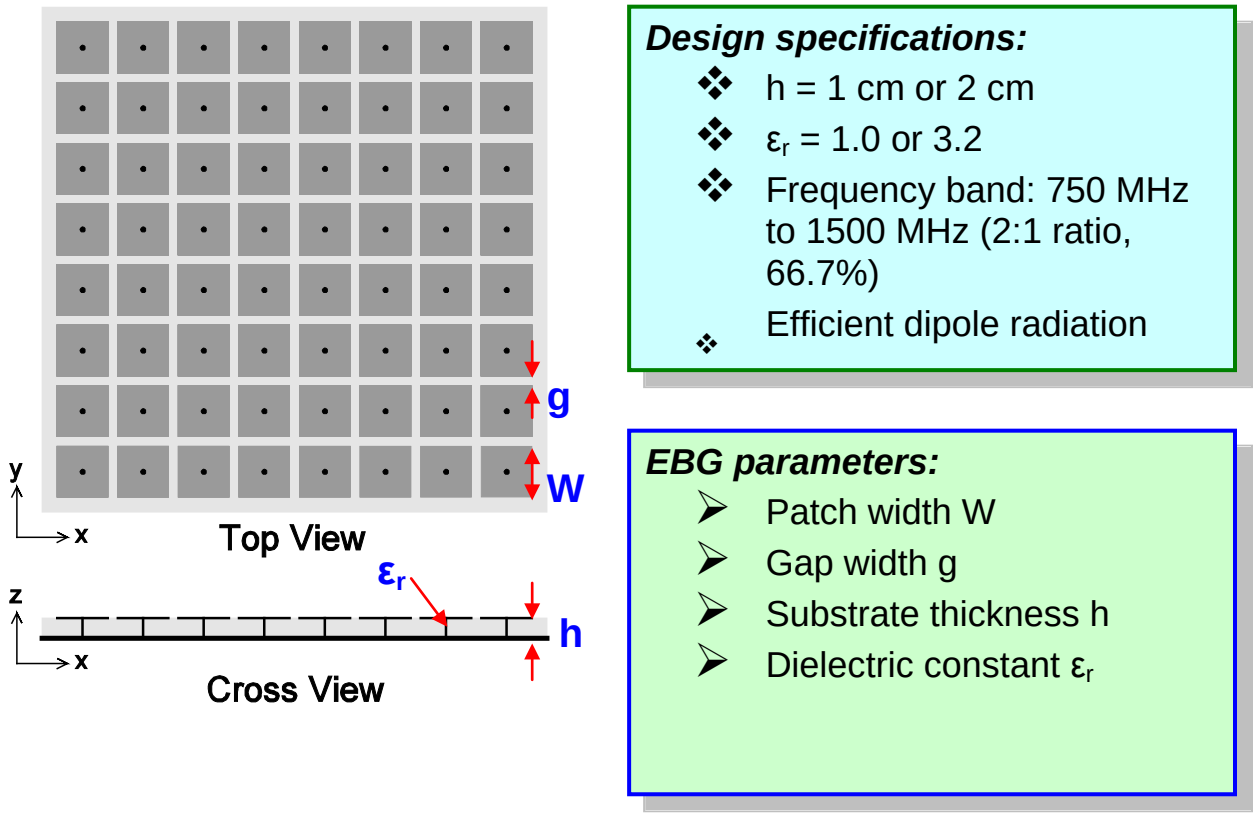

Figure 18. Geometry of an EBG ground plane

The four design parameters are indicated in Figure 18 as well.

The basic analysis of the EBG structure is illustrated in Figure 19.

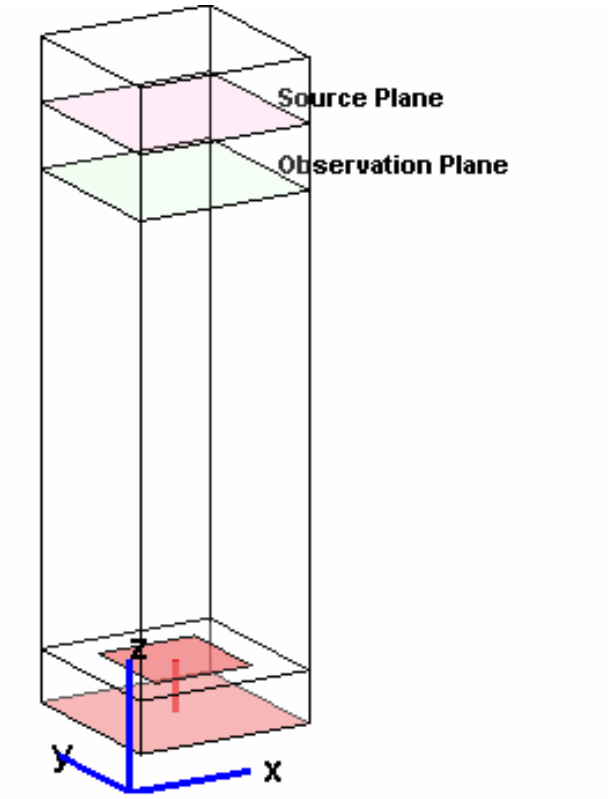

Figure 19. Numerical problem space for analyzing the EBG

The EBG structure is placed on the x-y plane as shown. The EBG structures are analyzed using a FDTD program. Plane wave sources are placed on the plane marked source plane at a certain height from the EBG structure. The plane wave travels down and interacts with the EBG structure and reflects back normally, for normal incidence as shown. In the observation plane, the phase of the reflected wave is calculated and plotted as a function of frequency for various geometrical and material parameters.

Initially, we have air as the substrate, i.e., $\varepsilon_r = 1$ and fix the height h = 2cm. Holding these two parameters constant, we vary the values of w (square patch size) and g (gap between the patches) The computed phase angle of the reflected signal as a function of frequency is plotted in Figure 20.

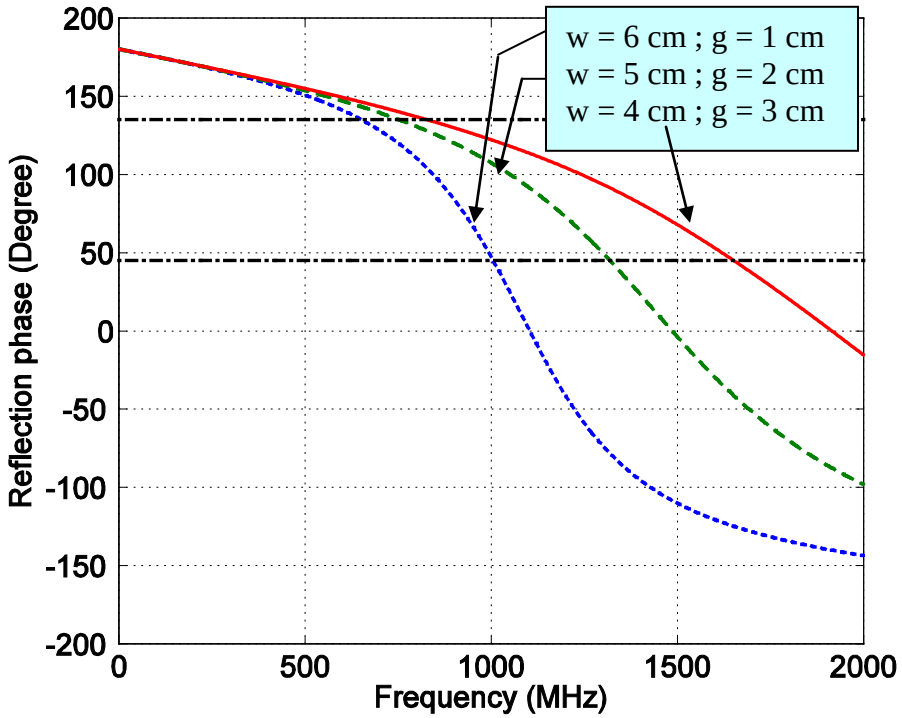

Case	(w, g)	Bandwidth MHz	Percent Bandwidth
1	(6 cm, 1cm)	651-1005	42.75%
2	(5 cm, 2 cm)	752-1319	54.76%
3	(4 cm, 3cm)	827-1651	66.51%

Figure 20. Reflection phase for varying patch and gap sizes for $\varepsilon_r = 1$ and height h = 2cm.

It is noted that the two horizontal marker lines in Figure 20 correspond to (90 degrees $\pm$ 45 deg) or delineate the frequencies where the reflected phase angle falls between 45 and 135 degrees. If there was no EBG structure, the phase of the reflected wave will be 180 degrees from the metal ground plane. However, the phase of the reflected wave ranges from -180 degrees to + 180 degrees in the presence of the EBG structure backed by the ground plane. A frequency where the

reflection phase is 0 degrees represents the resonance frequency of the structure. When the reflected phase is 90 degrees, the reflected wave interferes interacts with the incident wave in phase. The in-phase property makes it possible to design low-profile electrical antennas near metallic ground planes like the skin of an aircraft. This range of frequencies where the reflection phase is (90 degrees $\pm$ 45 deg) defines the bandwidth of the EBG structure. In this frequency range, basically the effect of the metallic ground plane is approximately eliminated and we reach the condition as though, the metal plane is absent. The bandwidths for the three cases studied are indicated in Figure 20, using this criterion on the reflected phase.

The EBG with w = 4 cm and g = 3 cm achieves a 2:1 bandwidth, when the substrate is air and the height of the structure is 2 cm.

We have also increased the dielectric constant of the substrate and also varied the height. The results are shown in Figure 21 and 22.

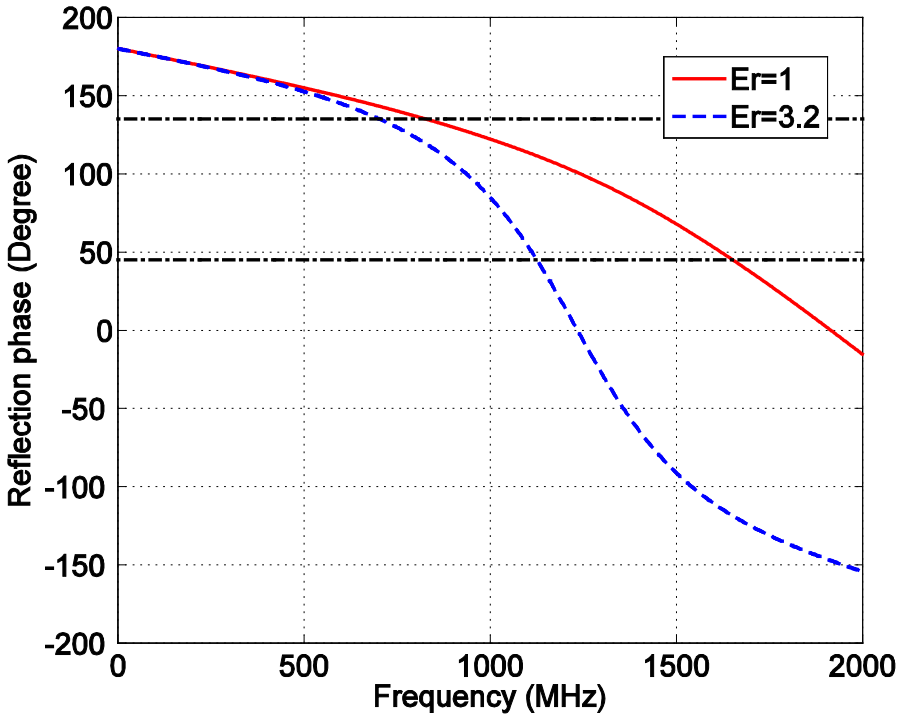

Dielectric constant	Bandwidth MHz	Percent Bandwidth
Er =3.2	702-1125	46.31%
Er =1	827-1651	66.51%

Figure 21. Reflection phase for varying dielectric constant of the substrate

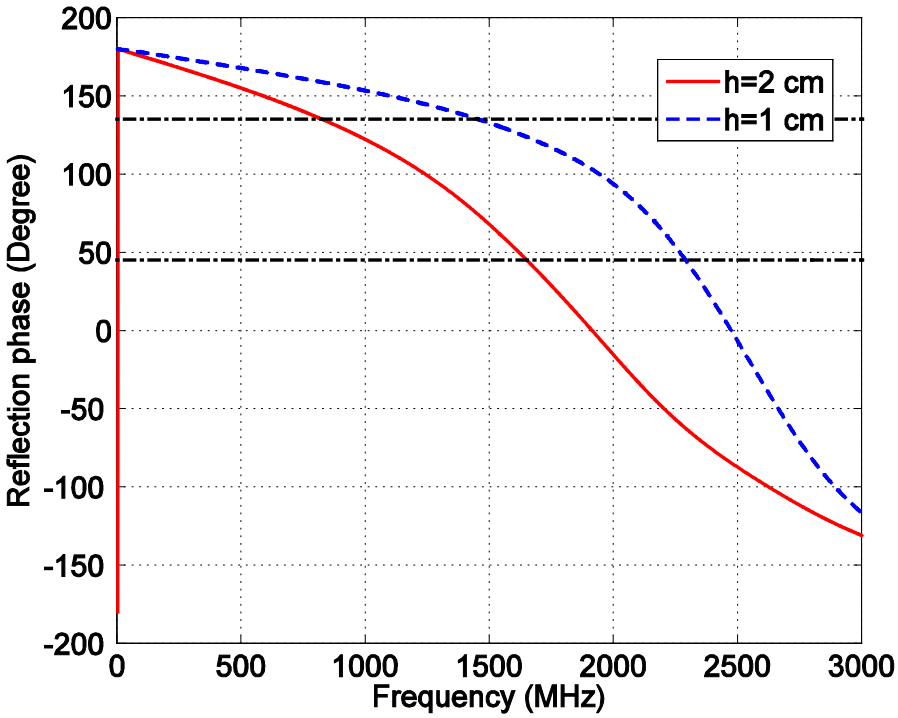

Height h	Bandwidth MHz	Percent Bandwidth
h = 1 cm	1455-2291	44.63%
h = 2 cm	827-1651	66.51%

Figure 22. Reflection phase for varying heights of substrate

We observe:

1. When the dielectric constant increases, the frequency decreases and the bandwidth becomes narrower.

2. When the substrate thickness decreases, the frequency increases but the percentage bandwidth becomes narrower.

Finally, we have arrived at the following geometry of the EBG structure for fabrication and measurements.

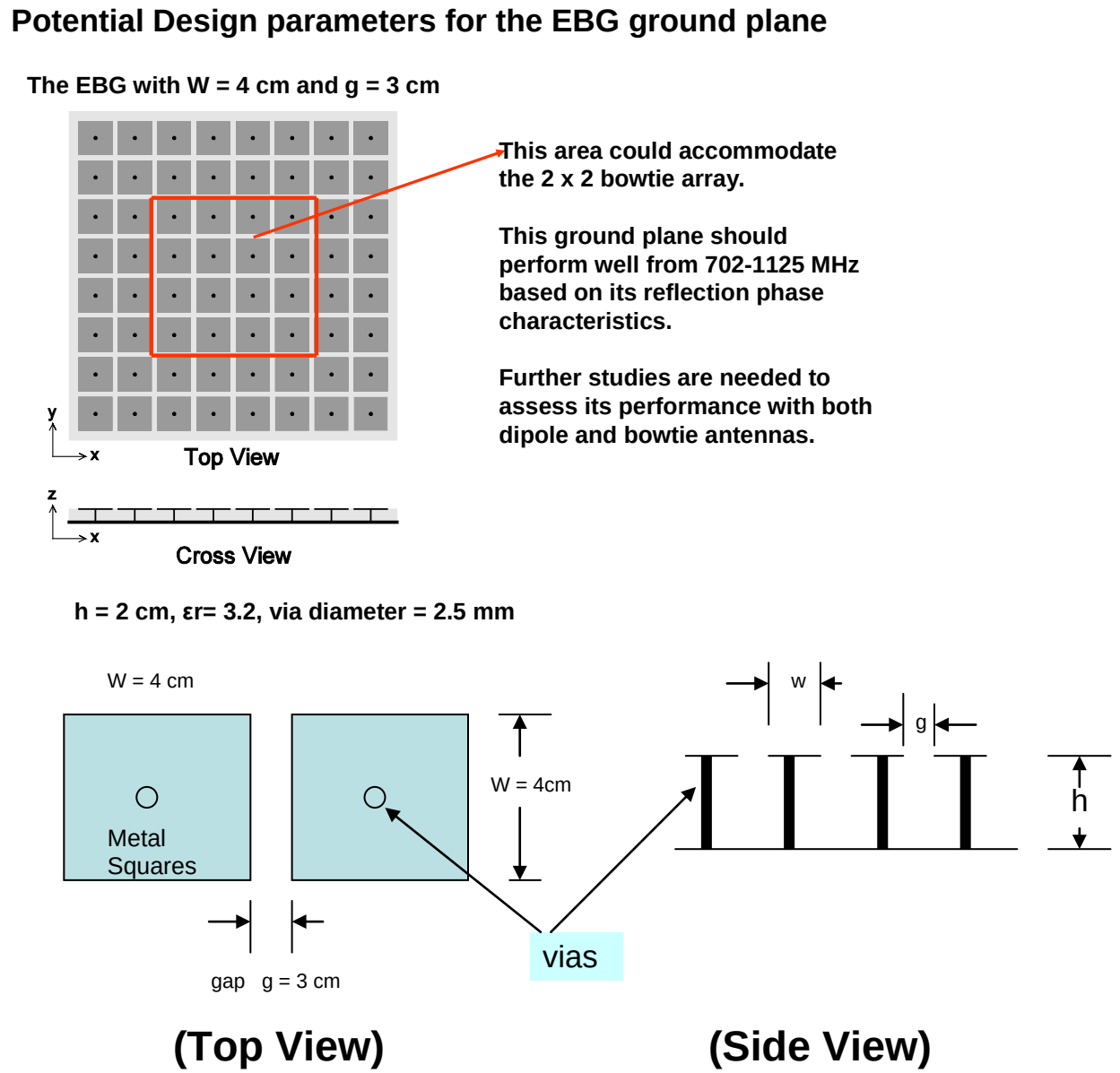

Figure 23. Geometrical details for the EBG for experimentation

It is noted that the design is not intended to meet the bandwidth requirements, but it is more of a proof-of-concept design. We have fabricated the EBG structure of Figure 23 and performed the TDR, S11 and VSWR measurements. The results, described in the next section are very encouraging. The EBG structure between the conformal array and the metal ground plane significantly improves the performance. Although we never get back the performance of an isolated conformal array, this sandwich structure of the EBG between the antenna and the metal plane, is far superior to the case of the antenna near a metal surface.

4.1 Dipole Antennas near the EBG Structure

We have analyzed and tested some dipole antennas on EBG structures prior to the conformal array. The dipole geometry is shown in Figure 24.

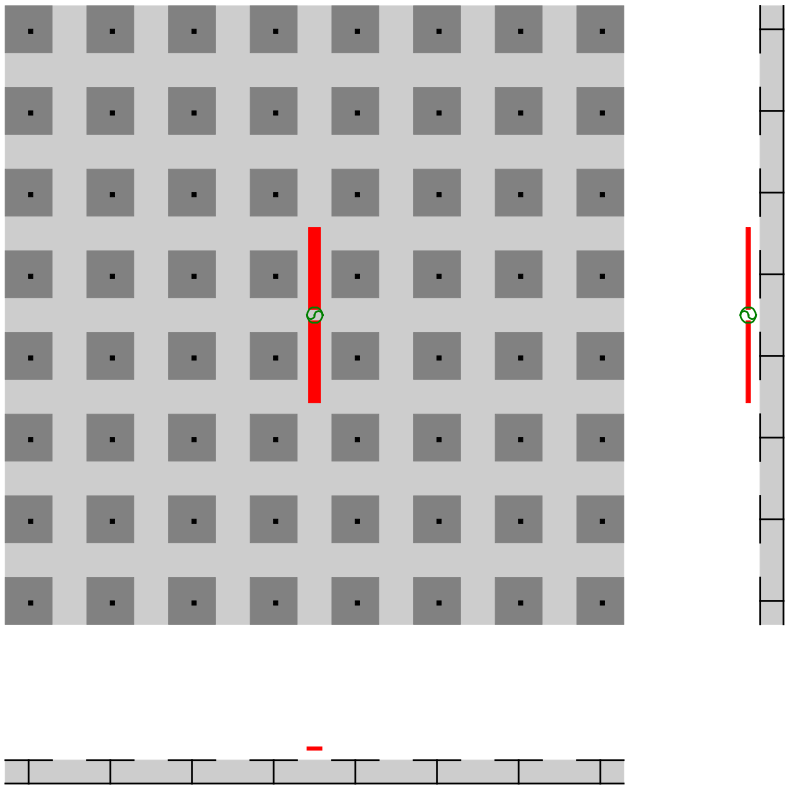

EBG parameters:

- **Patch width W: 4 cm**
- **Gap with g: 3 cm**
- **Substrate thickness h: 2 cm**
- **Dielectric constant ε_r : 1.0**

Dipole parameters:

- **Dipole width: 1 cm**
- **Dipole height: 1 cm**
- **Dipole length varies from 7 cm to 15 cm**

Figure 24. Geometry of dipole antennas over the EBG

The computed return loss (normalized to 50 Ohms) is shown in Figure 25a.

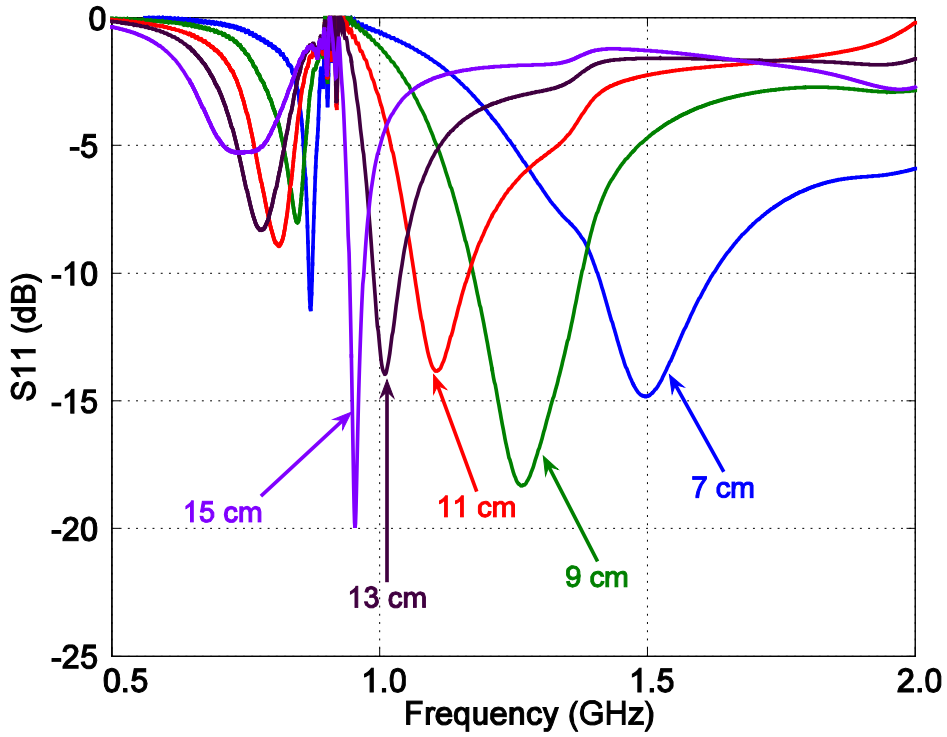

Figure 25a. Estimated S11 or return loss for the case of dielectric constant ε_r = 1

Remarks:

1. The half wavelength dipole realizes a good 50 ohms return loss close to the EBG ground plane (1 cm height).

2. The bandwidth for a given dipole is quite small.

3. When the dipole length is varied, the antenna can achieve a 50 ohms return loss better than -10 dB from 944 MHz ~ 1624 MHz (relates to the plane wave approach).

Next we repeat this calculation for the case of the dielectric constant = 3.2. The S11 estimates are shown in Figure 25b.

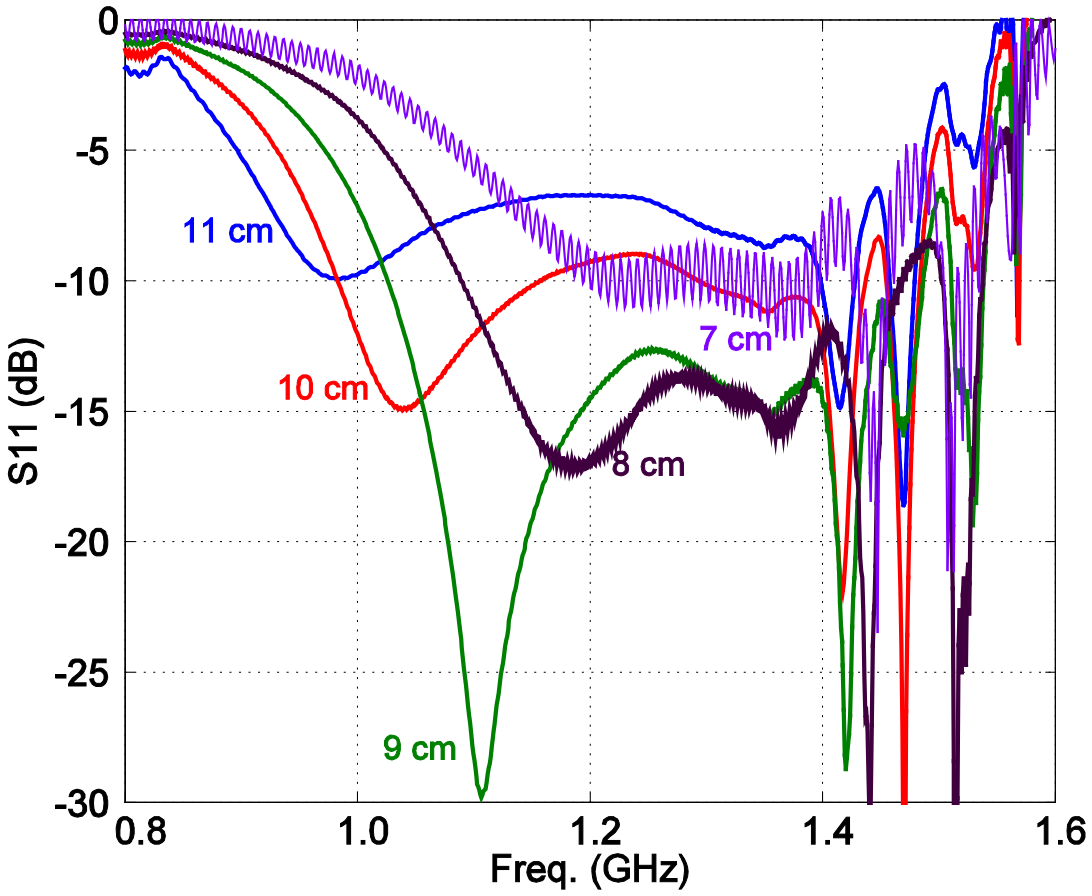

Figure 25b. Estimated S11 or return loss for the case of dielectric constant ε_r = 3.2

Remarks:

1. A dipole antenna can radiate efficiently near the EBG ground plane (2 cm height).

2. The resonant frequency can be tuned by adjusting the length of the dipole antenna.

We have calculated the radiation patterns of a dipole 9 cm, at 2 frequencies of 1.11 GHz and 1.42 GHz. This is shown in Figure 26.

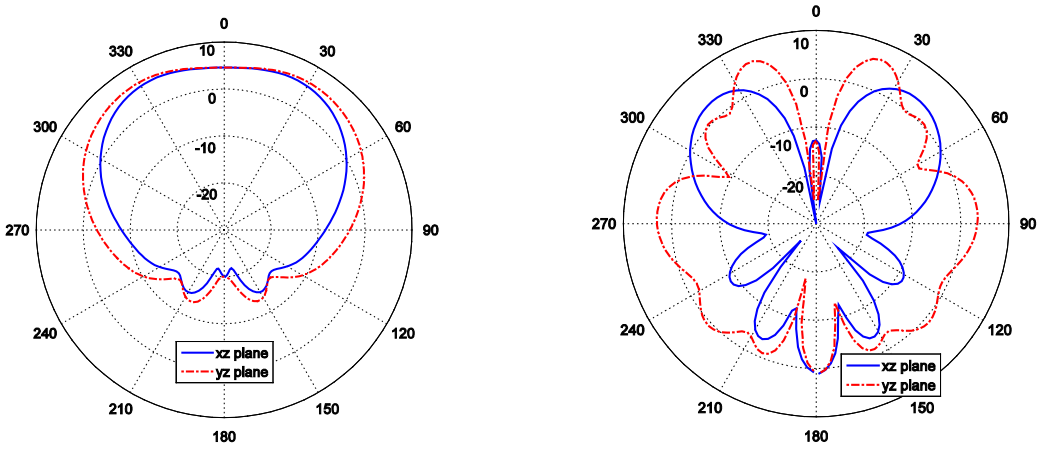

(a) Frequency = 1.1 GHz **(b) Frequency = 1.42 GHz**

Figure 26. Radiation Pattern of the 9 cm dipole near the EBG structure

Remarks:

1. At 1.11 GHz, a broadside radiation pattern is obtained from the dipole.

2. At 1.42 GHz, a broadside null is obtained, which indicates that the radiation is not from the dipole, but from the diffraction of excited surface waves.

3. This calculation shows the bandwidth limitation and shift in radiation patterns of the dipole near the EBG structure.

Next we turn our attention to simulate the bow tie antenna elements.

4.2 Bow-Tie Antennas near the EBG structure

Initially we use an FDTD code to obtain the input impedance of 1 and 2 bow-tie antenna elements. The numerical model for the bow tie is shown in Figure 27a and the impedances in Figure 27 b.

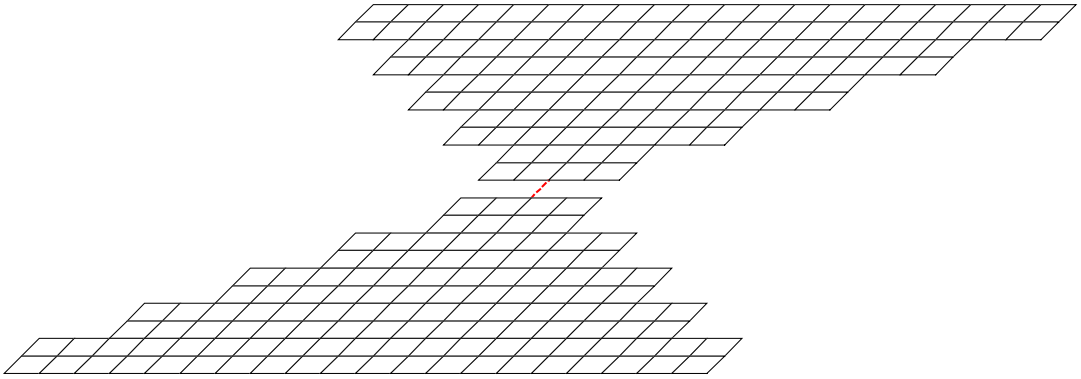

(a) A 10 cm x 10 cm bow –tie antenna model for FDTD calculations

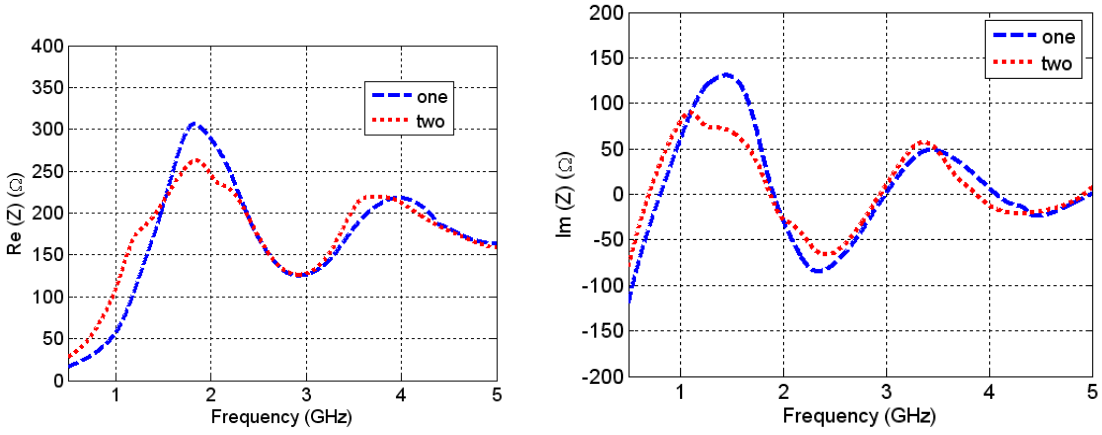

(b) Real and imaginary parts of 1 and 2 bow- tie antennas

Figure 27. The numerical model for the bow-tie and the impedances

The geometry for one and two bow-tie antennas are shown in Figure 28.

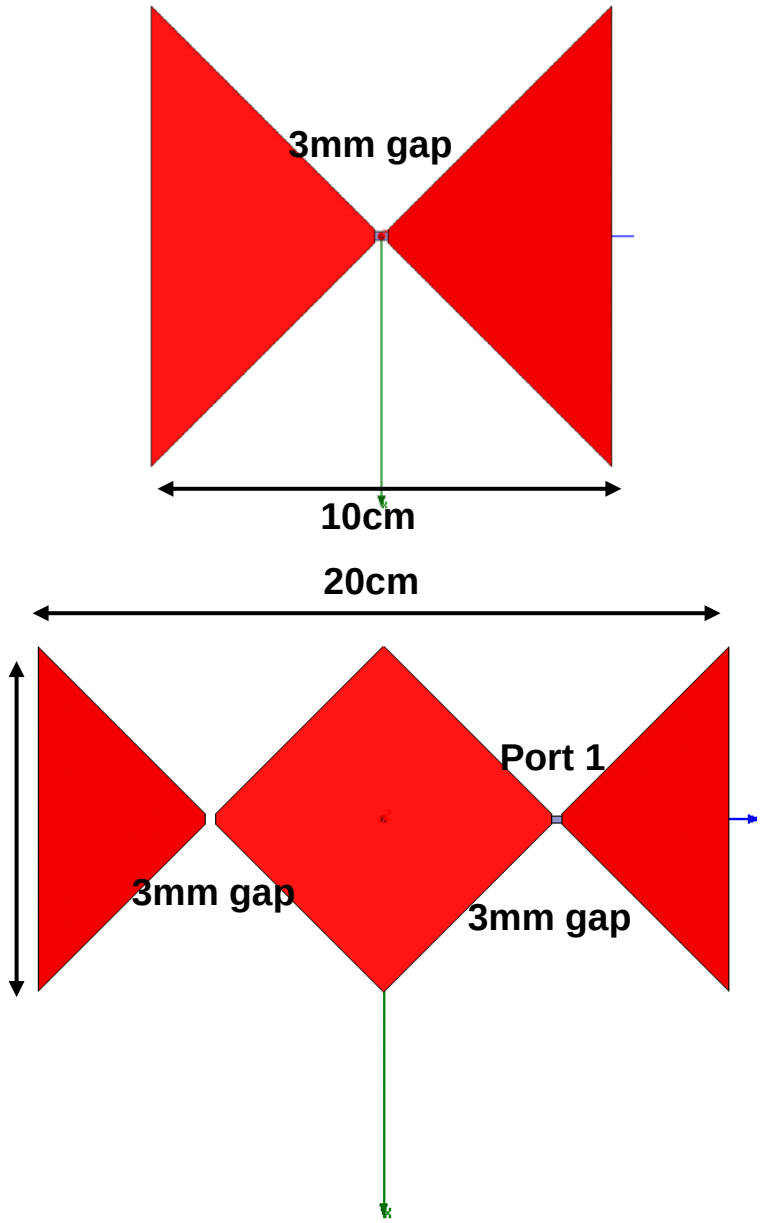

Figure 28. Geometry of one and 2 bow-tie antennas

In examining the simulated impedances, we find that the impedance oscillates around 188 Ohms, (half of free space characteristic impedance) as one would expect. The simulated S11 for one and two bow-tie antennas are shown in Figures 29 and 30.

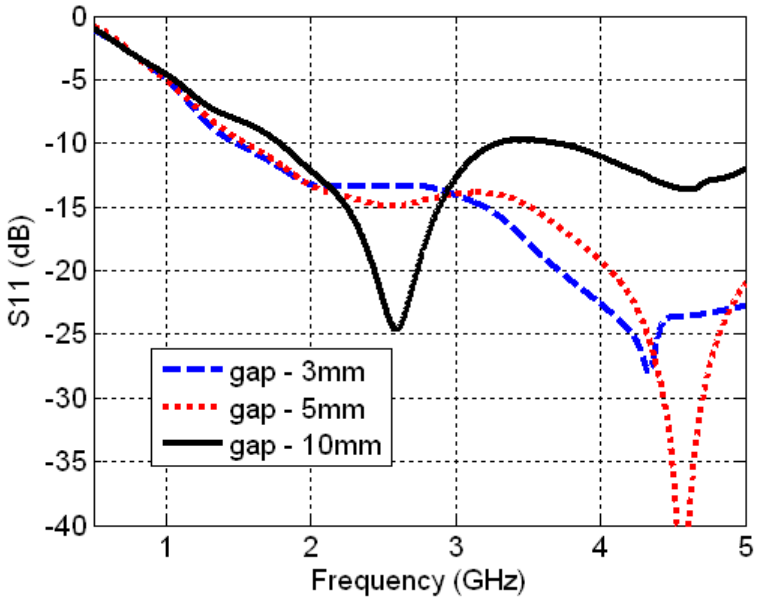

Figure 29. Simulated S11 (normalized to 188.5 Ohms) for a Bow-tie antenna with varying gap dimensions.

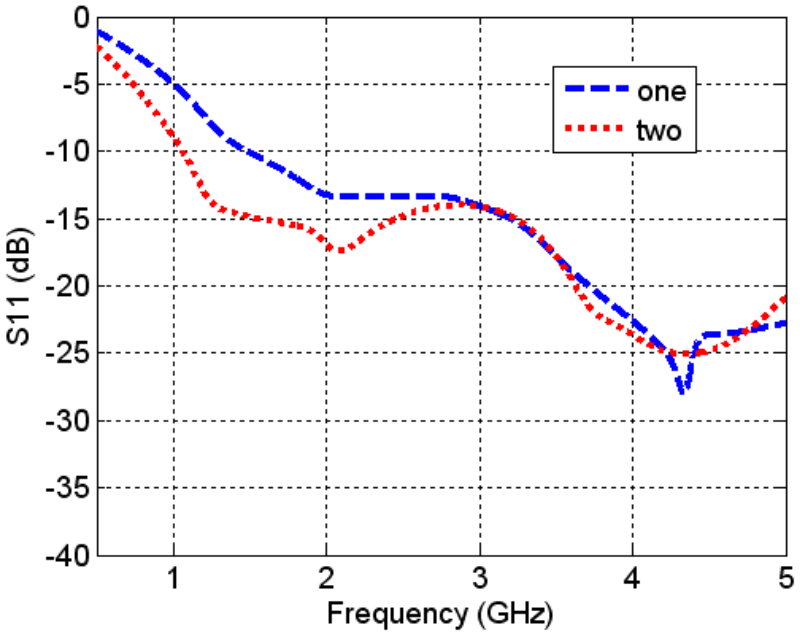

Figure 30. Simulated S11 (normalized to 188.5 Ohms) for two Bow-tie antennas of Figure 28, with a feed gap of 3 mm

It is clear that putting two bow–tie antennas together, the band width increases. One bow-tie starts to work at 1.5 GHz for a feed gap of 3 mm and when two antennas are connected, the lower limit reduces to 1 GHz. The reason is in an array of bow-ties that are series-parallel connected, currents from one element is permitted to flow into the neighboring antenna at low frequencies, thus enhancing the bandwidth. Generally speaking, in antenna arrays, the elements are not touching each other and the mutual interaction is less. Here we need to extend the bandwidth and the elements are deliberately made to touch each other. It is as though, the individual elements are working at high-frequencies and the array as a whole is working at low frequencies and hence the enhanced bandwidth for the array!

Having established the theoretical basis for the array antennas, we now proceed to report our experimental results.

5.0 Experimental Evaluation of an EBG Structure for use with a Conformal Antenna

5.1 Experimental Hardware

The EBG surface is composed of an array of 4 cm x 4 cm (w = 4 cm in the design) squares placed on a 1.87 cm (h = 2 cm in the design) thick dielectric material. The Polyvinylchloride (PVC) dielectric material has a dielectric constant of 3.2 (close to the assumed value in the design). The distance between the squares is 3 cm (g = 3 m in the design). The overall size of the panel is 61 cm by 61 cm (roughly 2 feet x 2 feet). The overall dimension was chosen to allow the conformal antenna to be placed well within the outer dimensions of the structure. The EBG structure is shown in Figure 31. A top view of the 2 x 2 conformal array that fits in the middle and above the EBG structure is shown in Figure 32.

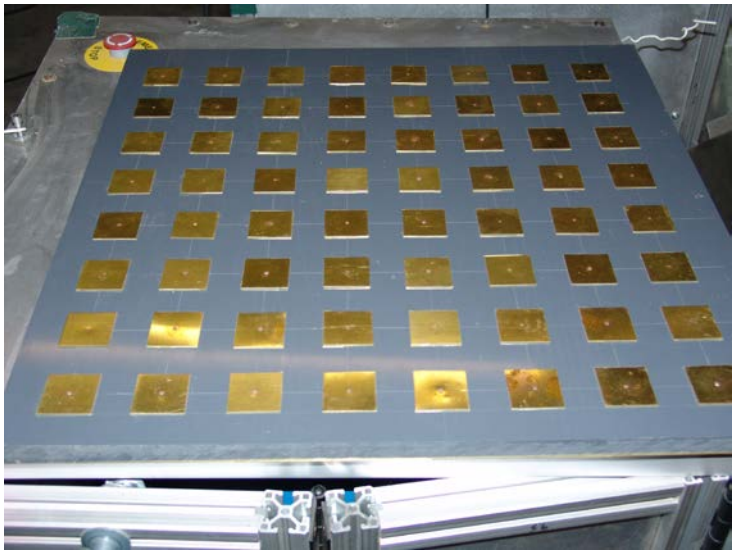

Figure 31. Photo of the fabricated EBG structure

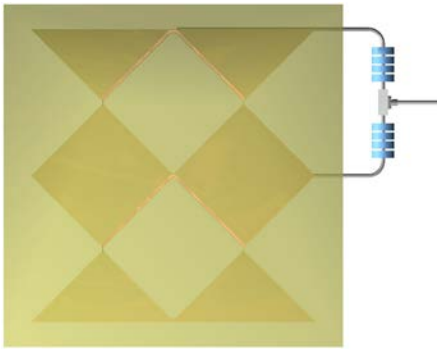

Figure 32. Top view of the prototype conformal array

A four element (2x2) prototype conformal antenna fabricated during phase I of this effort is utilized to test the effectiveness of the EBG structure. The array elements measure 10 cm x 10 cm (width x height) and were formed using 0.2 mm thick copper tape placed on a 6.35 mm thick polyethylene plate. A top view of the array is shown in Figure 32.

A Prodyn Technologies SB-10D (Serial Number 29) summing block is used to interface the two 100 Ω feed cables to the 50 Ω feed cable. The two 100 Ω feed cables interface with four 200 Ω strip transmission lines that are machined into the polyethylene substrate of the array (dielectric constant = 2.2). Three Ferrite cores were placed on each 100 Ω cable to provide isolation between the two arrays. The interface between the 100 Ω cable and the two 200 Ω cables is shown in Figure 32. The length of the center conductor required to connect to the 200 ohm line introduced a significant parasitic inductance that was partially compensated for by placing a small amount of epoxy (dielectric constant of 5.1) at the feed point. Wing extensions can be added to the array to improve the low frequency response of the array.

A variety of dipole antennas of different lengths were fabricated to test the EBG structure. A photo of the dipoles is shown in Figure 33. The lengths of the dipoles (overall length of one element) are 3.5 cm, 4.0 cm, 4.5 cm, 5.0 cm, 5.5 cm, 7.0 cm, 8.0 cm, 9.0 cm, 10.0 cm, and 11.0 cm. The effectiveness of the EBG structure is evaluated by making several measurements. The signal reflected by the antenna back to the source (S11) as a function of frequency is measured using an Agilent 8753ES network analyzer with an s-parameter test set (shown in Figure 34). The S11 measurement is then used to calculate the SWR for the antenna under test. A Tektronix 11801 with an SD24 TDR head is used to evaluate the time domain response of the antenna (shown in Figure 35).

5.2 Experimental Procedures and Dipole Data

The EBG structure was first evaluated using the dipoles as a radiating source. S11 and the SWR, and the TDR measurement are performed for each dipole in each of three configurations. The first configuration is with the dipoles placed on the EBG structure as is shown in Figure 36. The

S11 and the SWR measurements are shown in Figure 37- 40. The TDR measurements are shown in Figure 41-50.

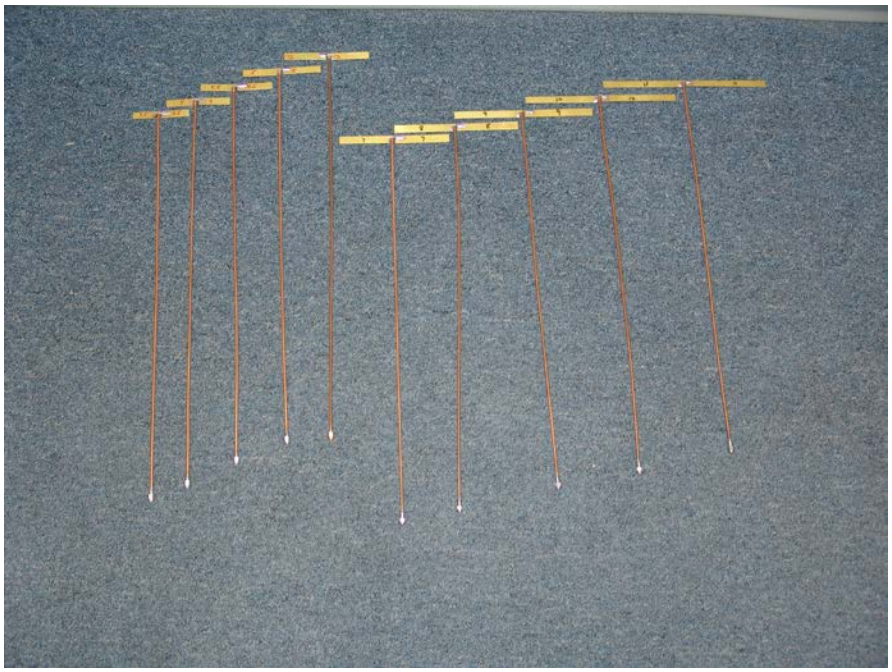

Figure 33. Photo of the dipoles of varying lengths (3.l5 cms to 11 cms) fabricated to evaluate the EBG.

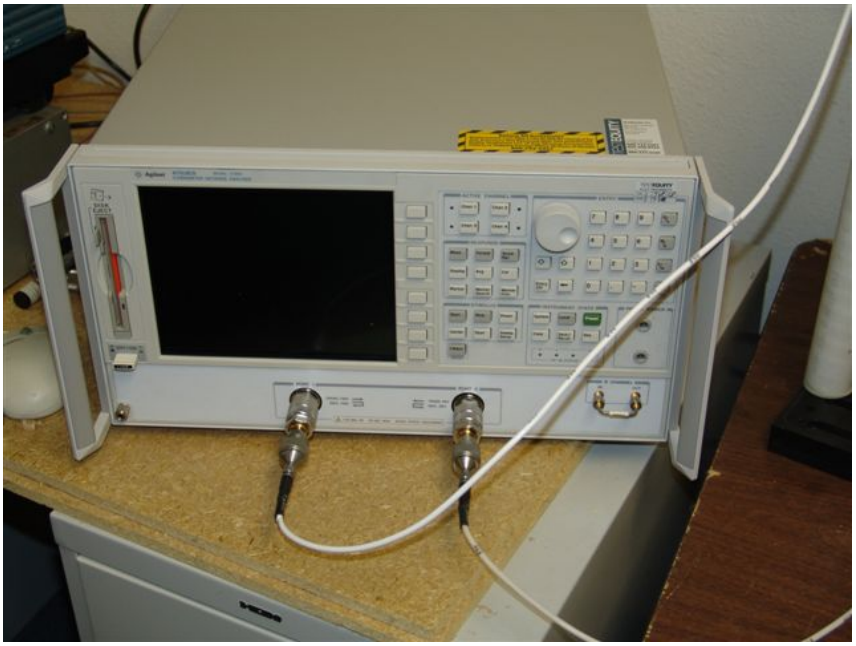

Figure 34. Photo of the 6811B network analyzer used in the measurement.

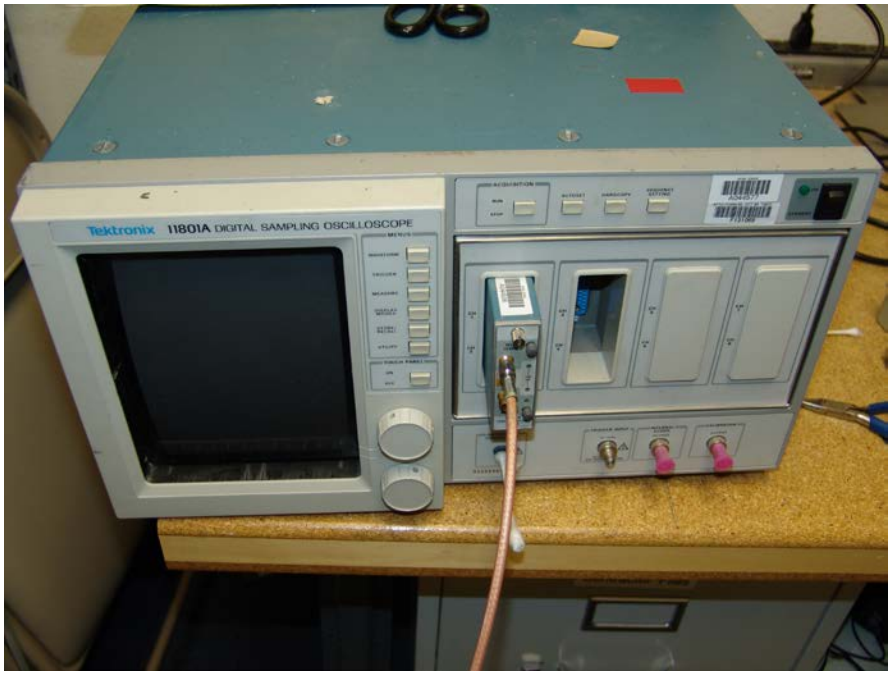

Figure 35. Tektronix 11801A oscilloscope with TDR sampling head.

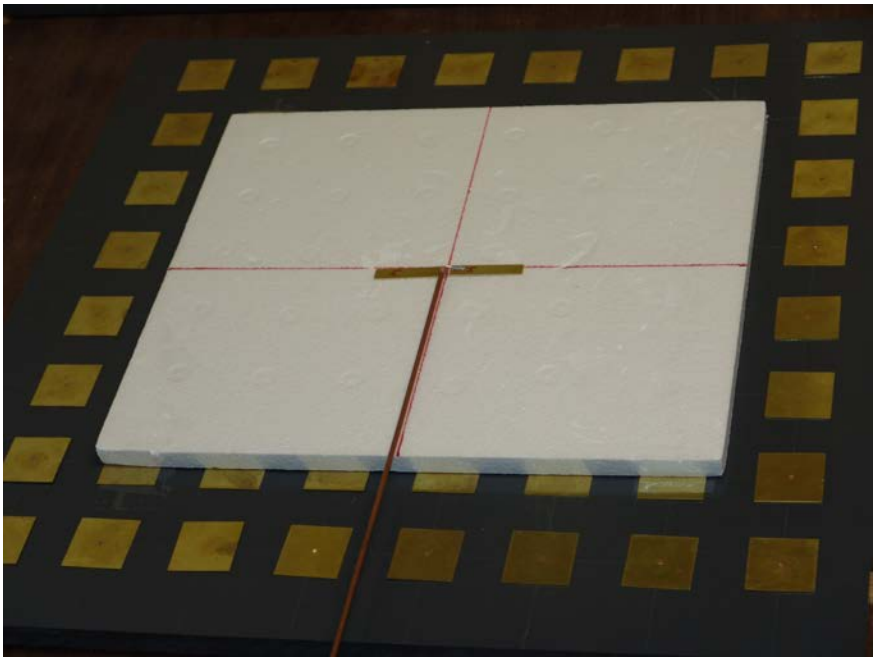

Figure 36. Photo of one of the dipole test configuration with the EBG Structure.

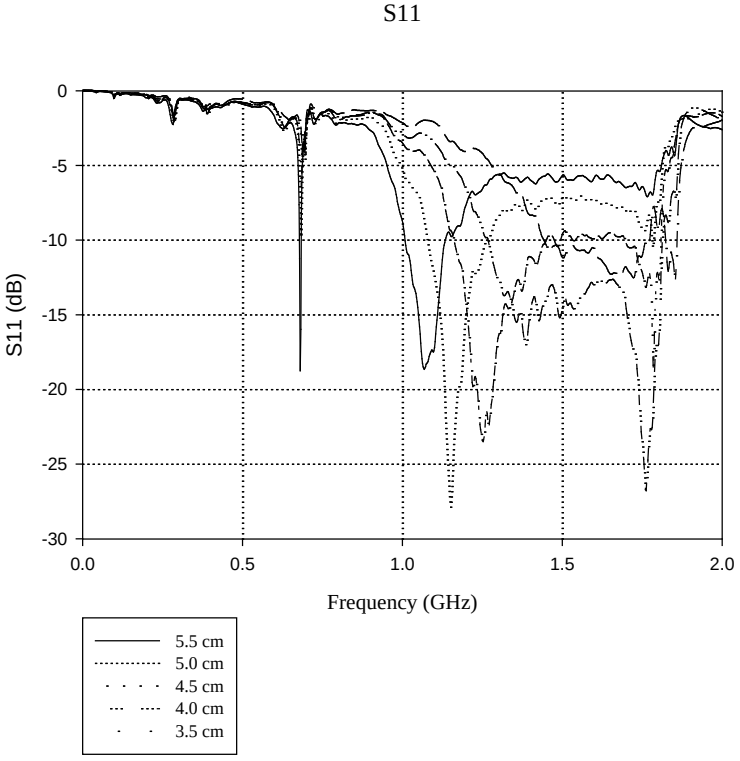

Figure 37. S11 measurements for the high frequency dipoles placed on the EBG structure.

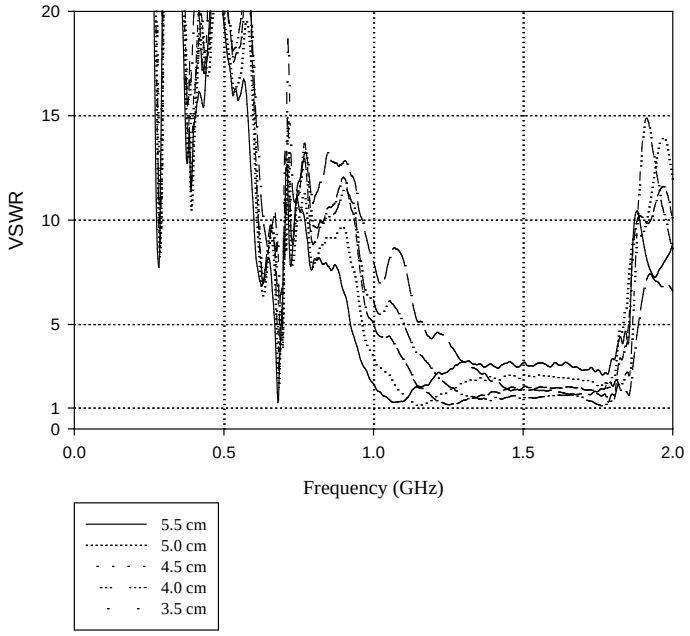

Figure 38. SWR measurement (calculated from S11) for the high frequency dipoles placed on the EBG structure.

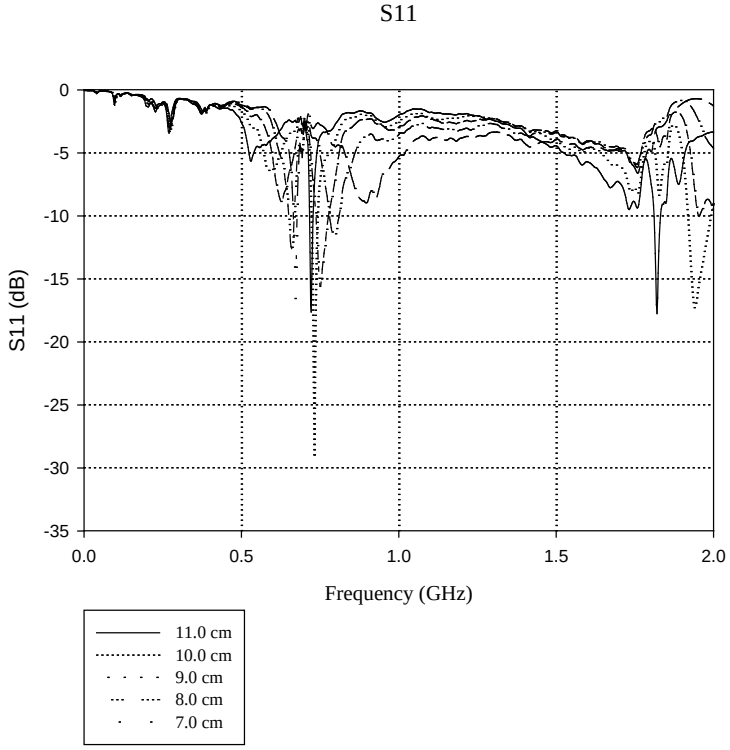

Figure 39. S11 measurements for the low frequency dipoles placed on the EBG structure.

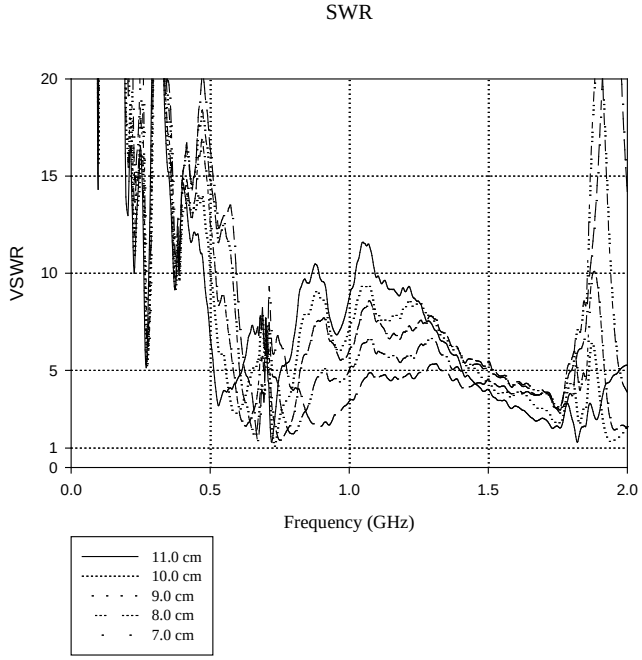

Figure 40. SWR measurement (calculated from S11) for the low frequency dipoles placed on the EBG structure.

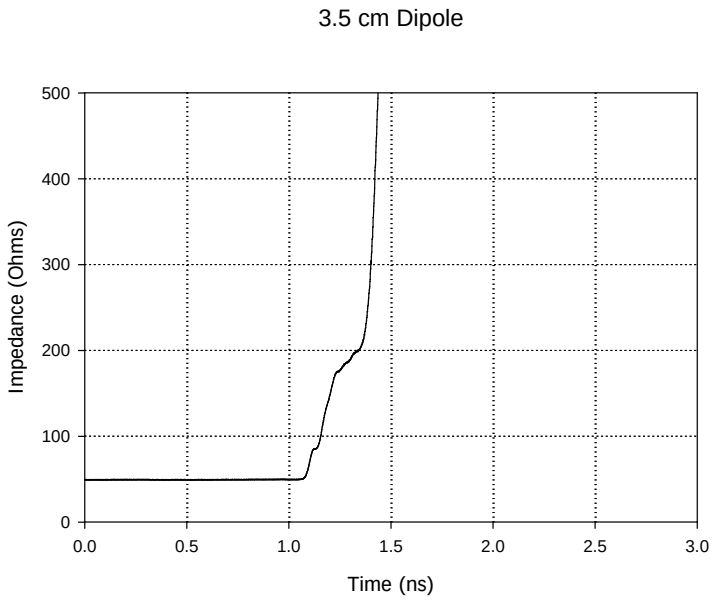

Figure 41. TDR measurement of the 3.5 cm dipole on the EBG structure.

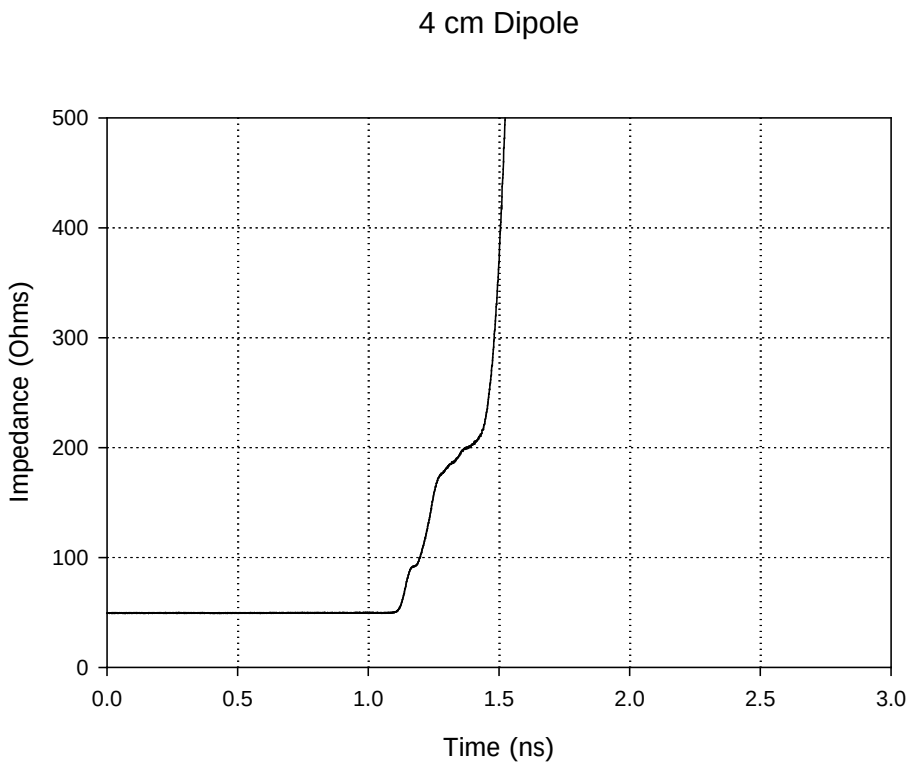

Figure 42. TDR measurement of the 4.0 cm dipole on the EBG structure.

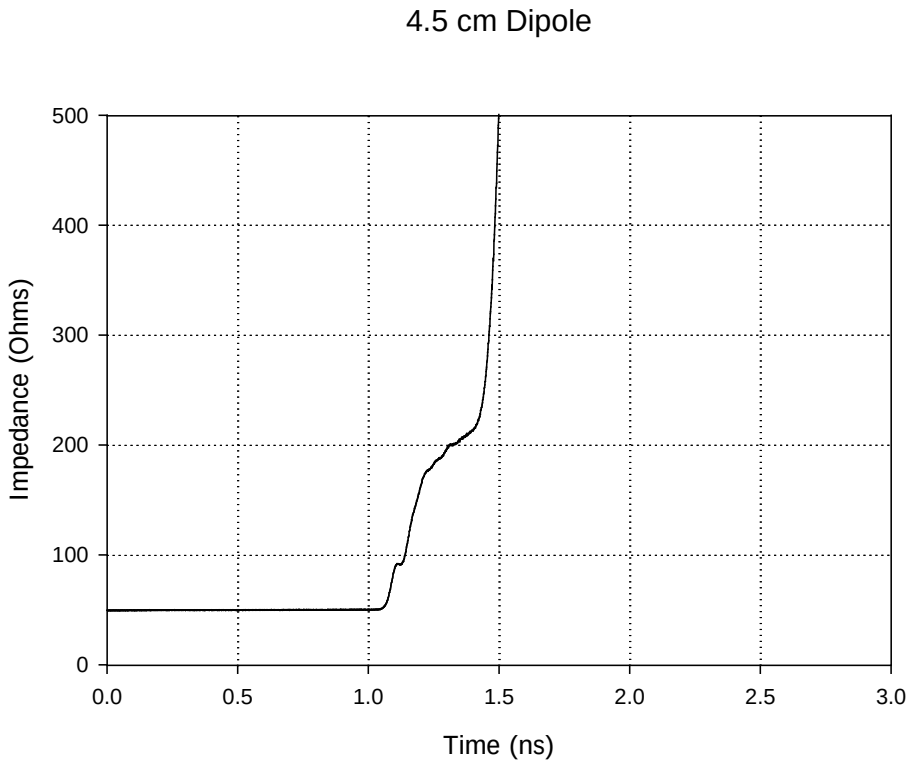

Figure 43. TDR measurement of the 4.5 cm dipole on the EBG structure.

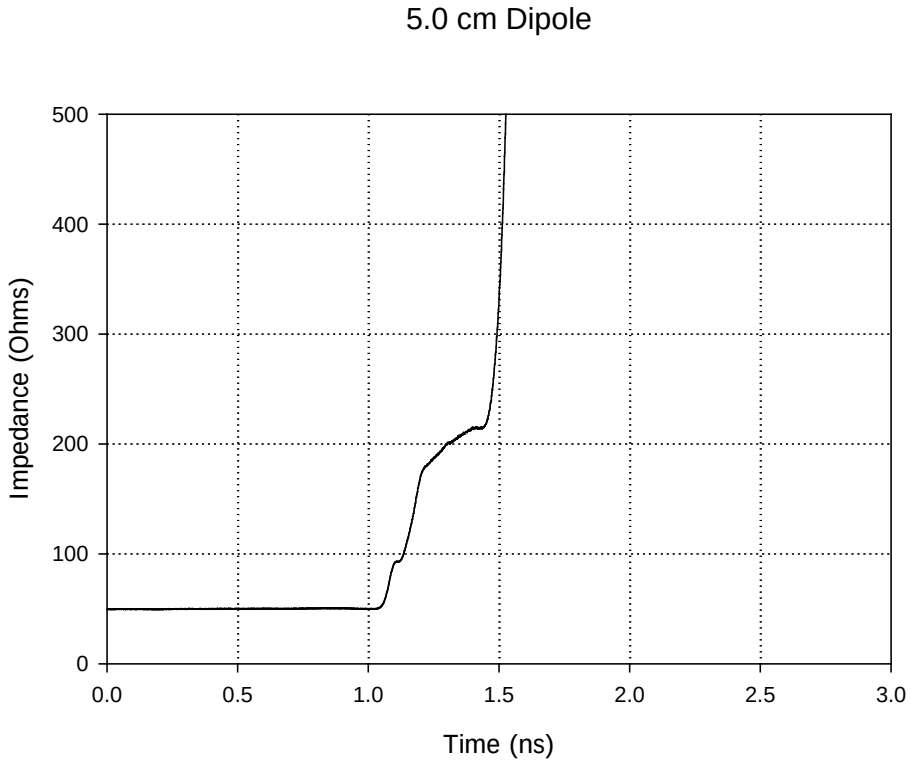

Figure 44. TDR measurement of the 5.0 cm dipole on the EBG structure.

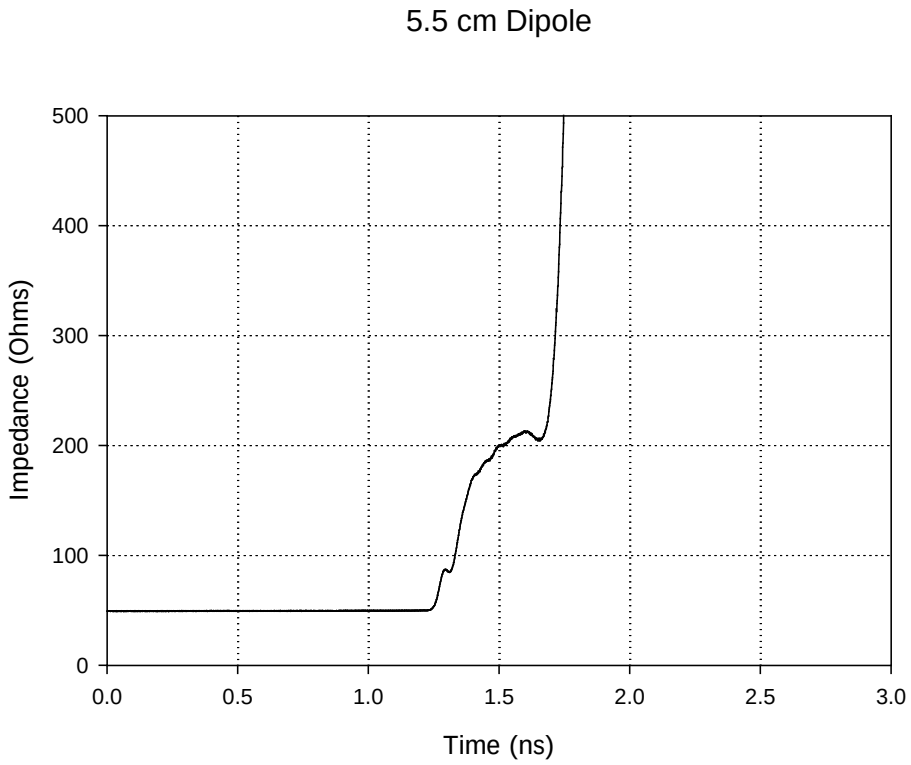

Figure 45. TDR measurement of the 5.5 cm dipole on the EBG structure.

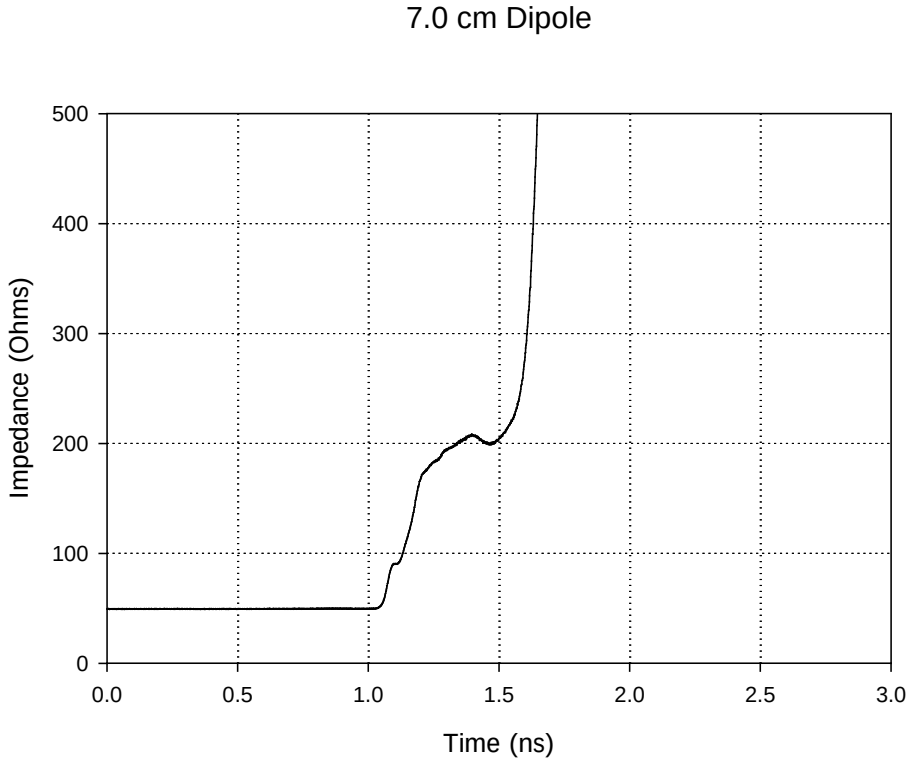

Figure 46. TDR measurement of the 7.0 cm dipole on the EBG structure.

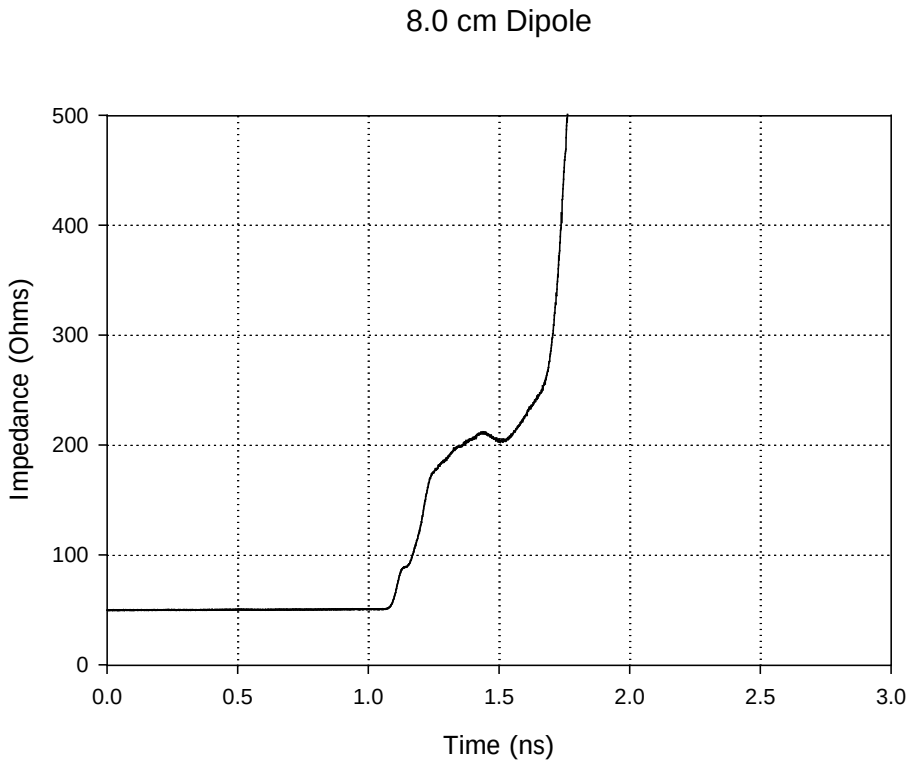

Figure 47. TDR measurement of the 8.0 cm dipole on the EBG structure.

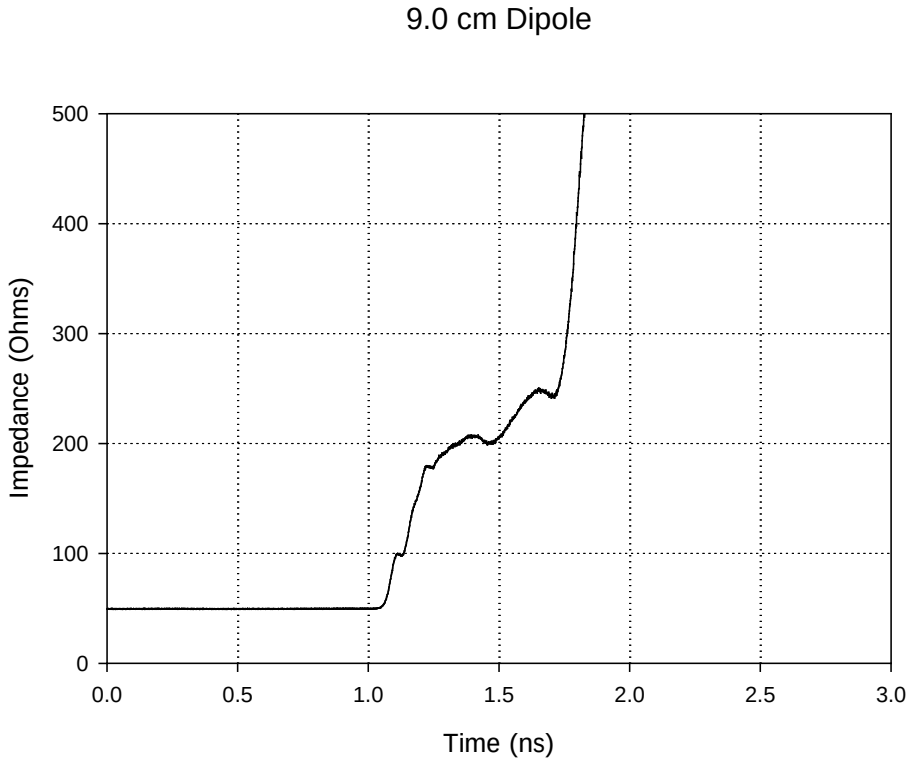

Figure 48. TDR measurement of the 9.0 cm dipole on the EBG structure.

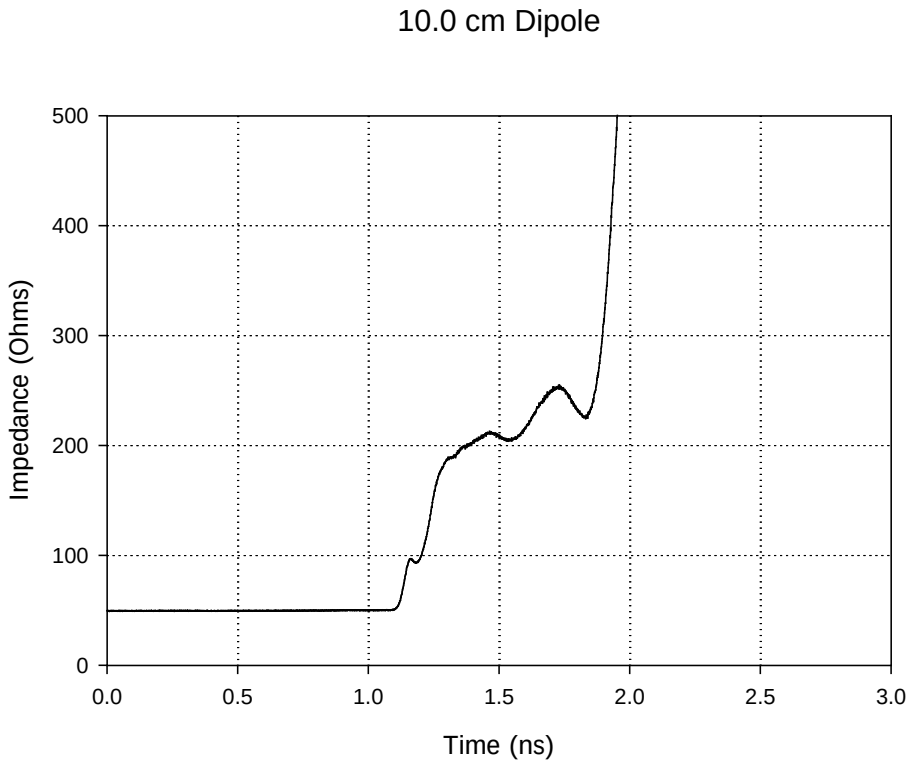

Figure 49. TDR measurement of the 10.0 cm dipole on the EBG structure.

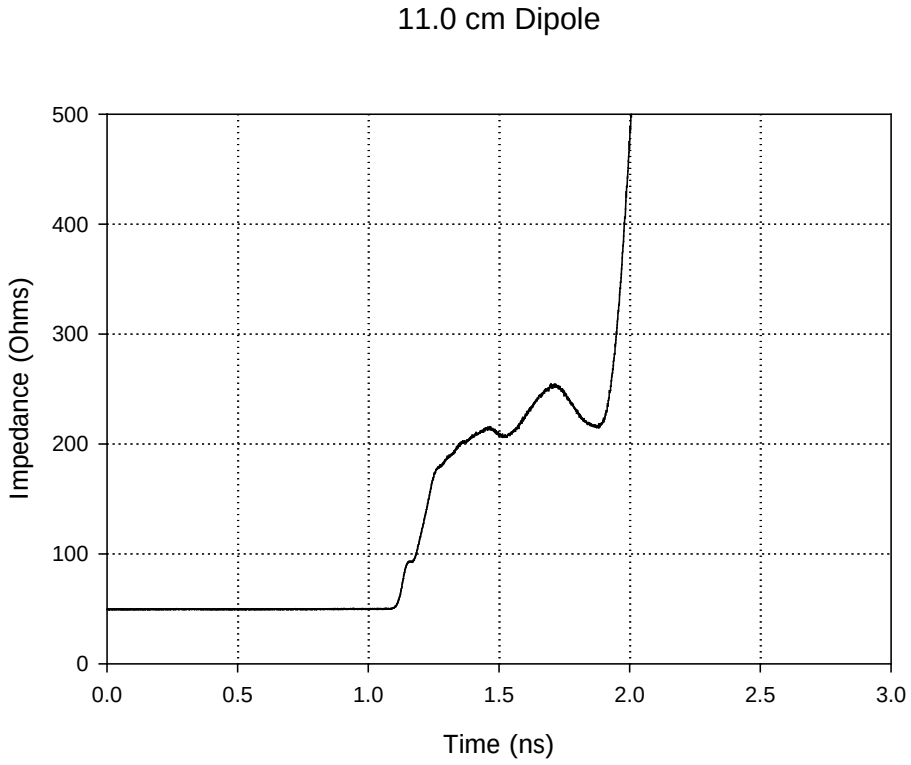

Figure 50. TDR measurement of the 11.0 cm dipole on the EBG structure.

The parameters are then measured with the dipoles located over a conductive ground plane as is shown in Figure 51. The S11 and the SWR measurements are shown in Figures 52-55. The TDR measurements for this configuration are shown in Figure 56-65. The final measurement configuration is with the dipoles located in free space as is shown in Figure 66. The S11 and the SWR measurements for the free space configuration are shown in Figure 67 – 70. The TDR measurements are shown in Figure 71- 80.

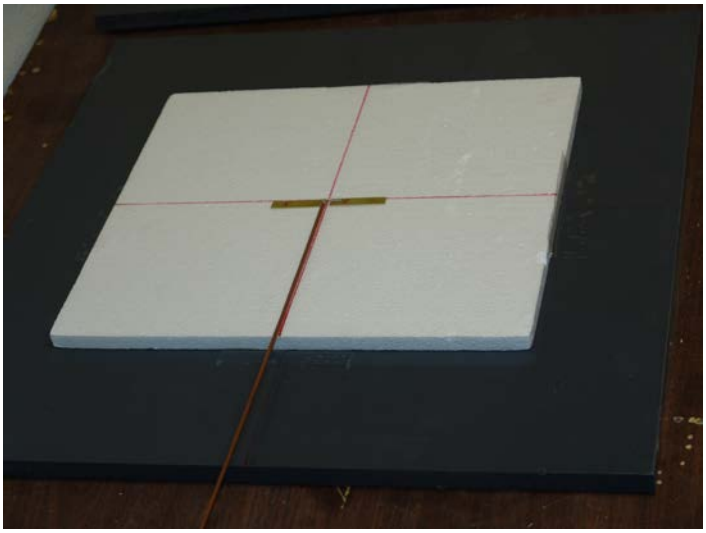

Figure 51. Photo of dipole test configuration with the ground plane Structure.

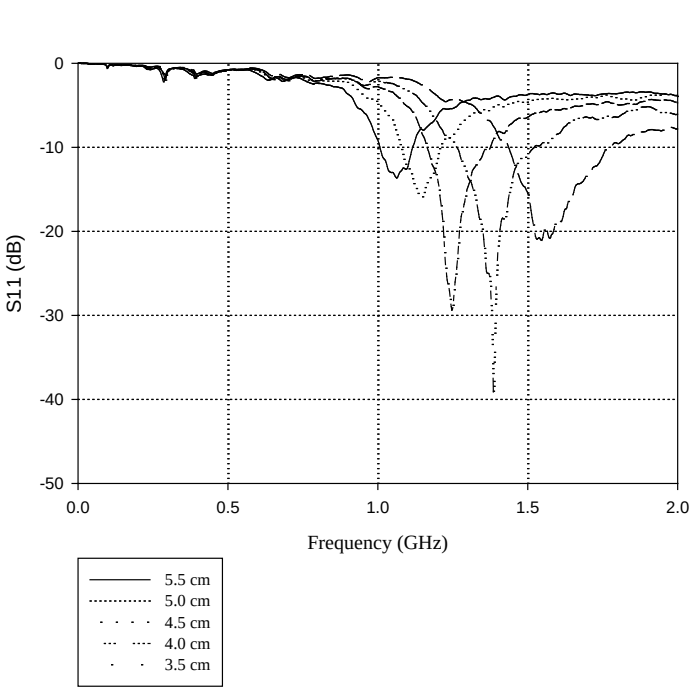

Figure 52 . S11 measurements for the high frequency dipoles placed on the ground plane structure.

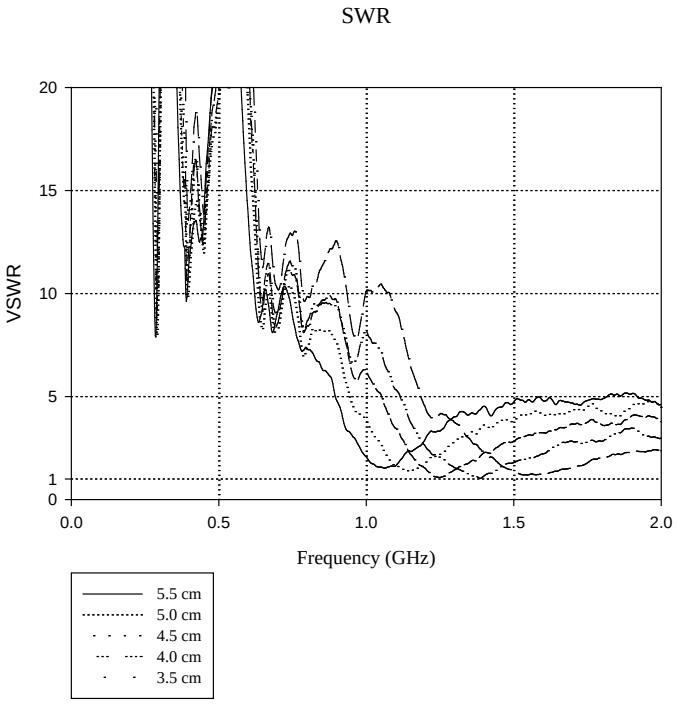

Figure 53. SWR measurement (calculated from S11) for the high frequency dipoles placed on the ground plane.

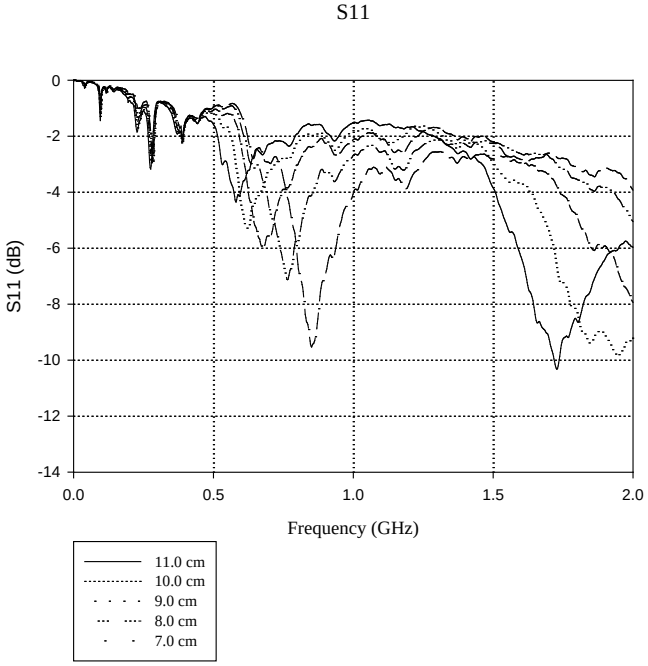

Figure 54. S11 measurements for the low frequency dipoles placed on the ground plane structure.

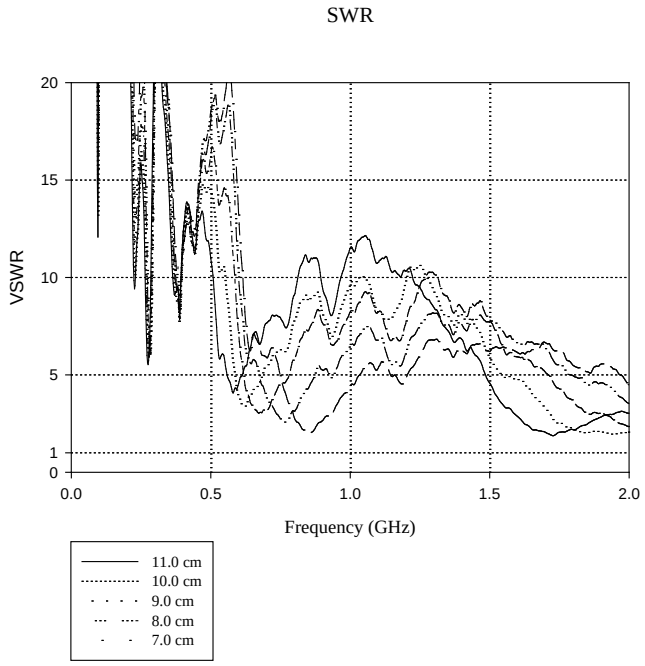

Figure 55. SWR measurement (calculated from S11) for the low frequency dipoles placed on the ground plane.

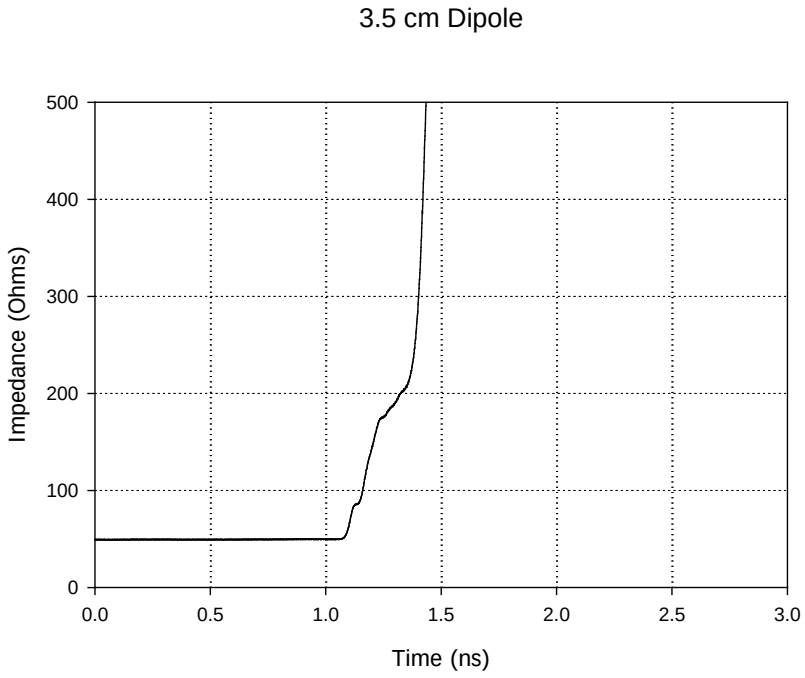

Figure 56. TDR measurement of the 3.5 cm dipole on the ground plane.

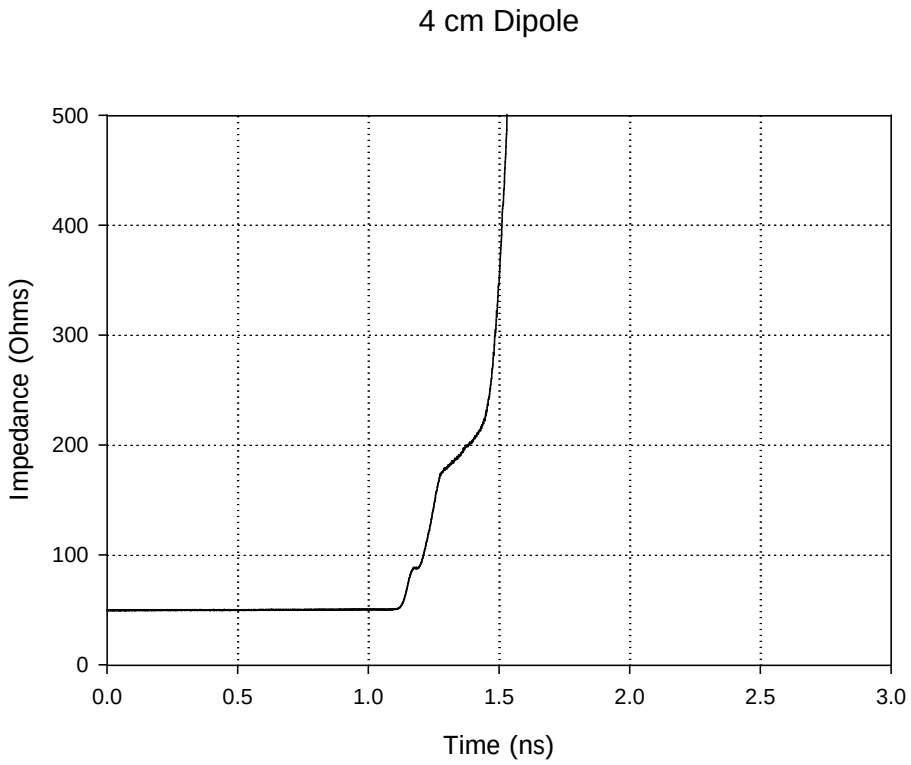

Figure 57. TDR measurement of the 4.0 cm dipole on the ground plane.

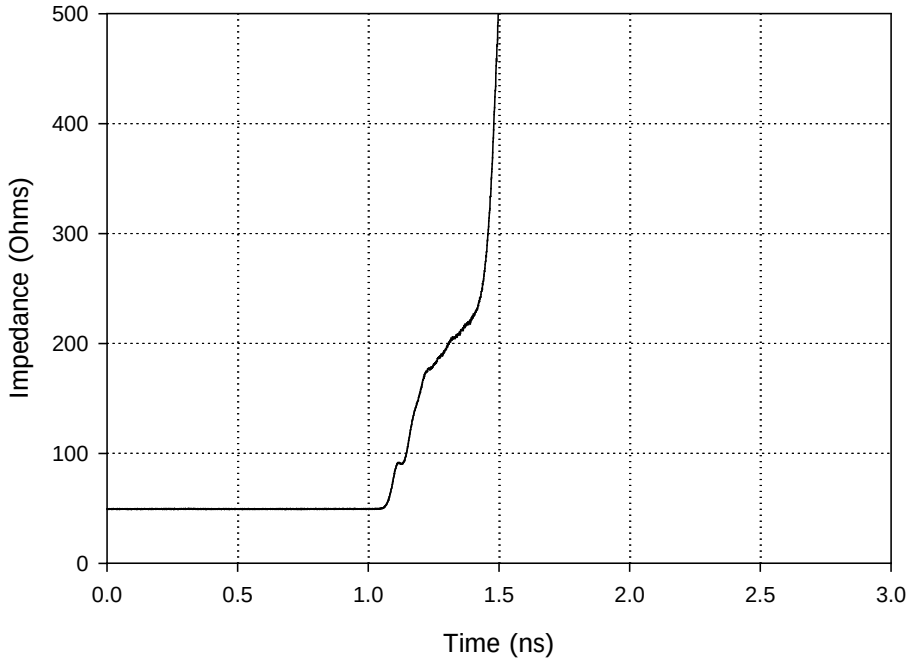

Figure 58. TDR measurement of the 4.5 cm dipole on the ground plane.

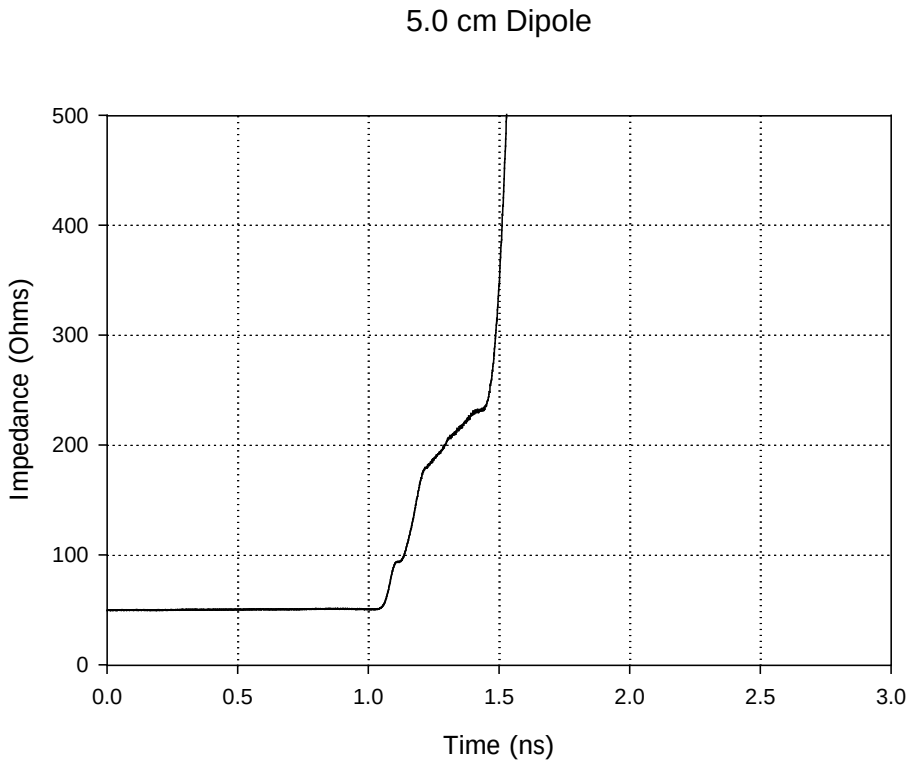

Figure 59. TDR measurement of the 5.0cm dipole on the ground plane.

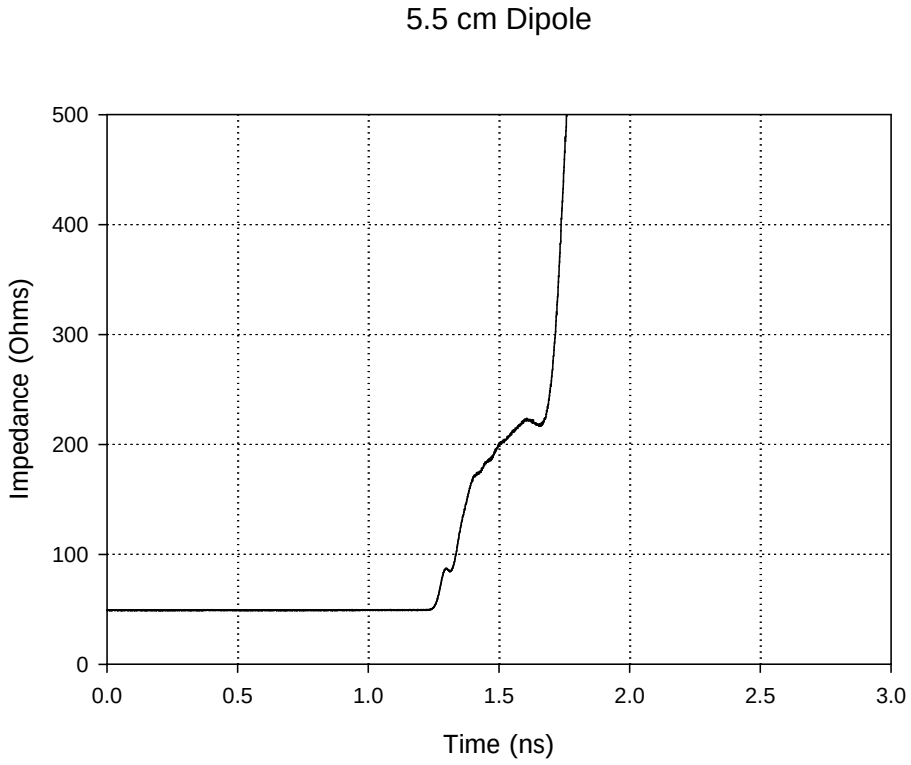

Figure 60. TDR measurement of the 5.5 cm dipole on the ground plane.

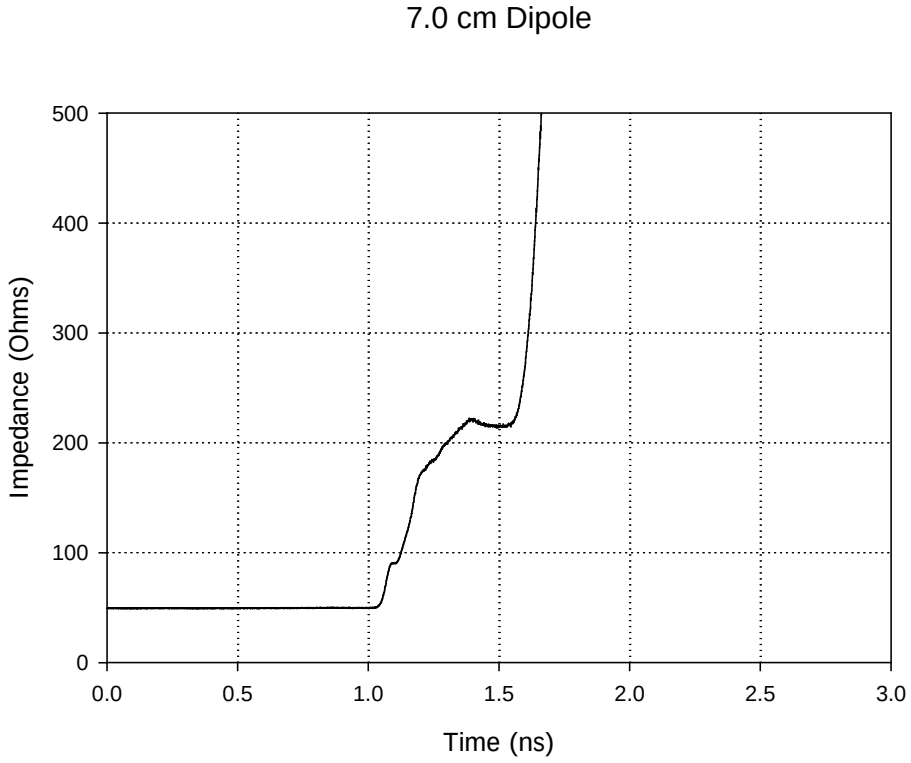

Figure 61. TDR measurement of the 7.0 cm dipole on the ground plane.

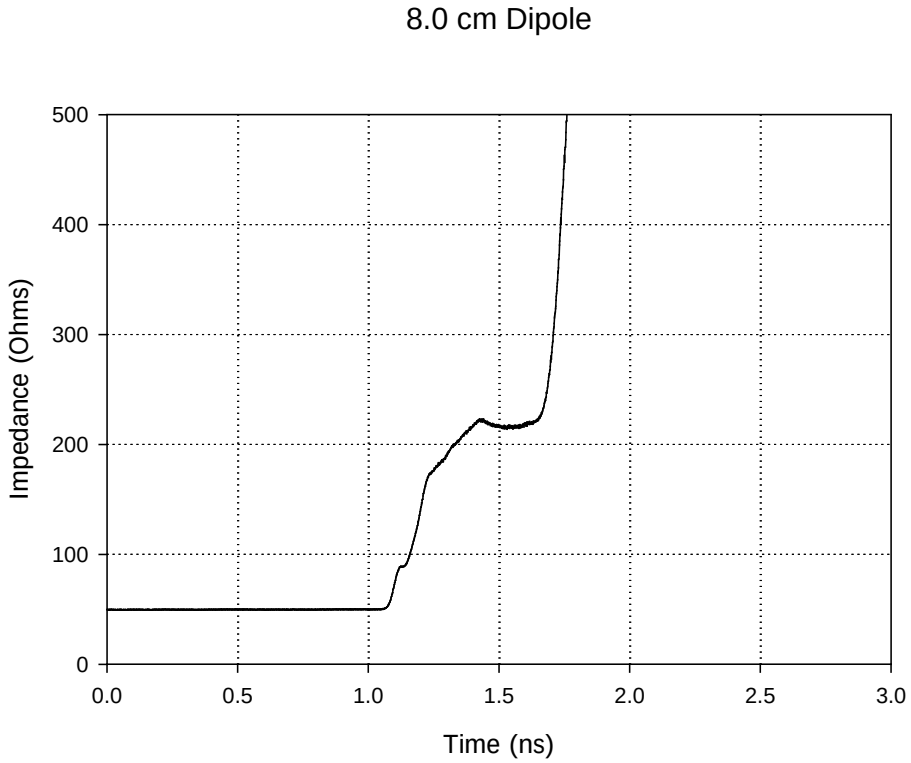

Figure 62. TDR measurement of the 8.0 cm dipole on the ground plane.

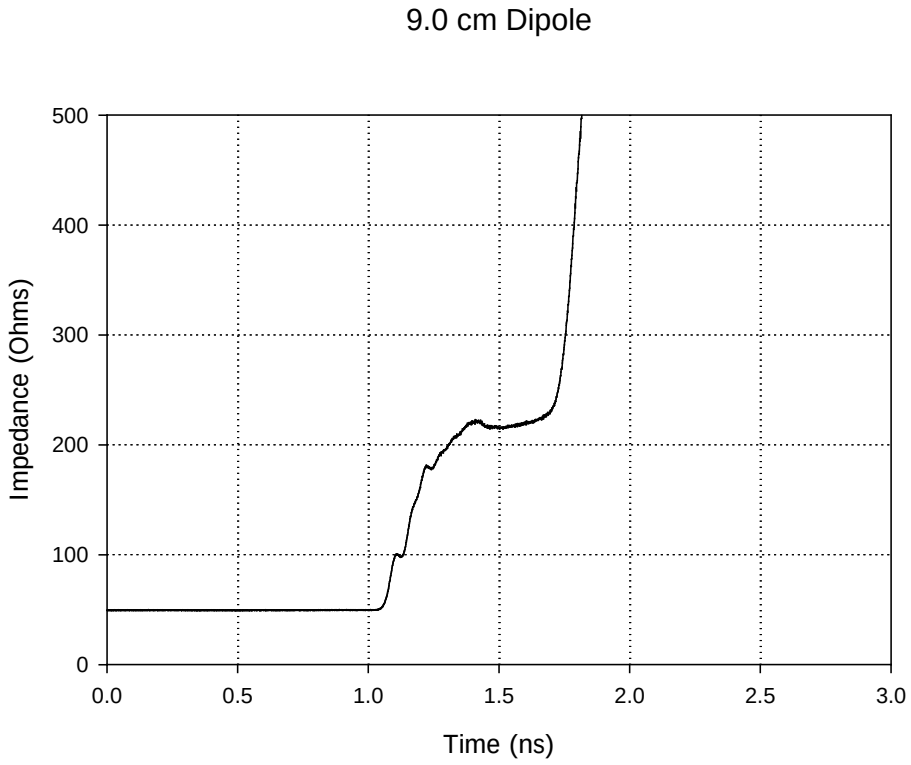

Figure 63. TDR measurement of the 9.0 cm dipole on the ground plane.

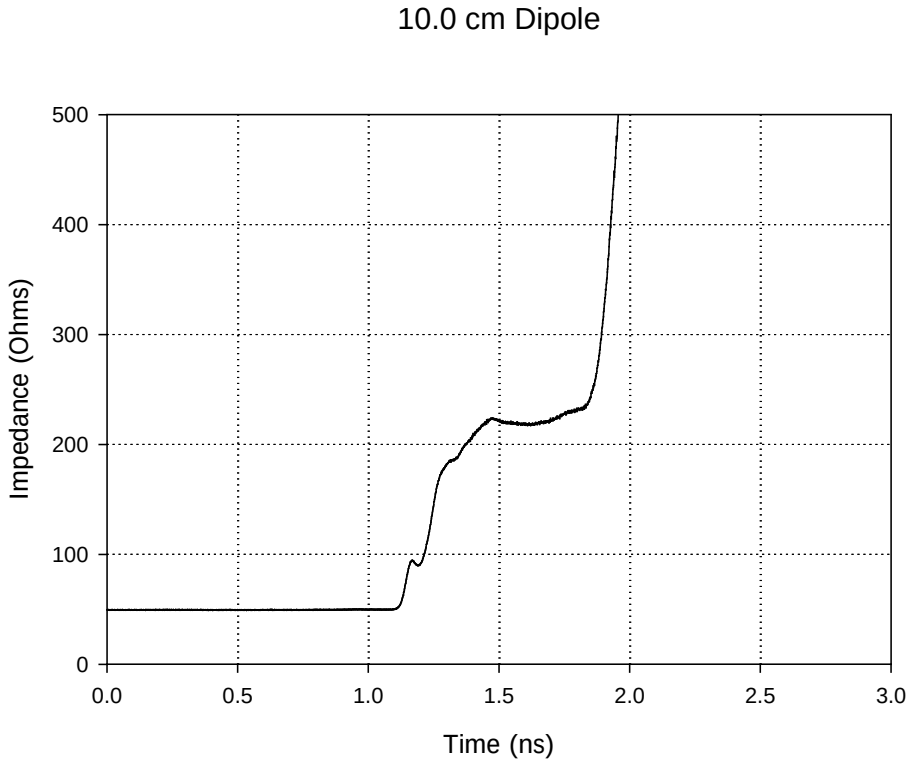

Figure 64. TDR measurement of the 10.0 cm dipole on the ground plane.

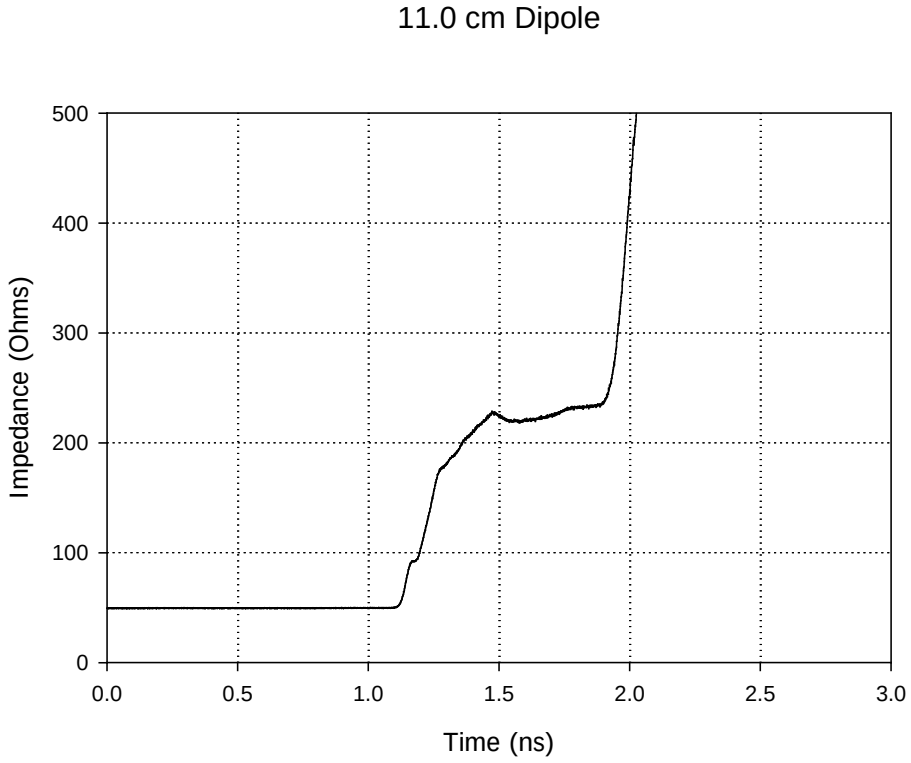

Figure 65. TDR measurement of the 11.0 cm dipole on the ground plane.

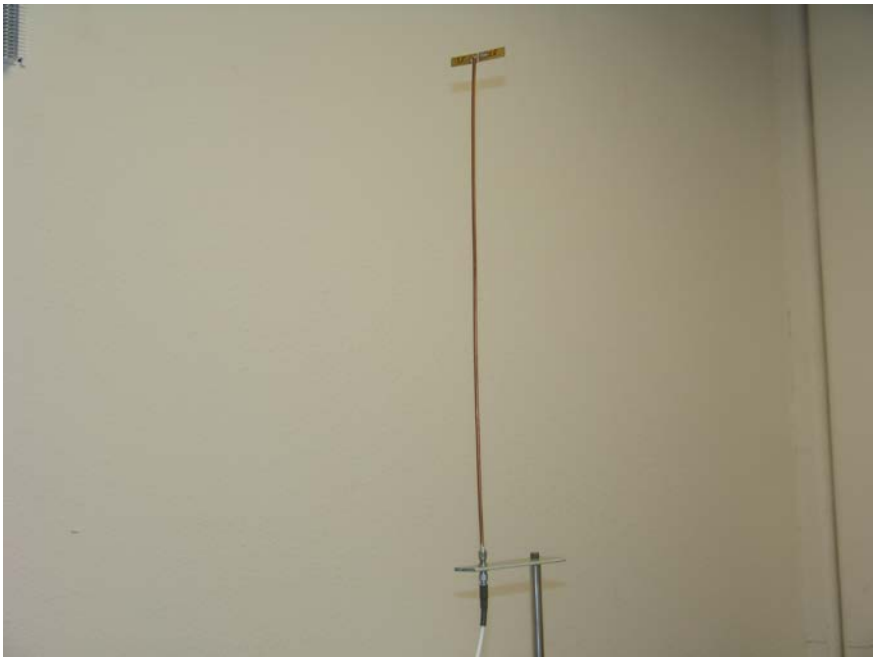

Figure 66. Photo of dipole test configuration in free space.

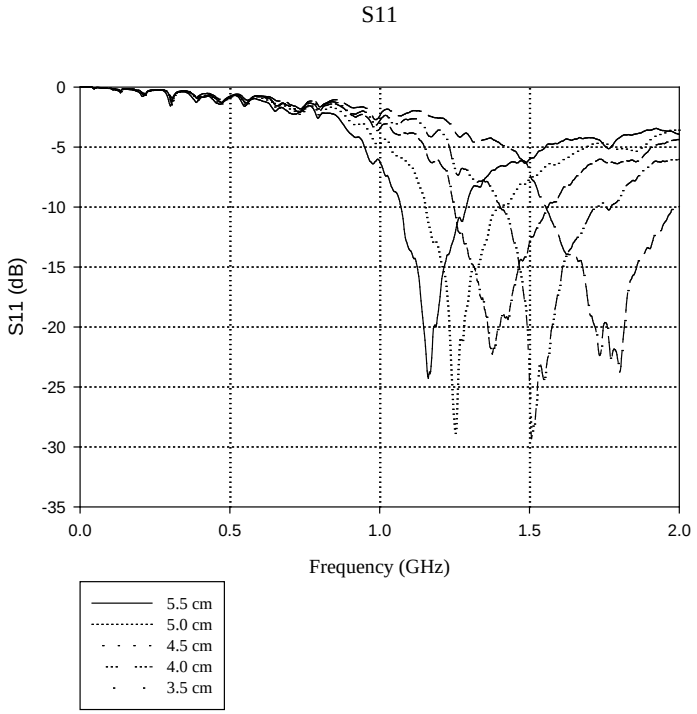

Figure 67. S11 measurements for the high frequency dipoles in free space.

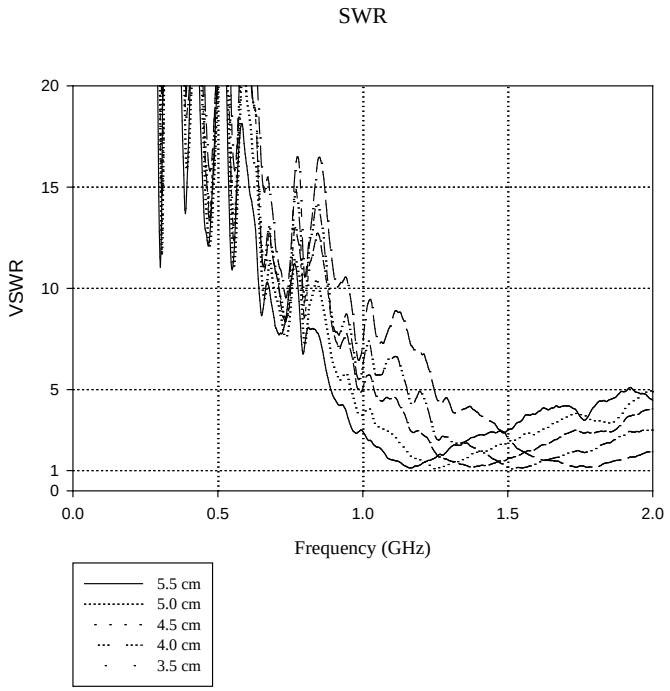

Figure 68. SWR measurement (calculated from S11) for the high frequency dipoles in free space.

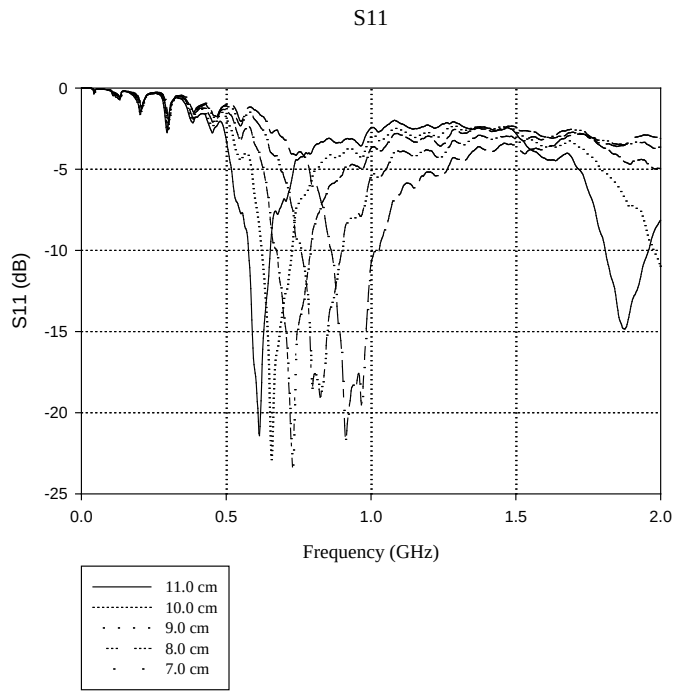

Figure 69. S11 measurements for the low frequency dipoles in free space.

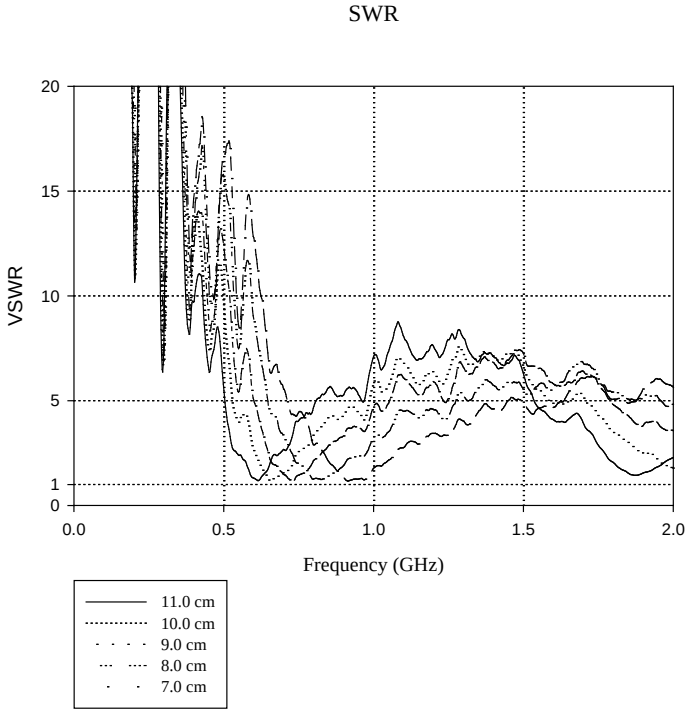

Figure 70. SWR measurement (calculated from S11) for the low frequency dipoles in free space.

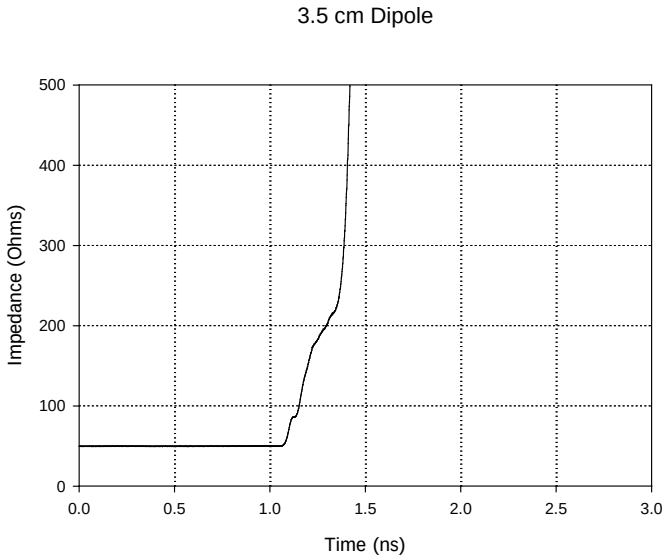

Figure 71. TDR measurement of the 3.5 cm dipole in free space.

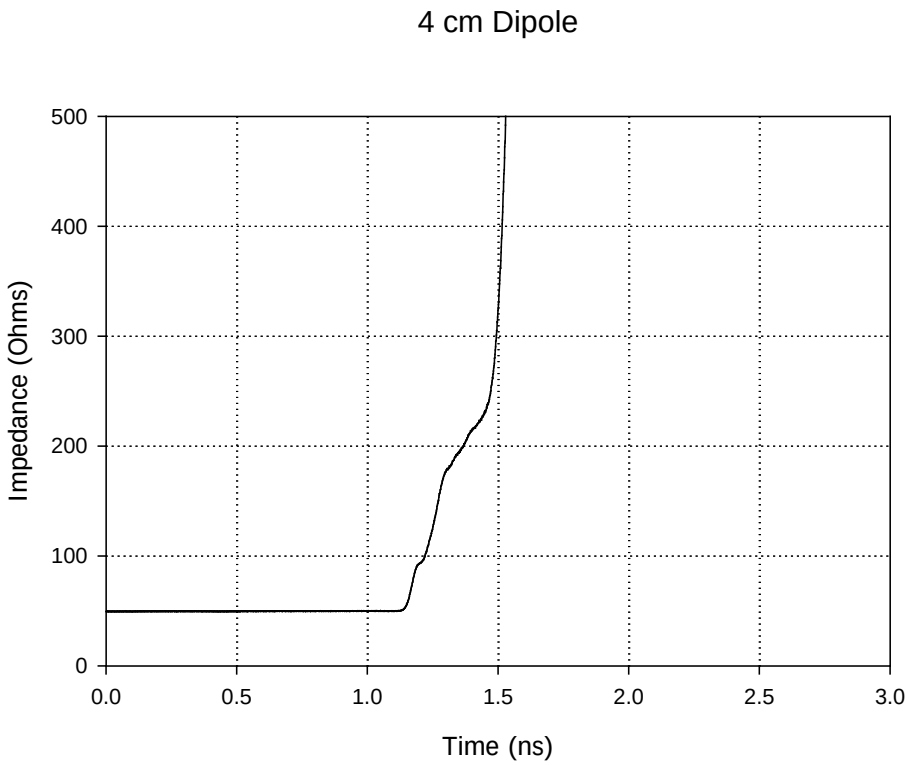

Figure 72. TDR measurement of the 4.0 cm dipole in free space.

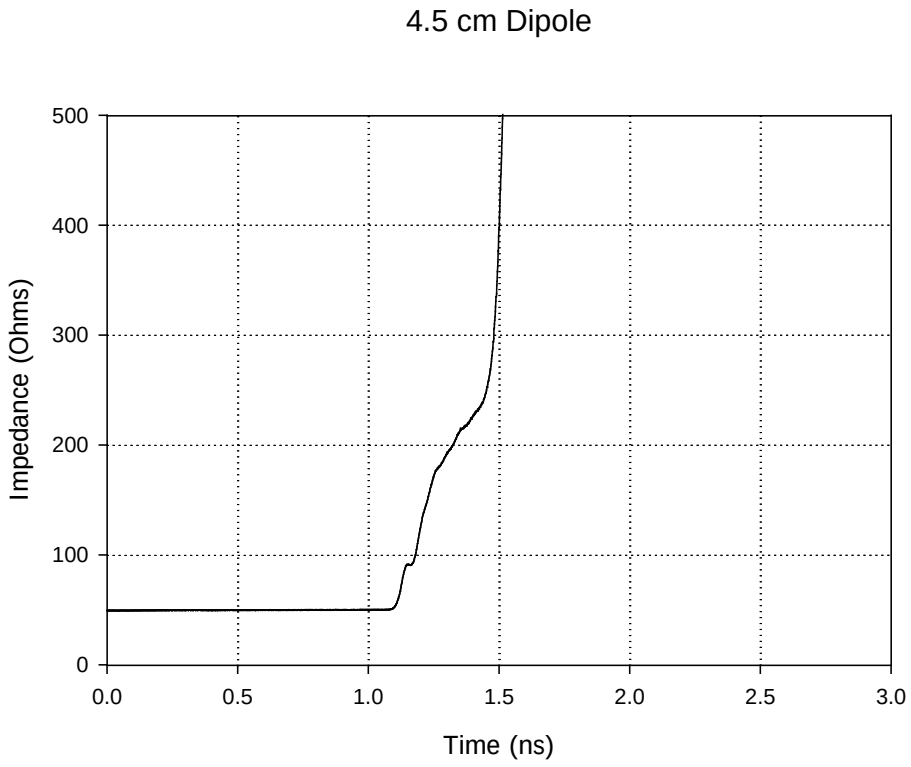

Figure 73. TDR measurement of the 4.5 cm dipole in free space.

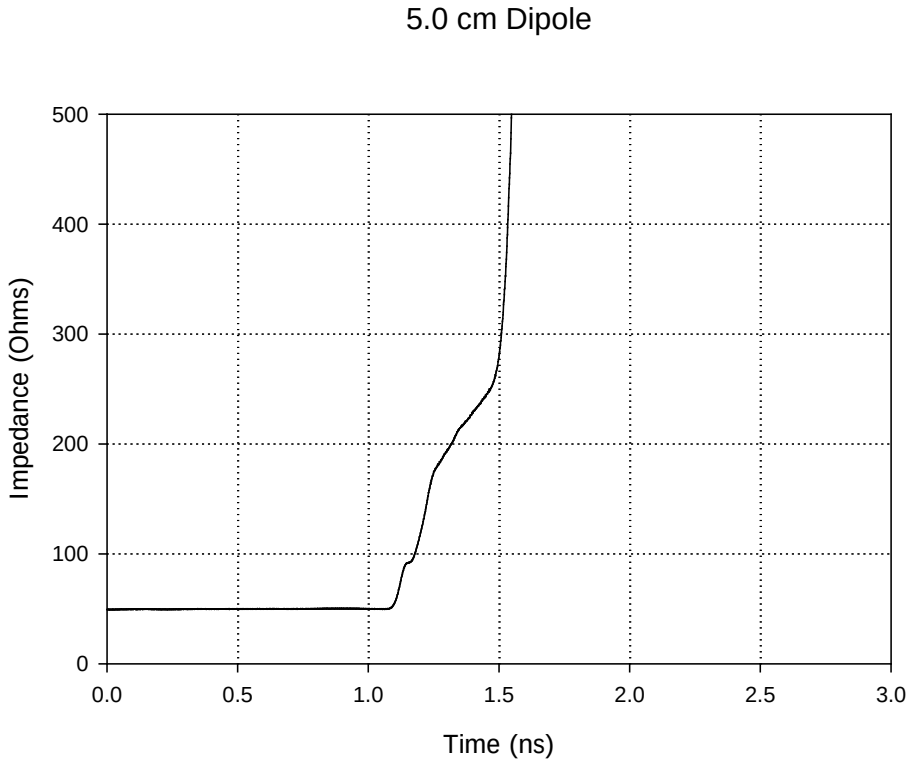

Figure 74. TDR measurement of the 5.0 cm dipole in free space.

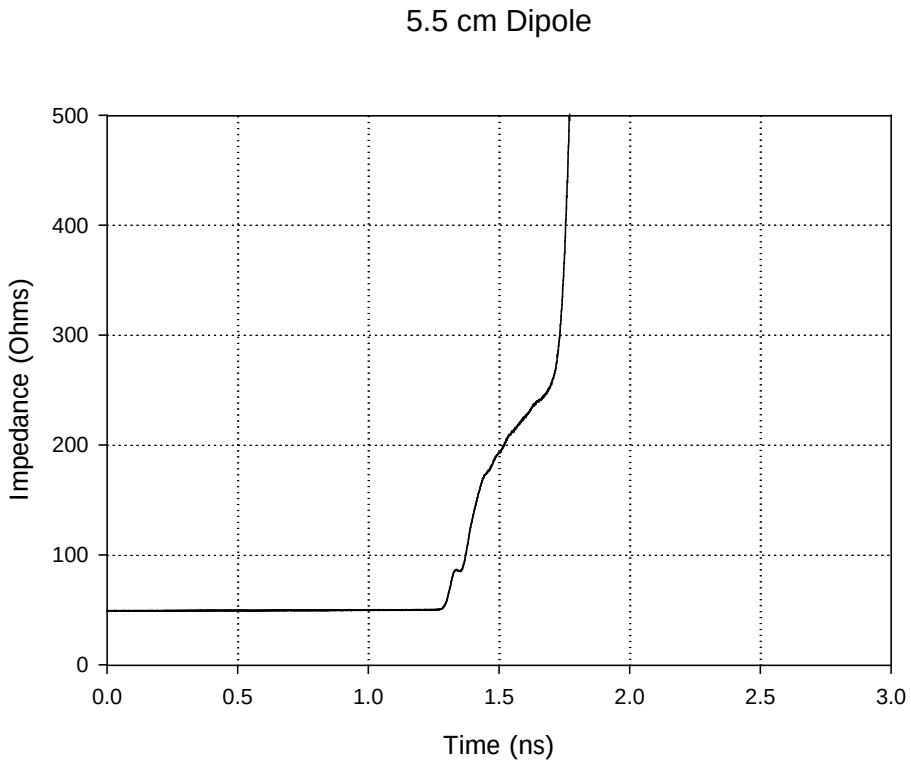

Figure 75. TDR measurement of the 5.5 cm dipole in free space.

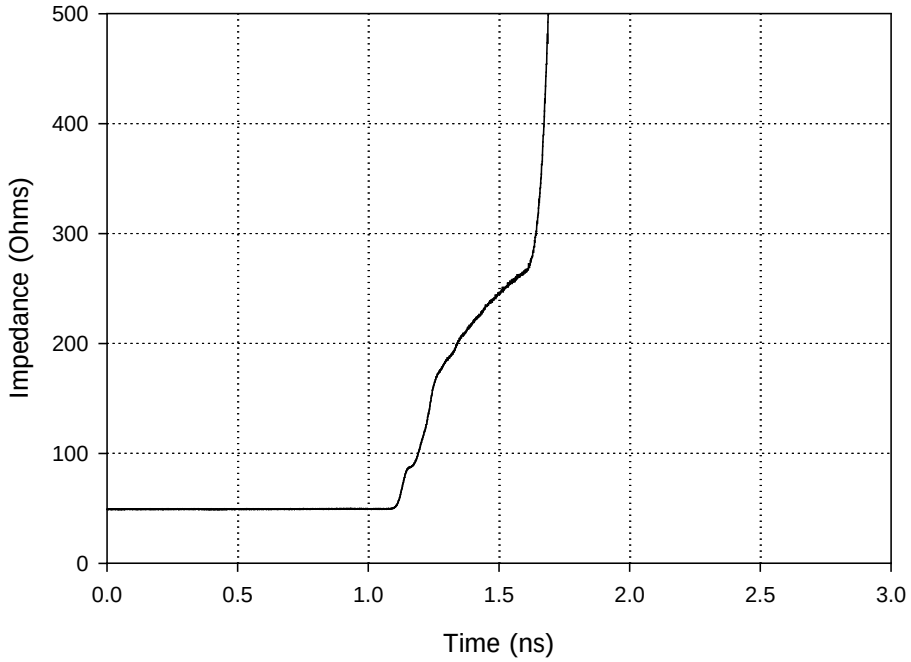

Figure 76. TDR measurement of the 7.0 cm dipole in free space.

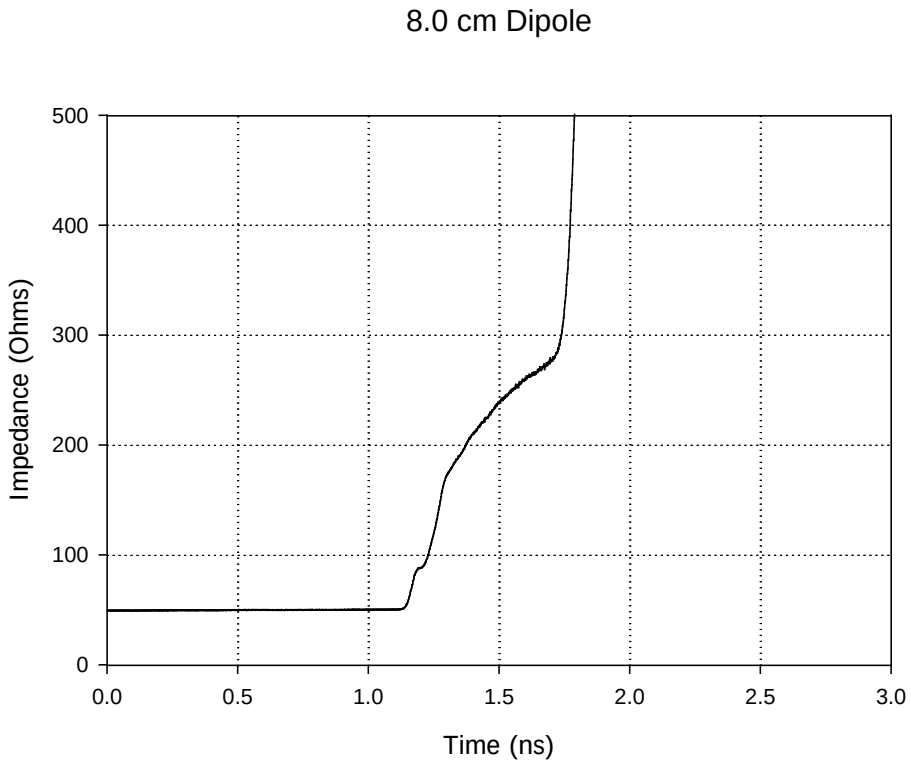

Figure 77. TDR measurement of the 8.0 cm dipole in free space.

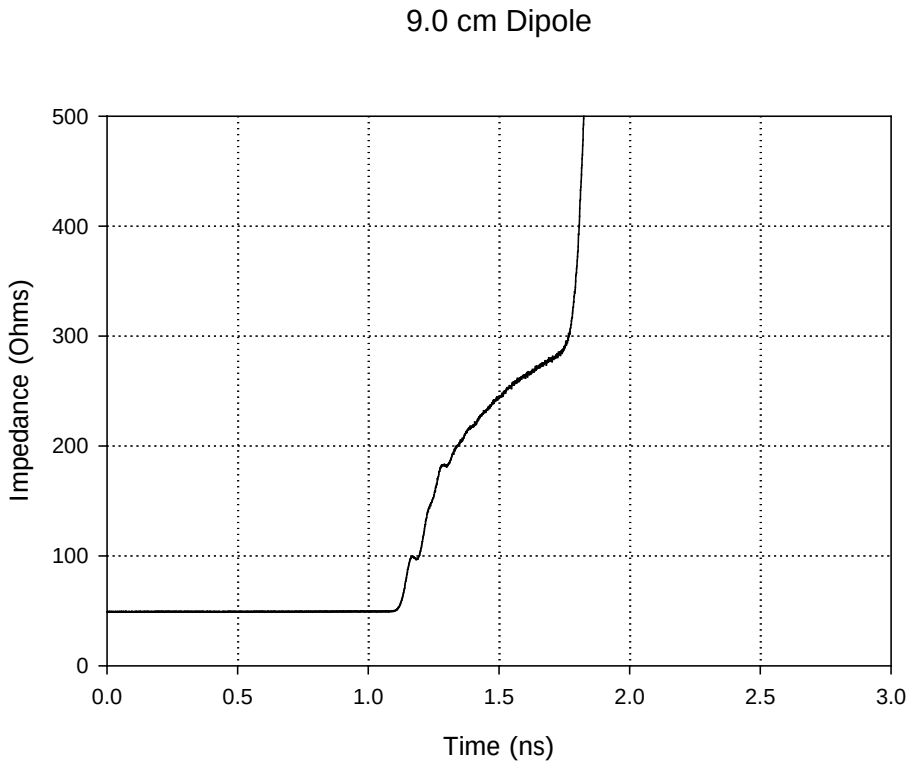

Figure 78. TDR measurement of the 9.0 cm dipole in free space.

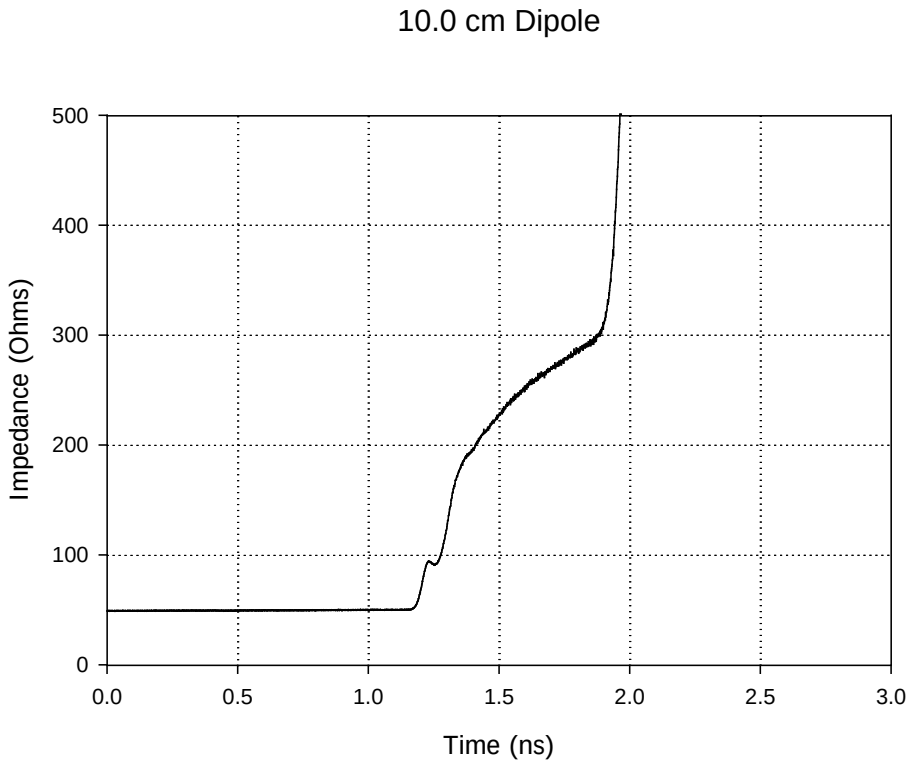

Figure 79. TDR measurement of the 10.0 cm dipole in free space.

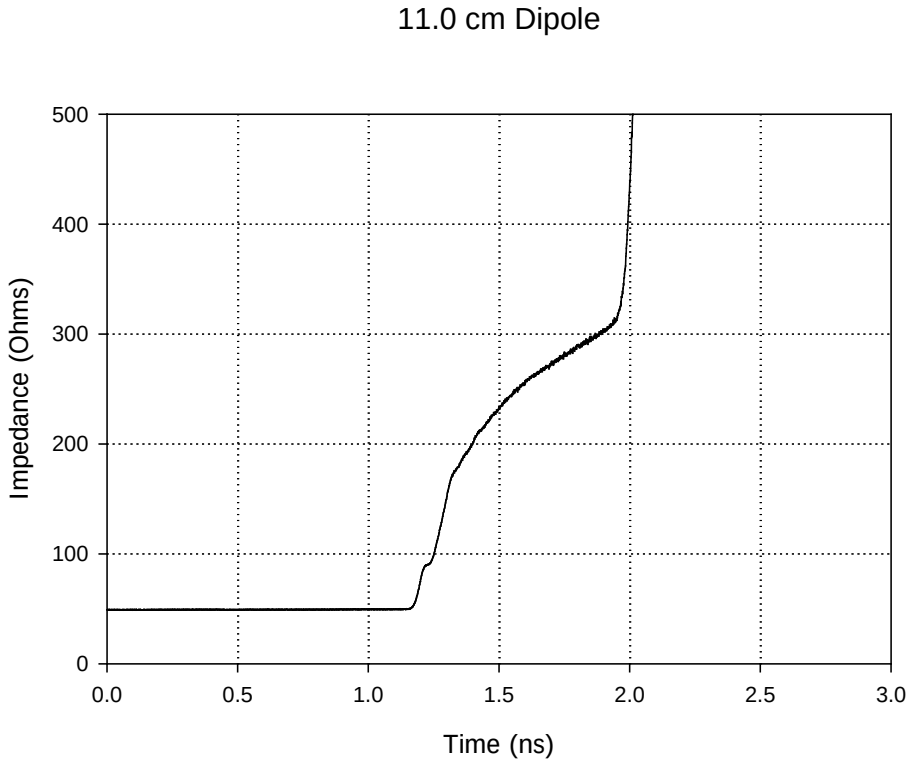

Figure 80. TDR measurement of the 11.0 cm dipole in free space.

5.3 Experimental Data on the Conformal Array on a Nylon Substrate

S11, the SWR, and the TDR measurements are performed on the prototype conformal array for the three different configurations. The first configuration is with the array on a non-conductive structure as is shown in Figure 81. These results are found in Figures 82 to 84. Measurements are then performed with the array sitting on the conductive ground plane (Figure 85) and reported in Figures 86-88. The conformal array is then placed on the EBG structure (Figure 89) and the measurements are to be found in Figures 90-92. All measurements are repeated with the wing extensions installed (Figure 93, Figure 97 and Figure 101) and the results reported respectively in Figures 94-96, Figures 98-100 and Figures 102- 104.

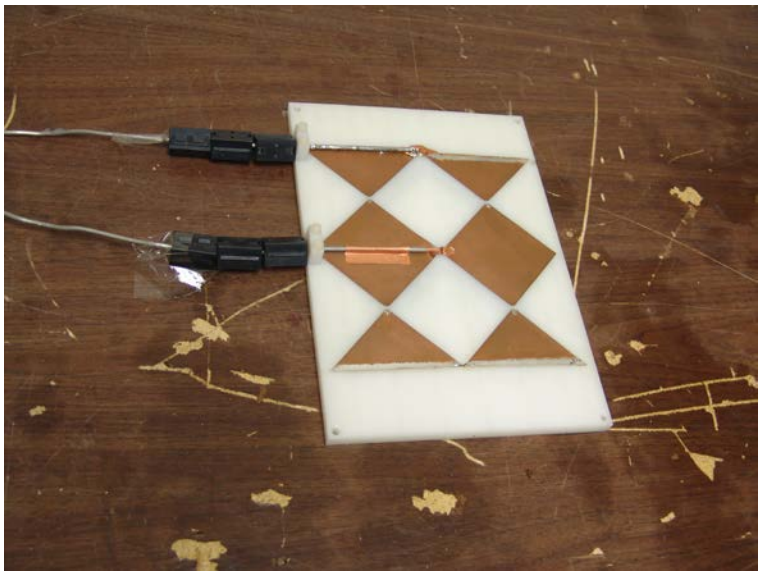

Figure 81. Photo of conformal antenna on non-conductive structure without wing extensions.

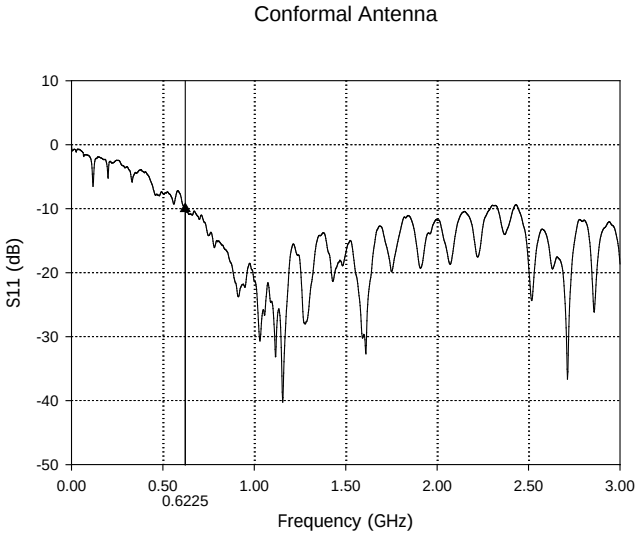

Figure 82. S11 measurement of conformal antenna placed on non-conductive structure.

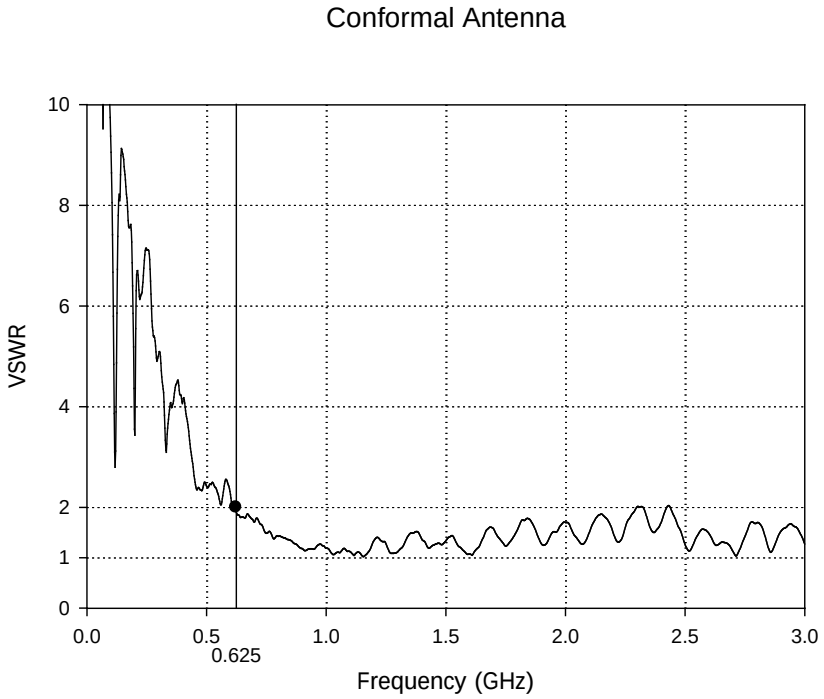

Figure 83. SWR measurement (calculated from S11) of conformal antenna placed on non-conductive structure.

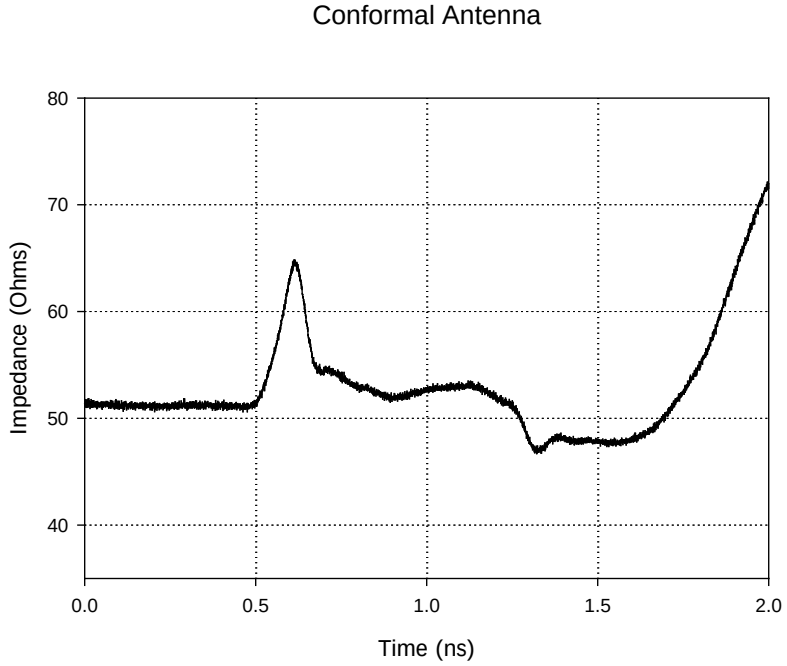

Figure 84. TDR measurement of conformal antenna placed on non-conductive structure.

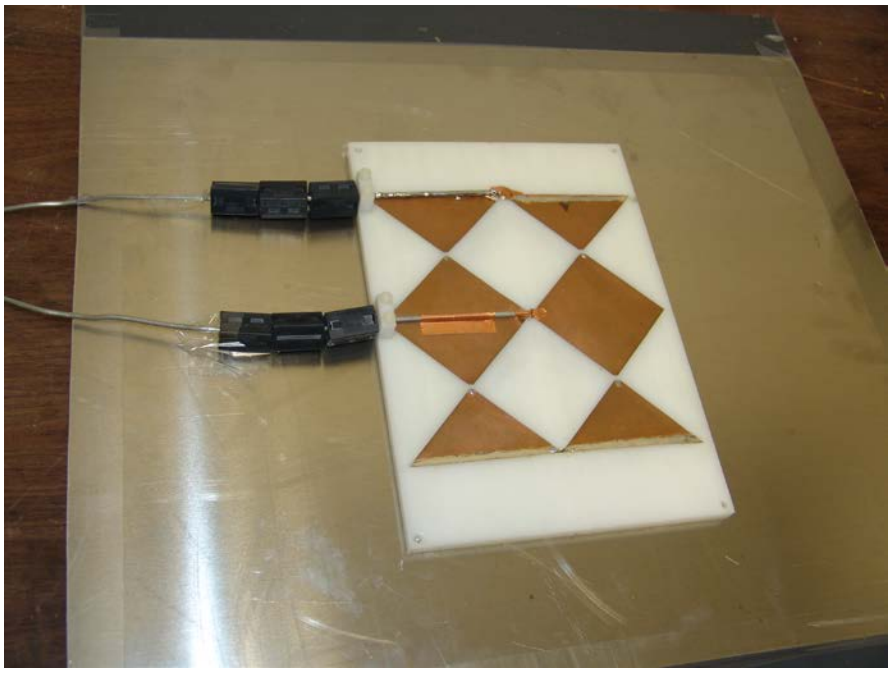

Figure 85. Photo of conformal antenna on conductive ground plane.

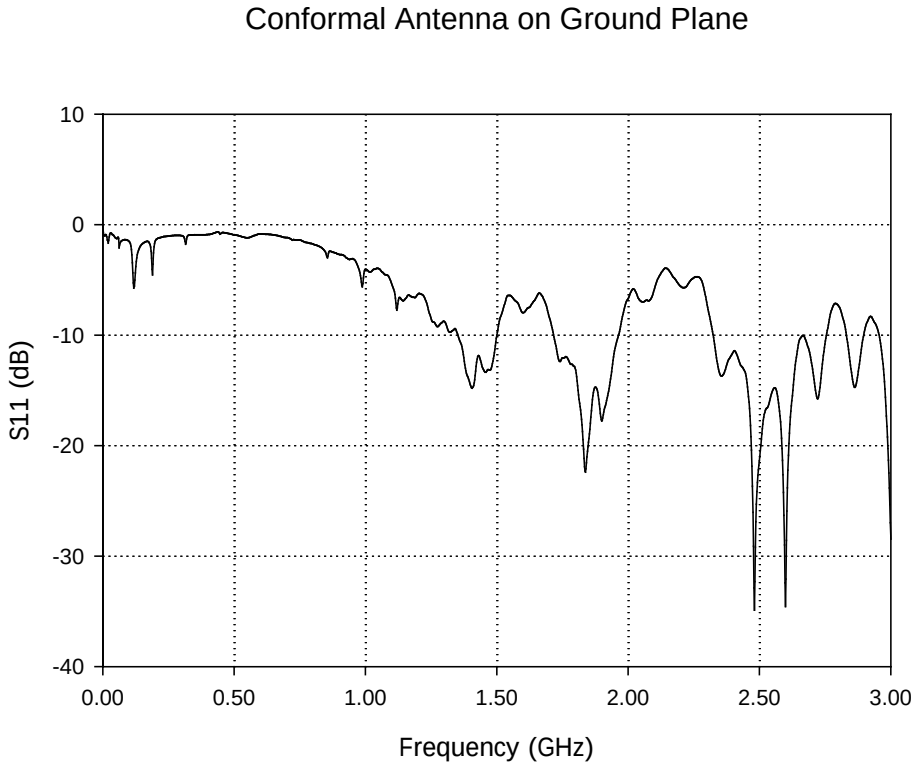

Figure 86. S11 measurement of conformal antenna placed on conductive ground plane.

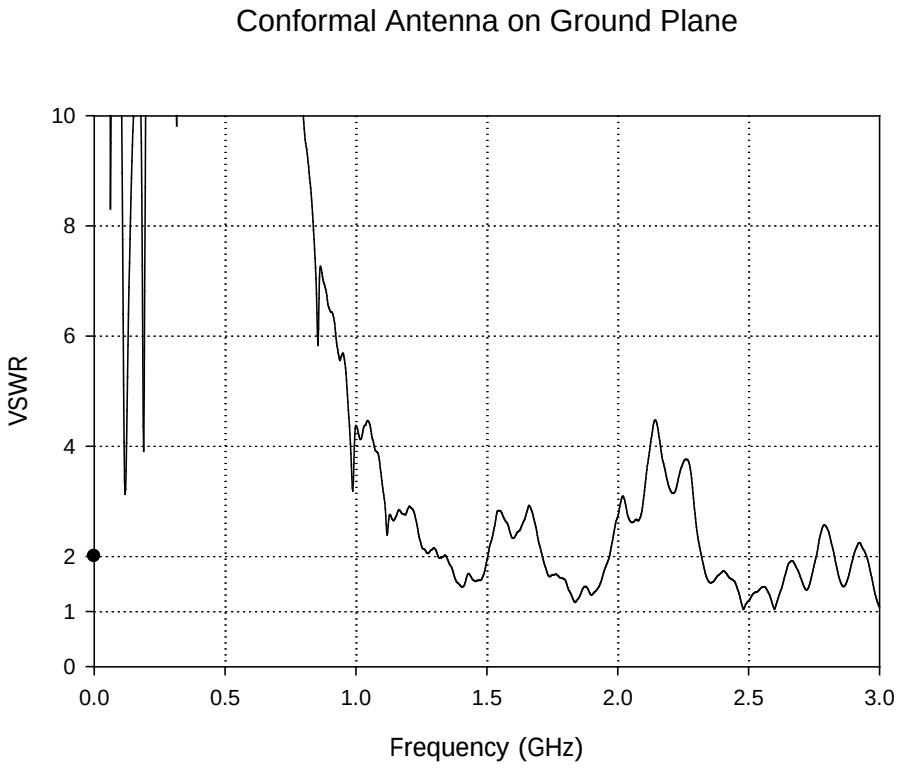

Figure 87. SWR measurement (calculated from S11) of conformal antenna placed on conductive ground plane.

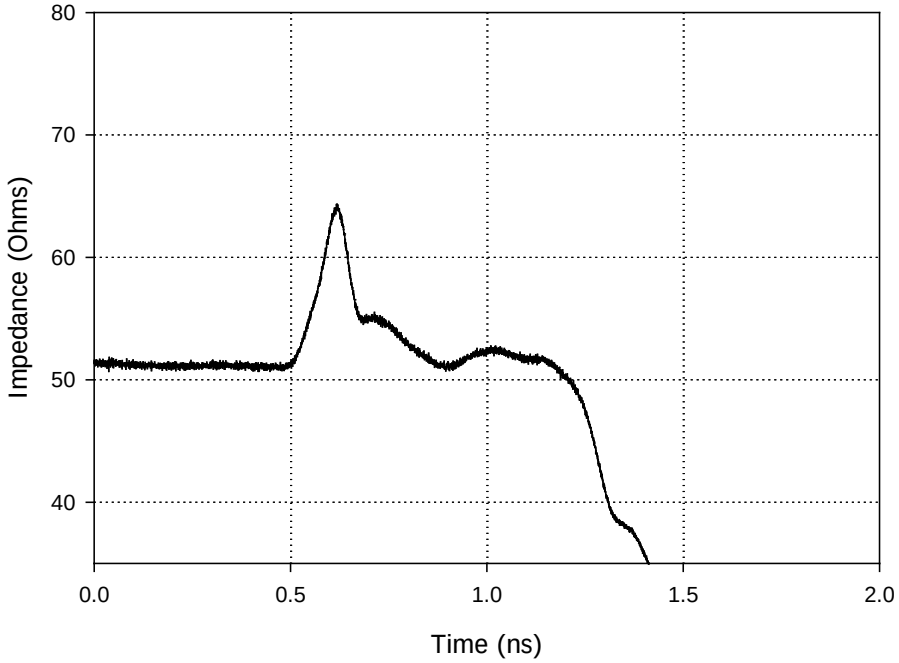

Figure 88. TDR measurement of conformal antenna placed on conductive ground plane.

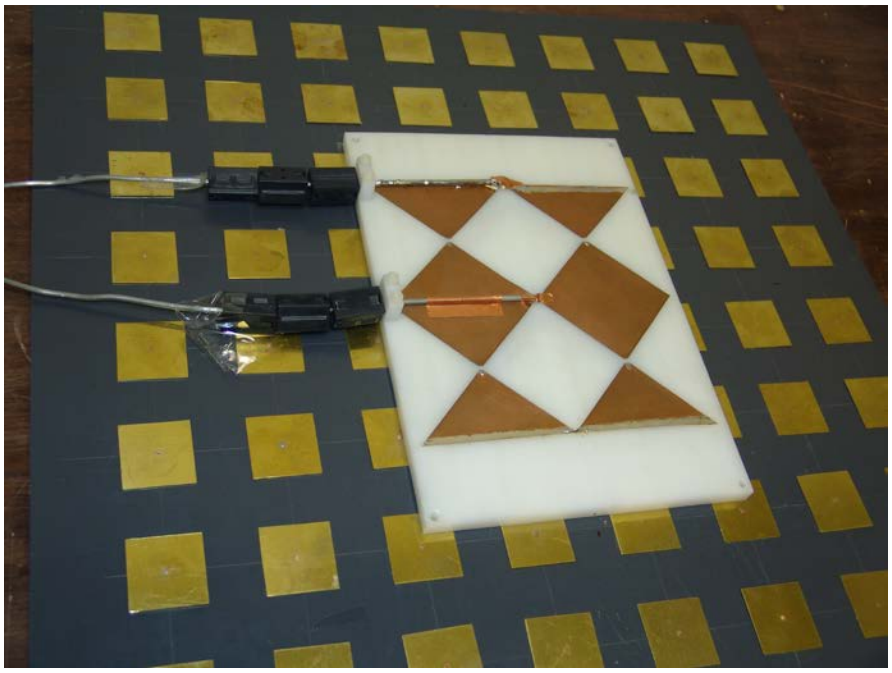

Figure 89. Photo of conformal antenna on EBG structure.

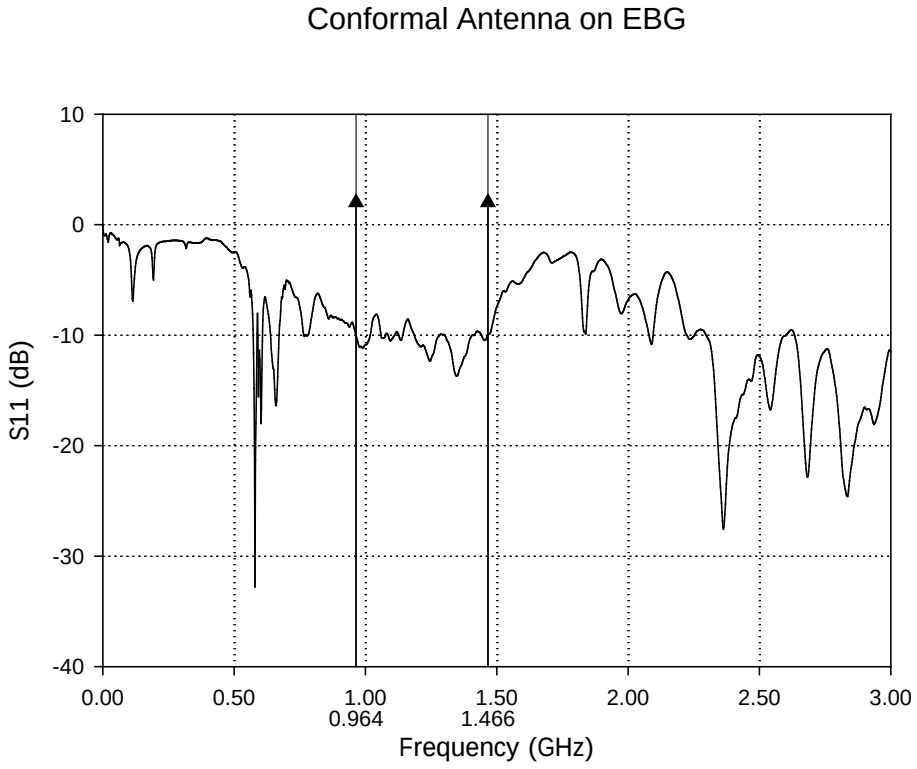

Figure 90. S11 measurement of conformal antenna placed on EBG structure.
The vertical bars show the limit frequencies where the S11 is (-10 dB) acceptable.

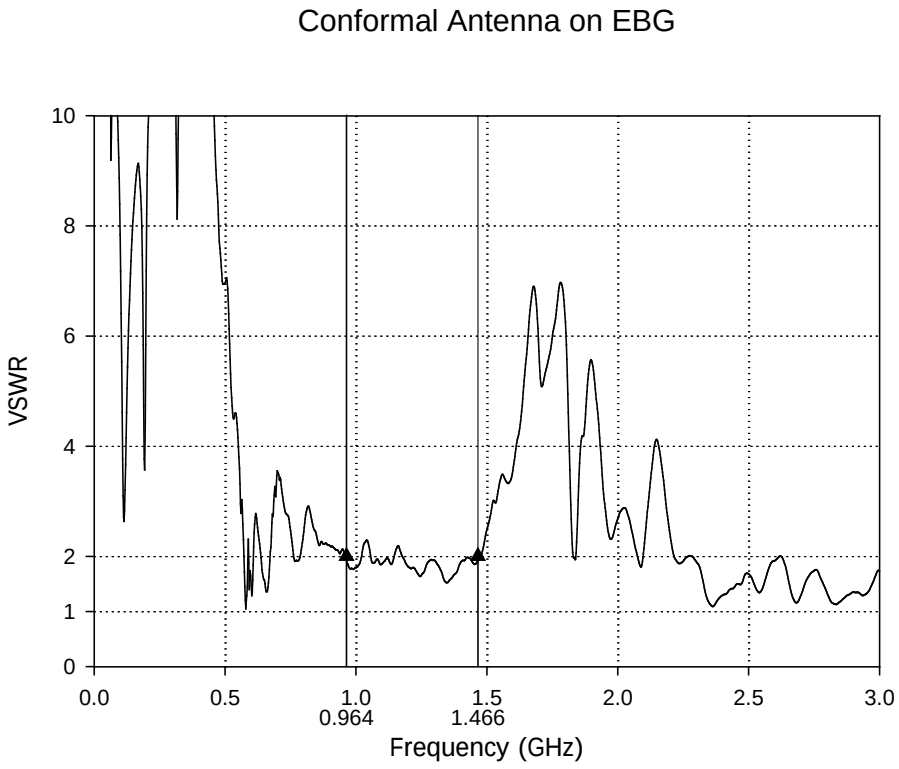

Figure 91. SWR measurement (calculated from S11) of conformal antenna placed on EBG structure.

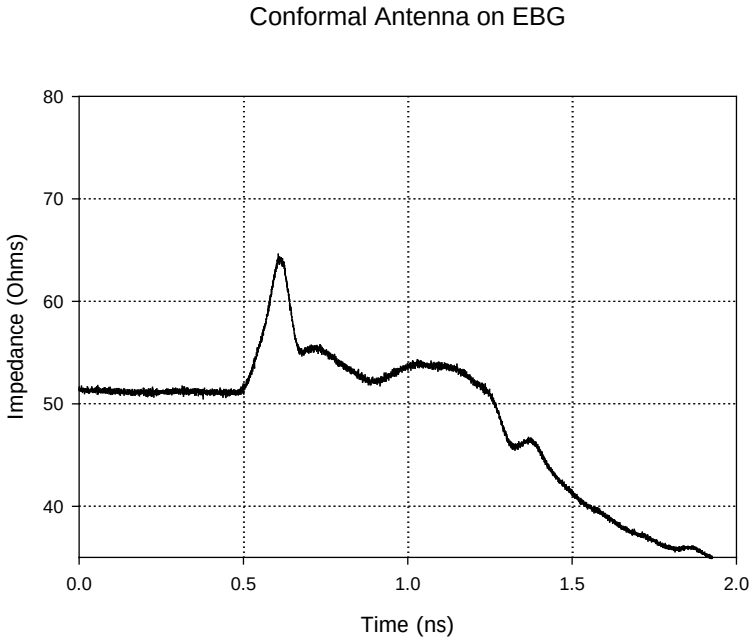

Figure 92. TDR measurement of conformal antenna placed on EBG structure.

Figure 93. Photo of conformal antenna with wing extension on non-conductive structure.

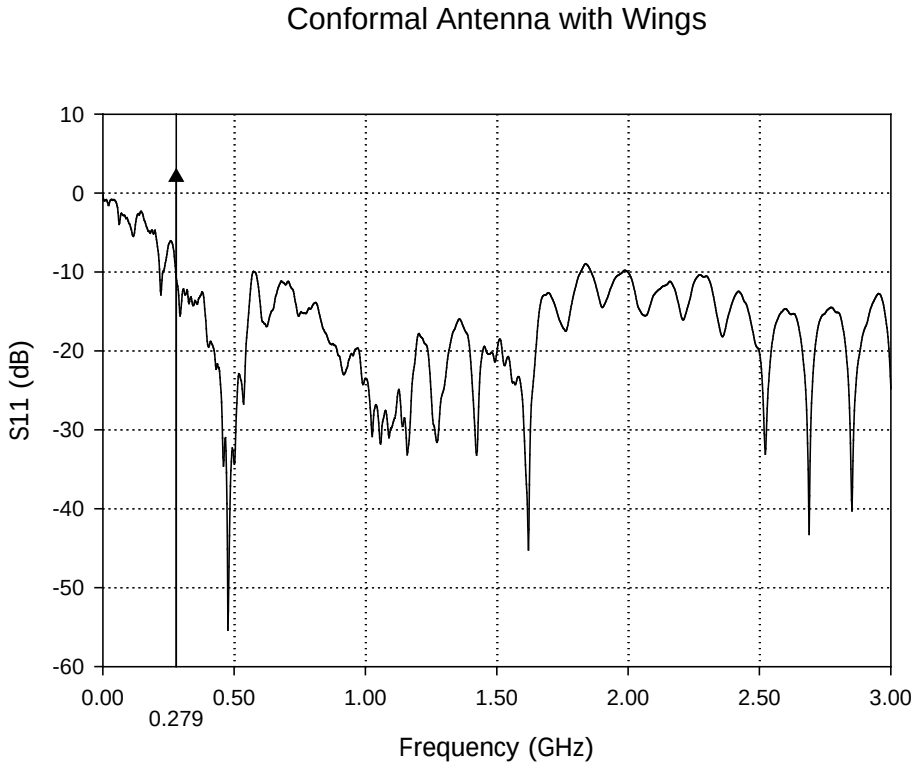

Figure 94. S11 measurement of conformal antenna with wing extensions placed on non-conductive structure.

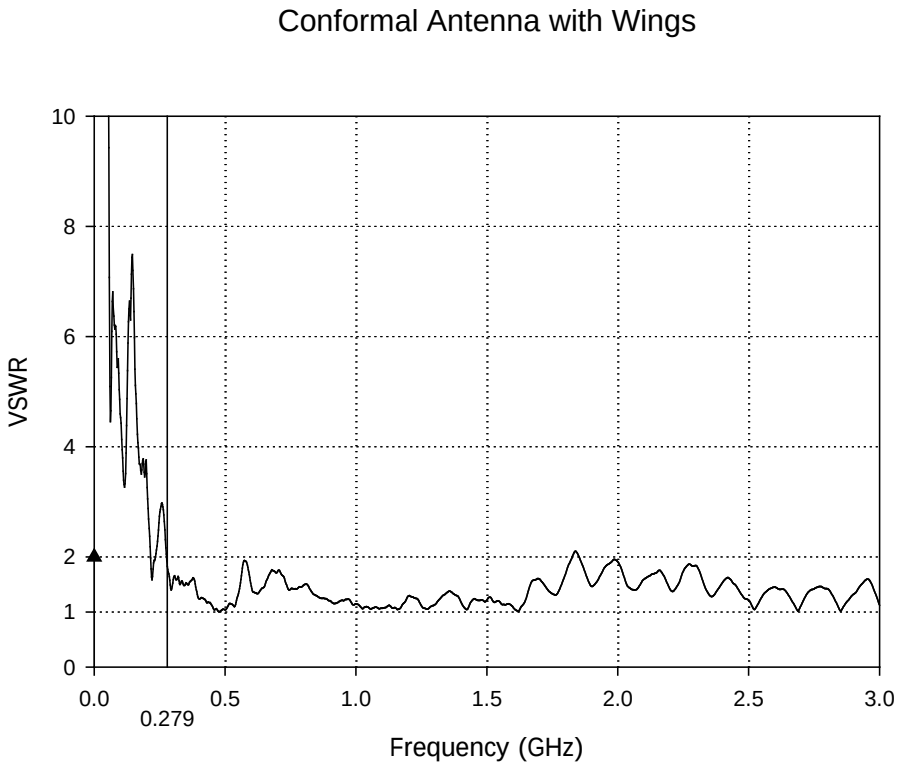

Figure 95. SWR measurement (calculated from S11) of conformal antenna with wing extensions placed on a non-conductive structure.

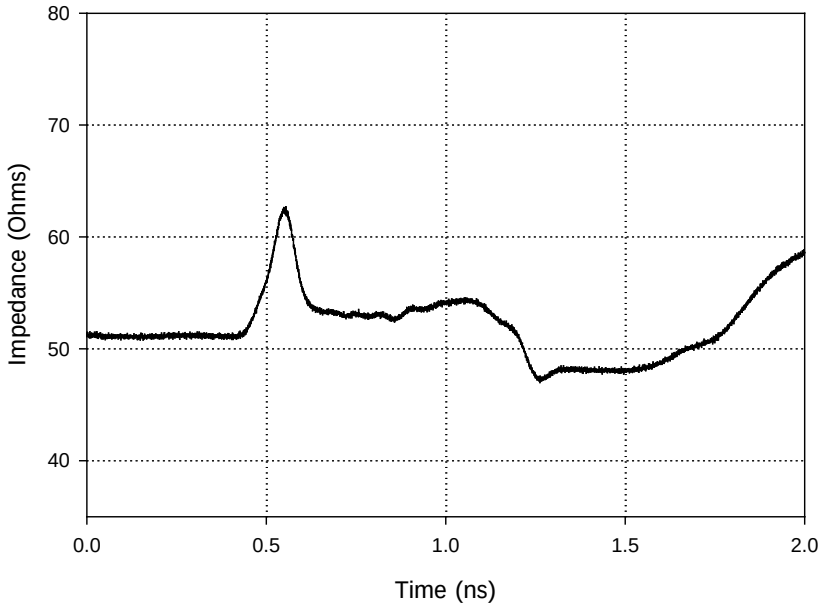

Figure 96. TDR measurement of conformal antenna with wing extensions placed on non-conductive structure.

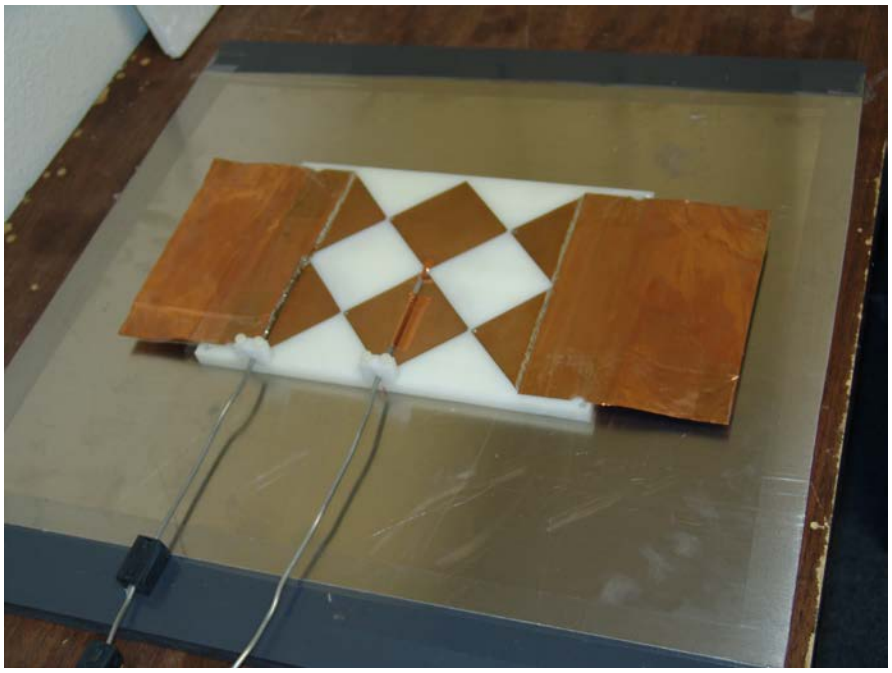

Figure 97. Photo of conformal antenna with wing extensions on ground plane structure.

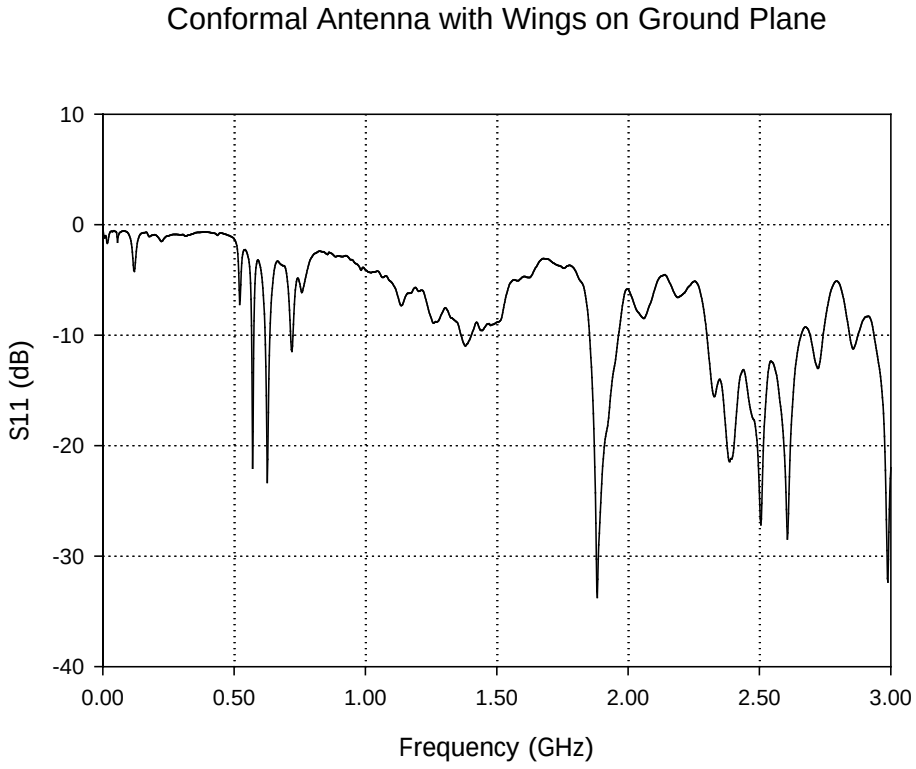

Figure 98. S11 measurement of conformal antenna with wing extensions placed on conductive ground plane.

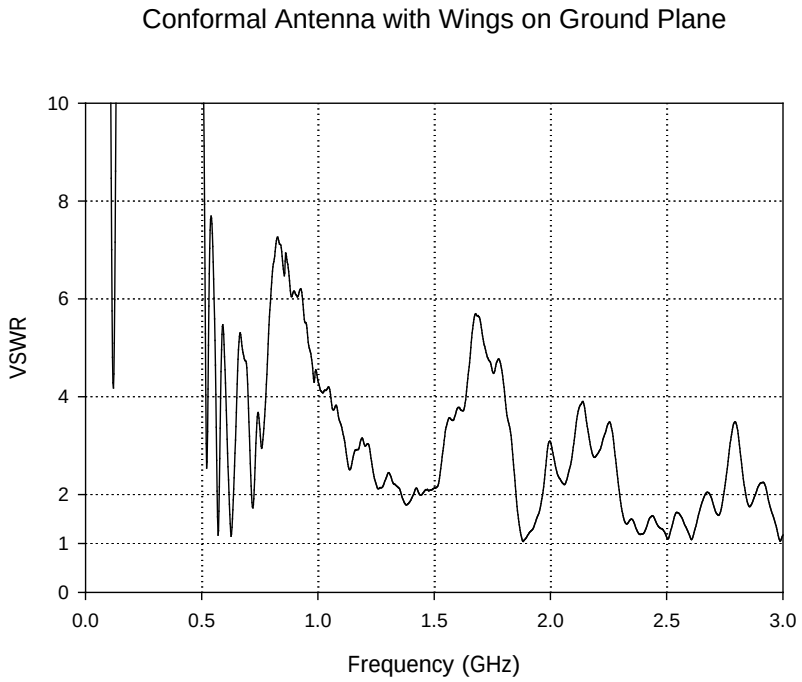

Figure 99. SWR measurement (calculated from S11) of conformal antenna with wing extensions placed on conductive ground plane.

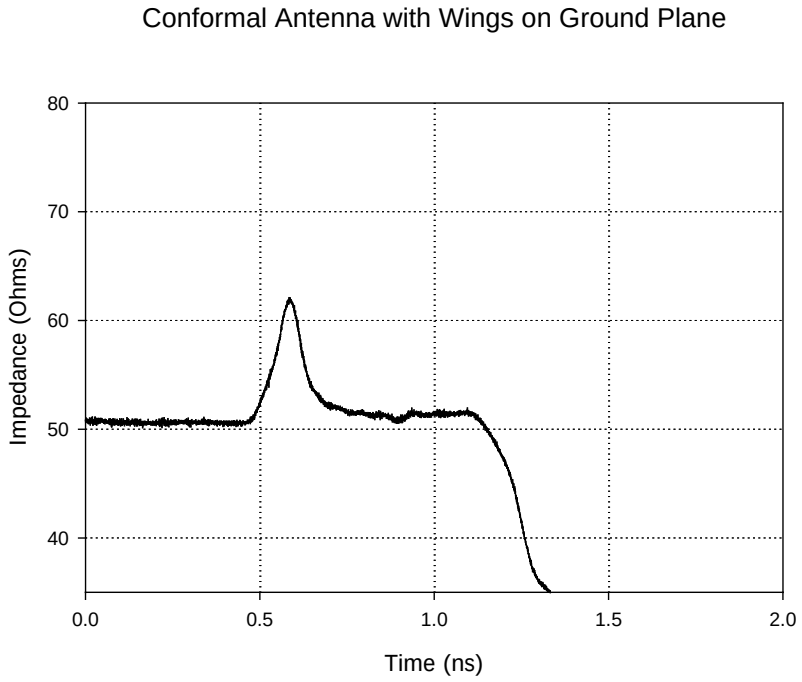

Figure 100. TDR measurement of conformal antenna with wing extensions placed on conductive ground plane.

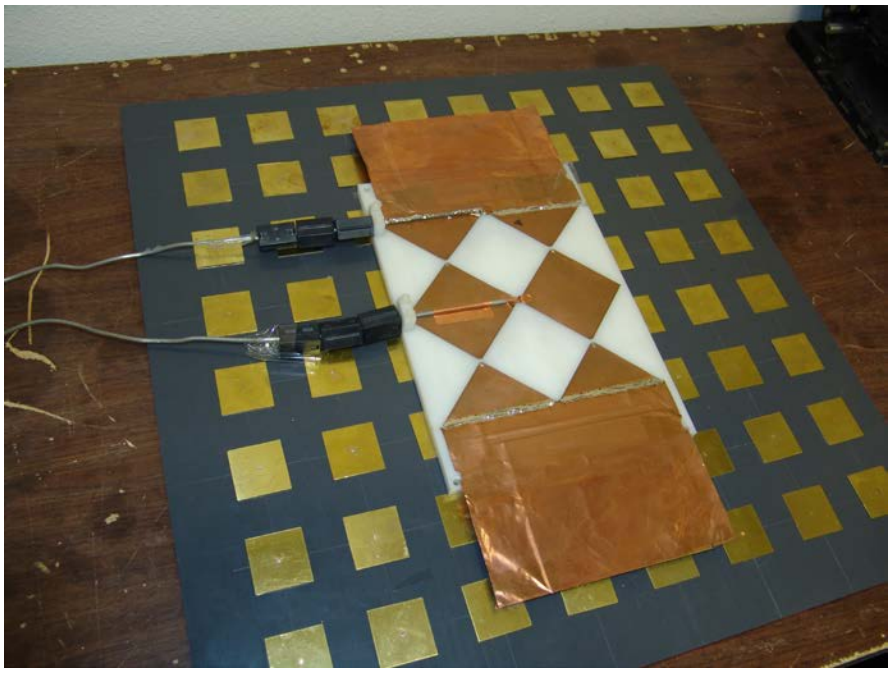

Figure 101. Photo of conformal antenna with wing extension on EBG structure.

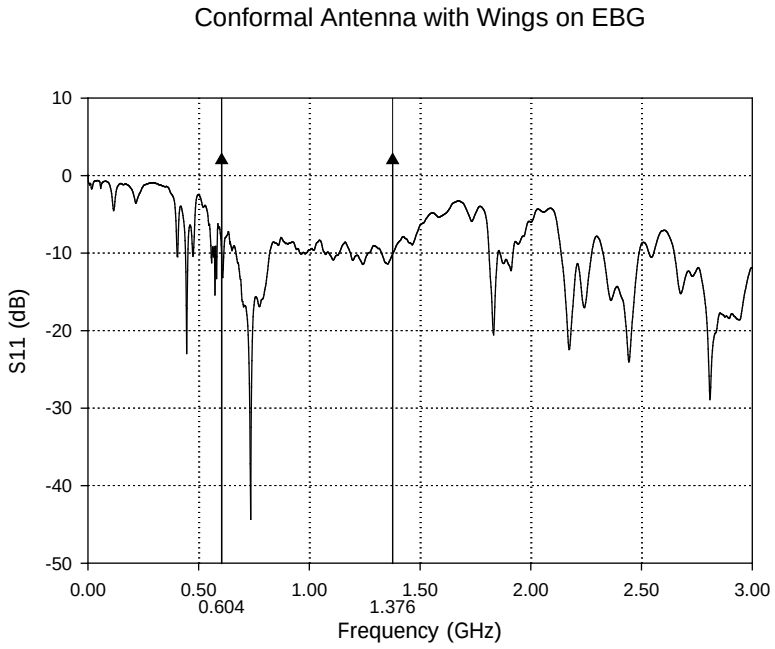

Figure 102. S11 measurement of conformal antenna with wing extensions placed on conductive on EBG structure.

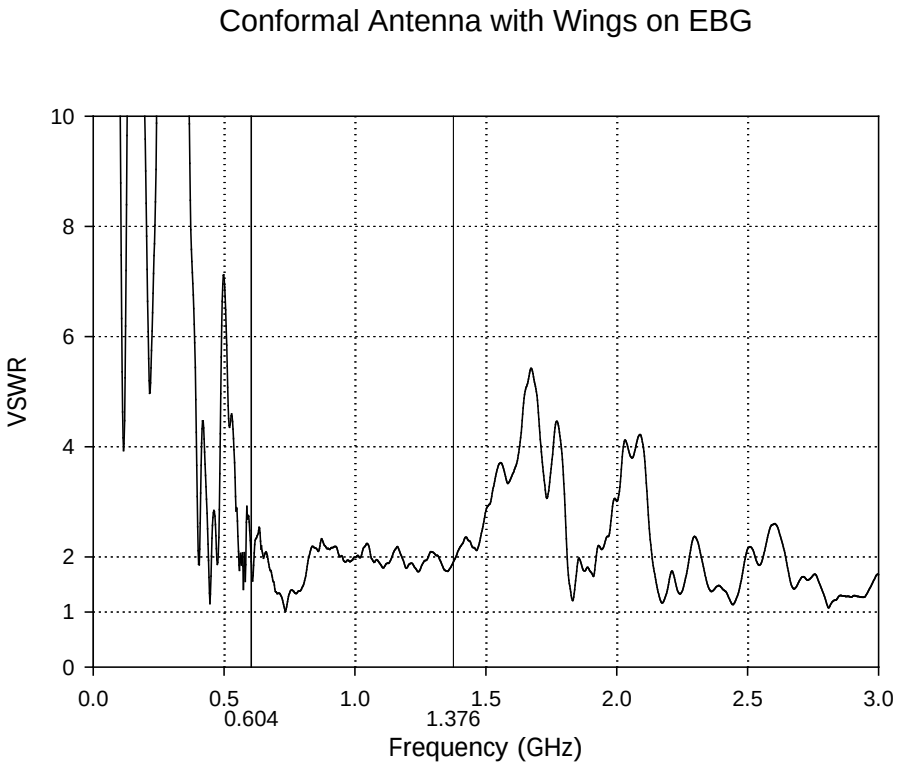

Figure 103. SWR measurement (calculated from S11) of conformal antenna with wing extensions placed on EBG structure.

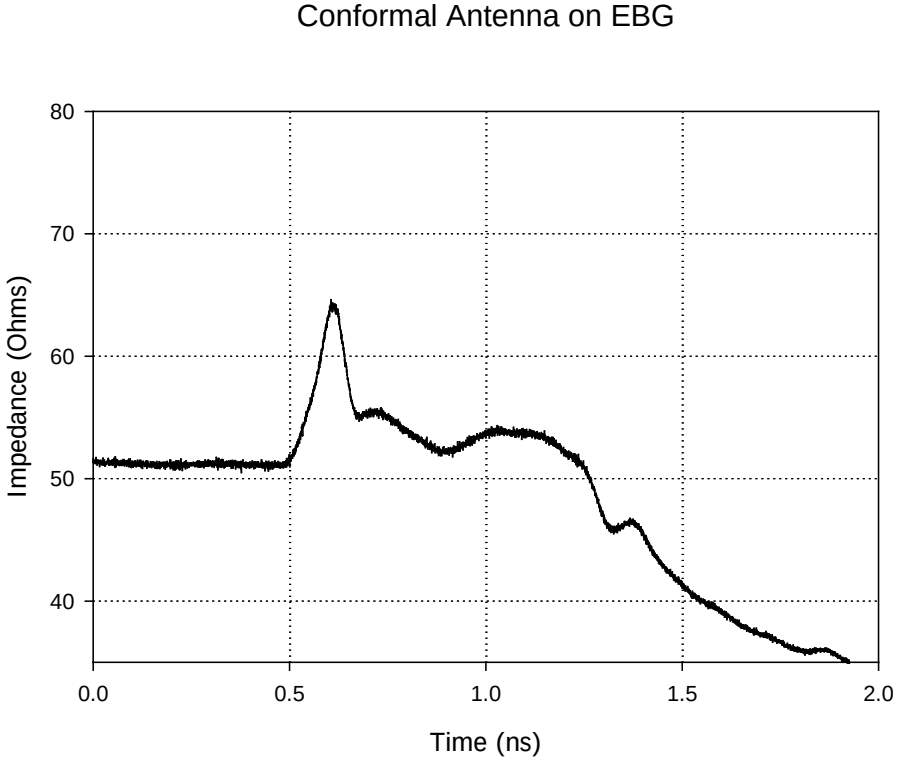

Figure 104. TDR measurement of conformal antenna with wing extensions placed on EBG structure.

5.4. Evaluation of an Updated Conformal Antenna

An updated version of the conformal array was fabricated using improved components to facilitate test of a conformal array on an actual piece of an aircraft skin. The prototype array was fabricated on a ***rigid structure*** that does not allow the antenna to be contoured to the surface shape. The updated conformal array is fabricated using ***flexible material*** allowing installation of the array on the skin.

The updated array was built using the dimensions of the prototype array and the wings were included as a non-removable element since it was determined that a significant performance enhancement is realized with the wings. The new antenna is fabricated using two sheets of 3.2 mm thick RT/duroid 5870 manufactured by Rogers Corporation for high frequency applications. The relative dielectric constant for the material is 2.33. The 2 x 2 array is placed on one sheet and the 200 ohm transmission lines feeding each element are formed on the back side of the duroid sheet using 0.74 mm diameter wire. A photo of the transmission lines is shown in Figure 105. The diameter of the wire was chosen to achieve the 200 ohm impedance with the duroid material. The second sheet of duroid is placed on the back side to isolate the 200 ohm lines from the aircraft skin. This locates the updated conformal 6.35 mm from the surface of the skin. A photo of the updated array is shown in Figure 106.

S11, the SWR, and the TDR measurements are performed on the updated conformal array for several different configurations. The first configuration is with the updated array on a non-conductive structure as is shown in Figure 106. The measurements are shown in Figures 107, 108 and 109.The measurements are then performed with the array sitting on the conductive ground plane (see Figure 110). The measurements for the conductive ground plane are shown in Figures 111-113. The updated conformal array is then placed on the EBG structure (Figure 114). The measurements of the updated conformal array on the EBG structure are presented in Figures 115-117.

The updated conformal antenna is then installed on the curved aircraft skin supplied by Northrop Grumman Corporation. This skin surface is slightly curved. The measurements are repeated to evaluate the effect of the skin on the performance of the array. The updated conformal antenna installed on the skin is shown in Figure 118 and the measurements are shown in Figures 119 to 121. The final measurements are performed with a metal surface under the skin and with the EBG structure under the skin. It must be noted that for these final measurements, it is not

possible due to the skin curvature for the metal surface and the EBG structure to be conformed to the back of the aircraft skin. This problem was overcome by foiling the back of the aircraft skin. The measurements are shown in Figures 122 to 129.

Figure 105. Photo of the 200 ohm transmission lines on the back side of the duroid material.

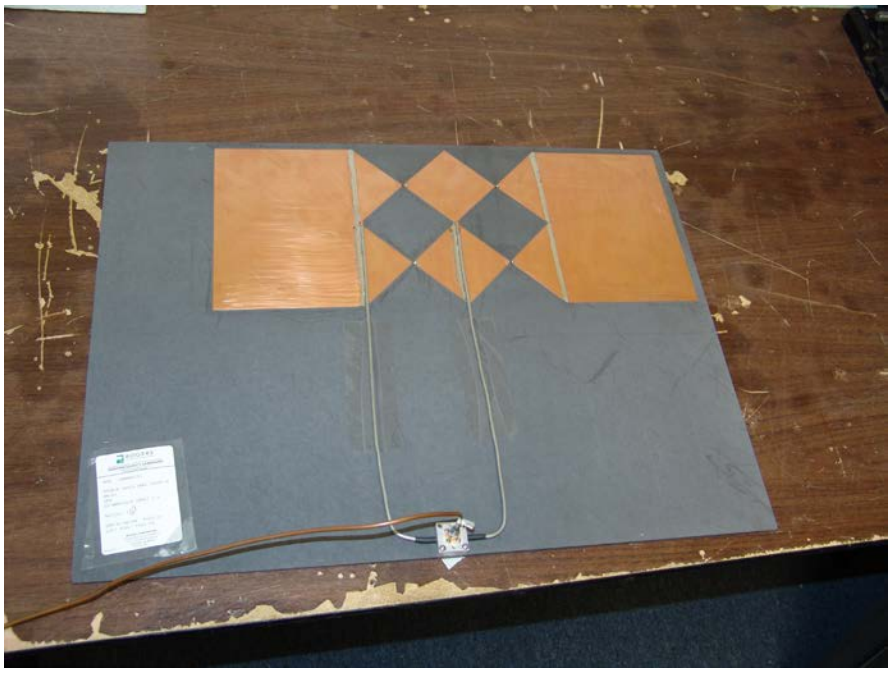

Figure 106. Photo of the updated conformal antenna.

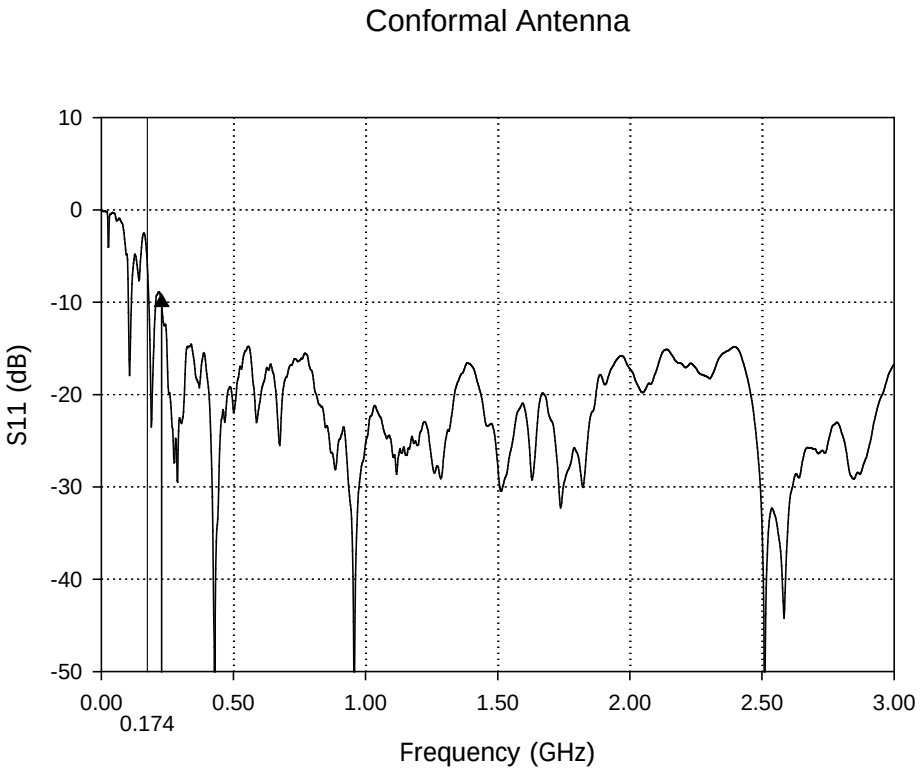

Figure 107. S11 measurement of updated conformal antenna placed on non-conductive structure.

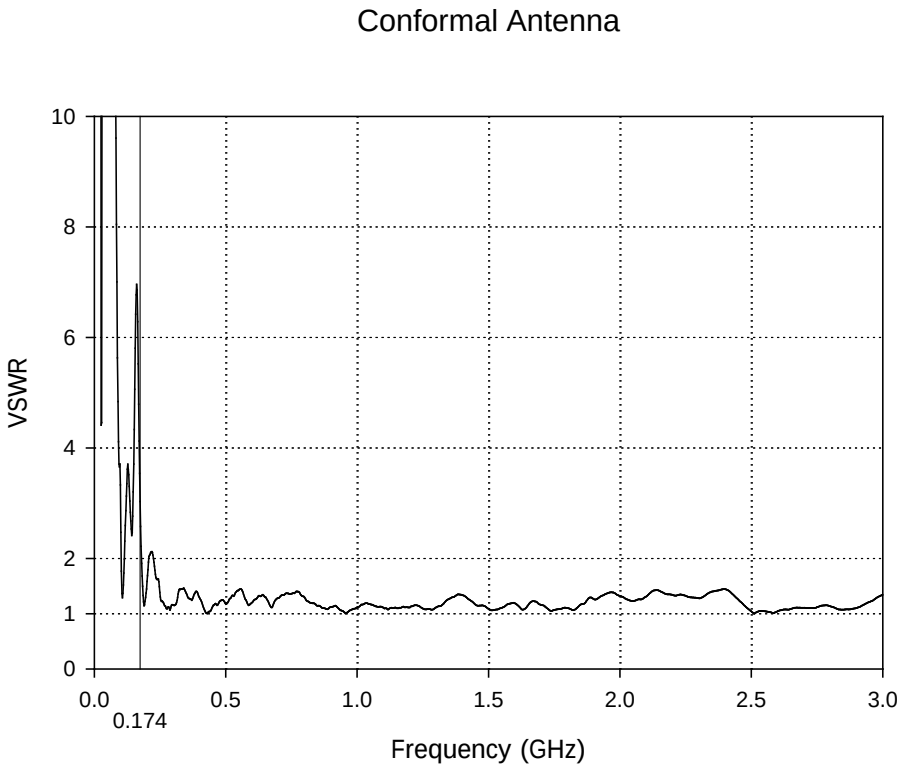

Figure 108. SWR measurement (calculated from S11) of updated conformal antenna placed on a non-conductive structure.

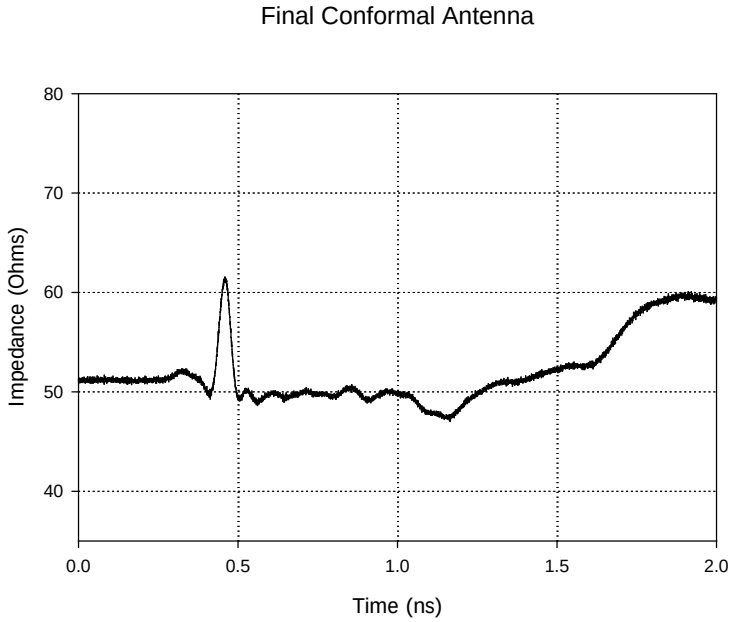

Figure 109. TDR measurement of updated conformal antenna placed on non-conductive structure.

Figure 110. Photo of updated conformal antenna on the conductive ground plane.

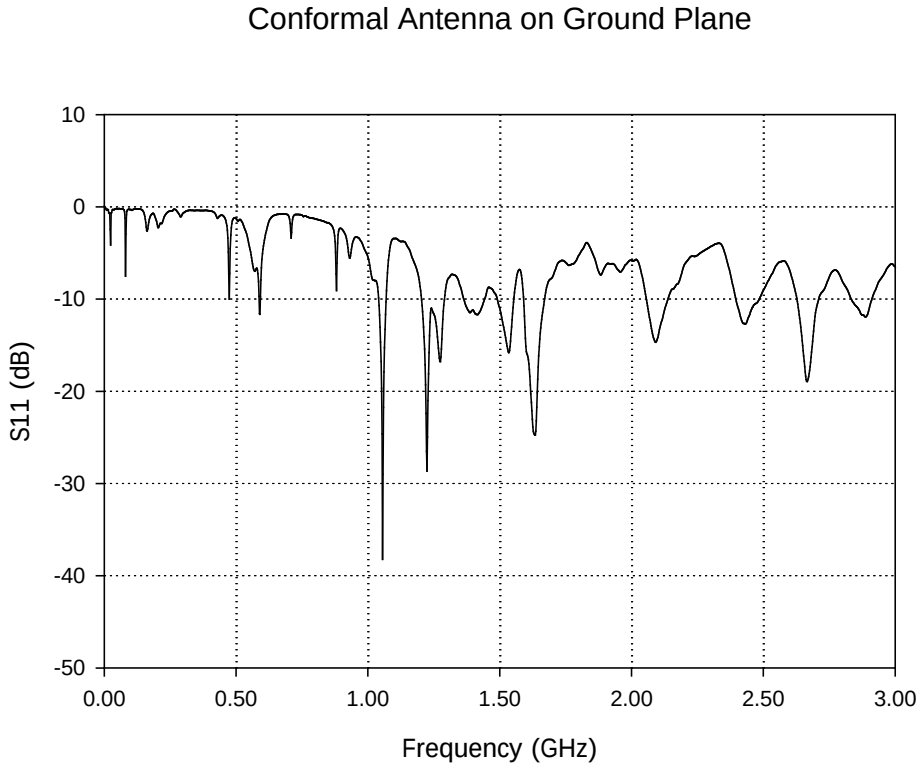

Figure 111. S11 measurement of updated conformal antenna placed on a conductive ground plane.

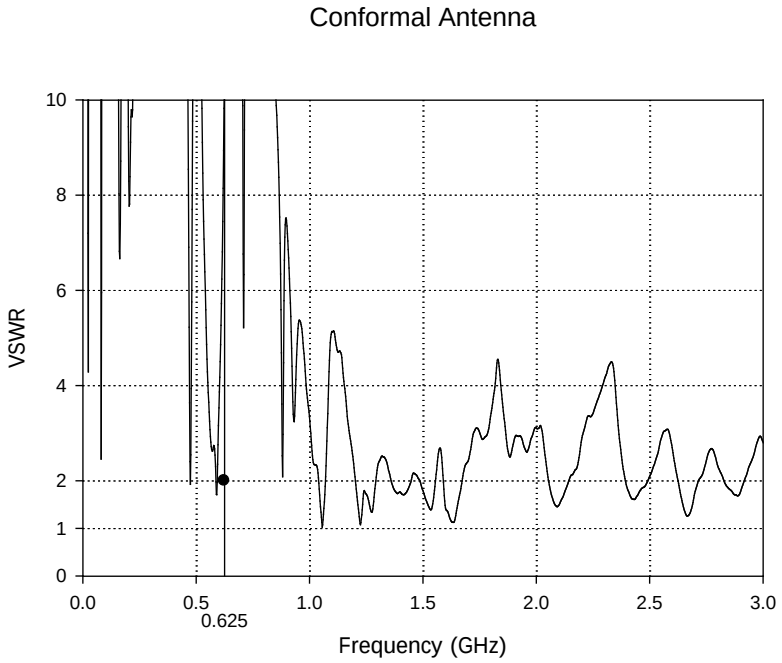

Figure 112. SWR measurement (calculated from S11) of updated conformal antenna placed on a conductive ground plane.

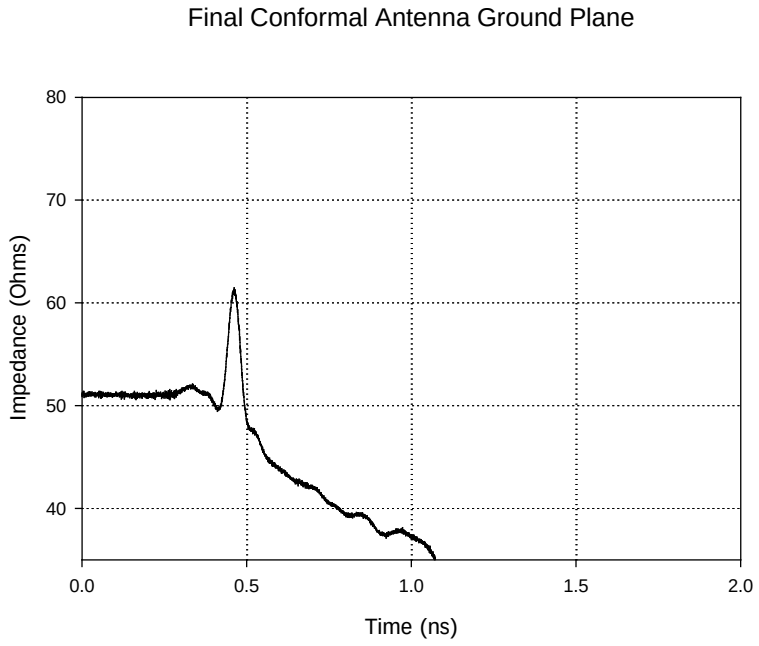

Figure 113. TDR measurement of updated conformal antenna placed on conductive ground plane.

Figure 114. Photo of the updated conformal array on the EBG structure.

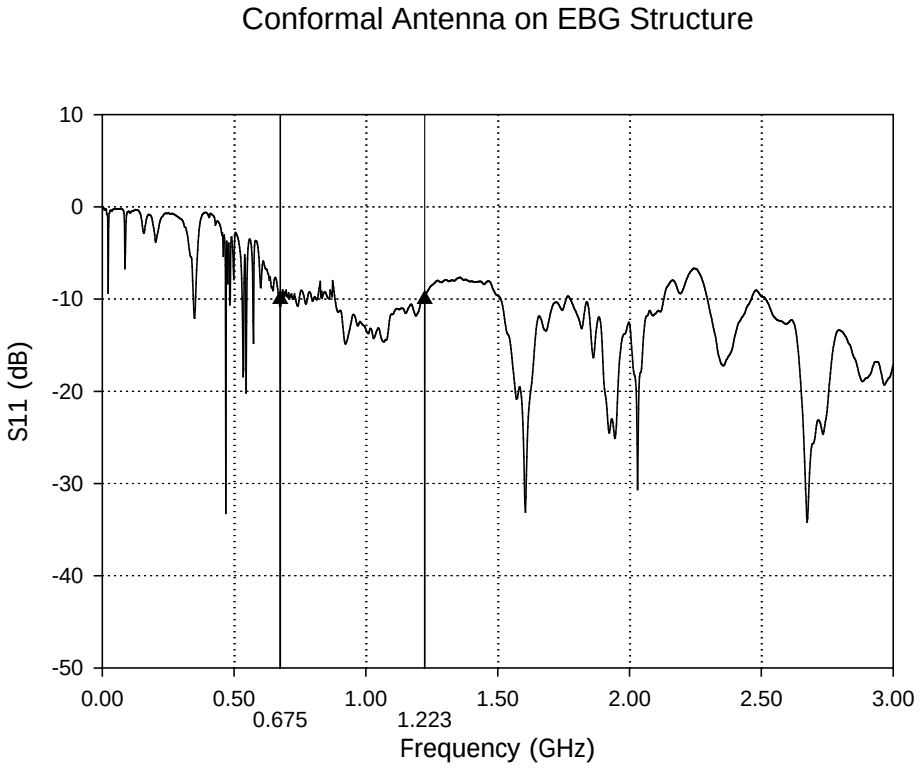

Figure 115. S11 measurement of updated conformal antenna placed on the EBG structure.

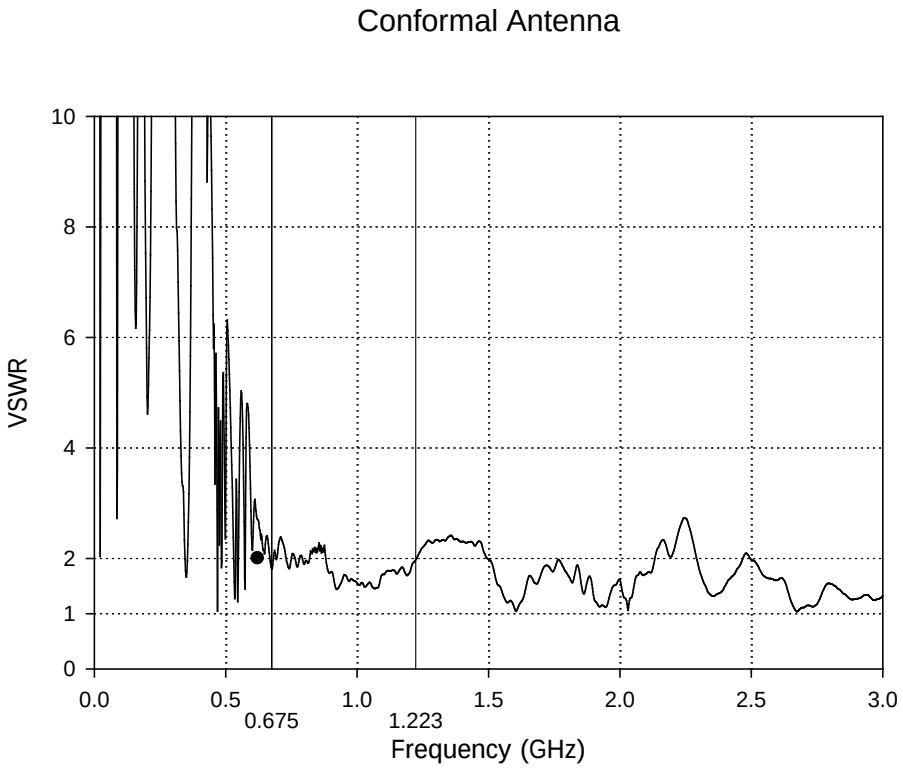

Figure 116. SWR measurement (calculated from S11) of updated conformal antenna placed on the EBG structure.

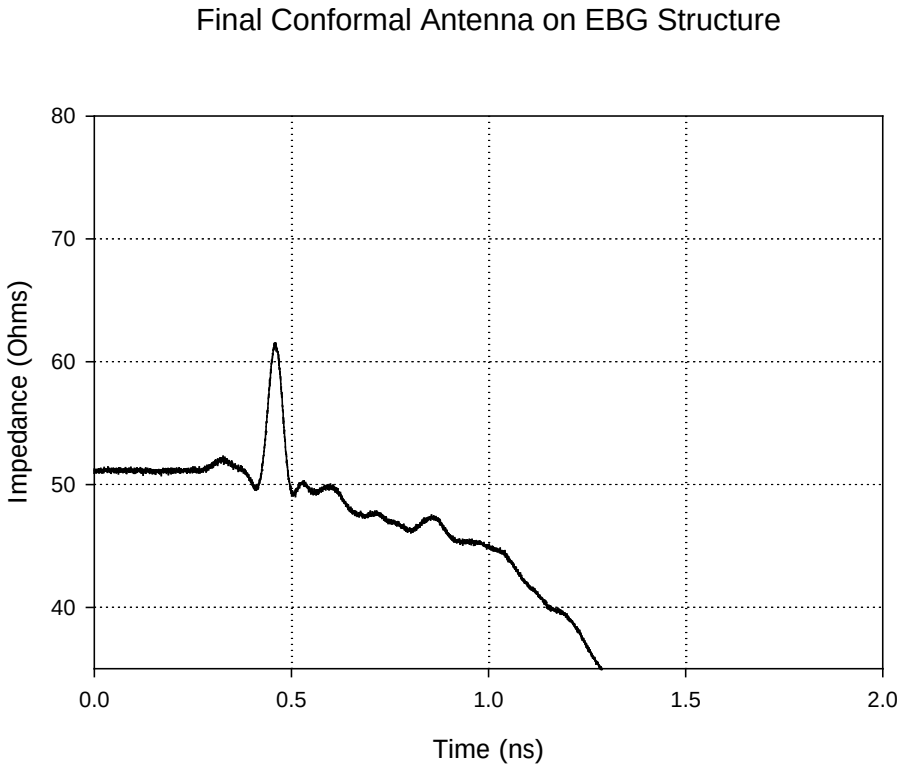

Figure 117. TDR measurement of updated conformal antenna placed on EBG structure.

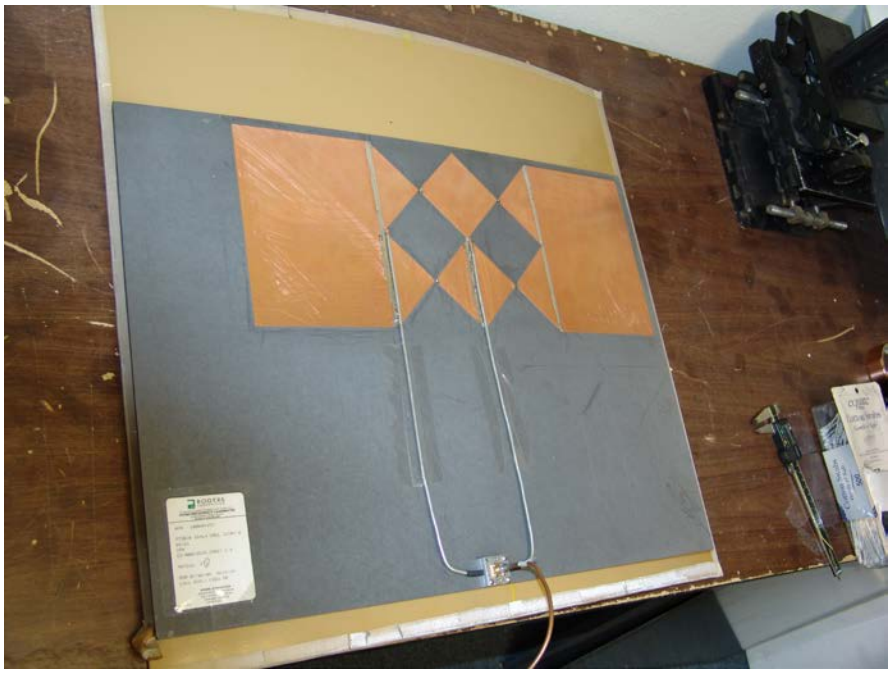

Figure 118. Photo of conformal antenna installed on the aircraft skin.

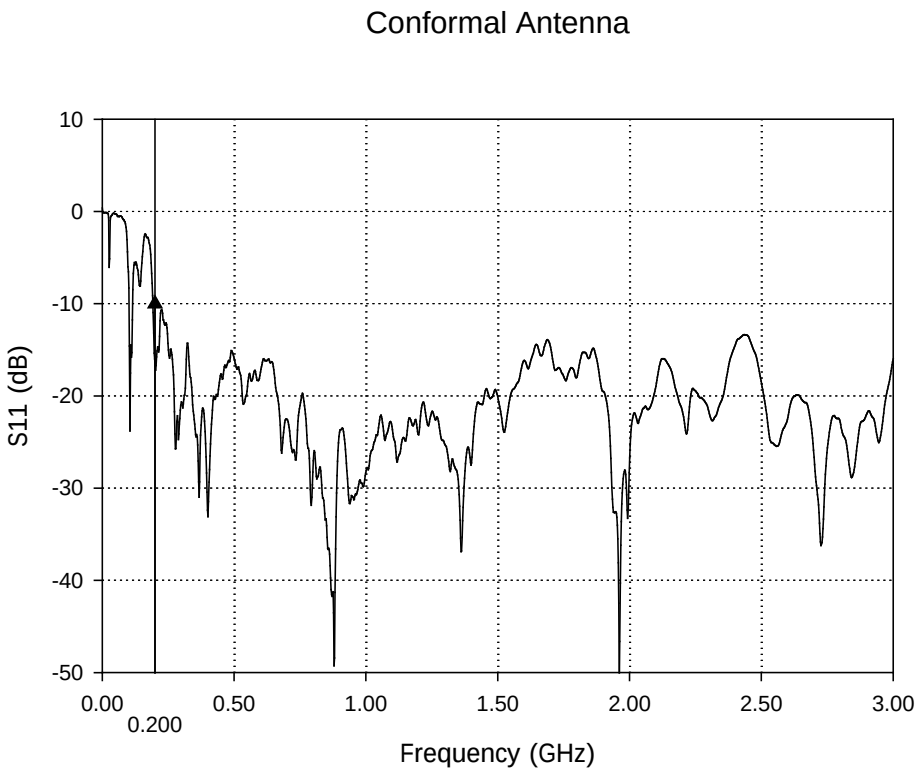

Figure 119. S11 measurement of conformal antenna on the aircraft skin place on a non conductive structure.

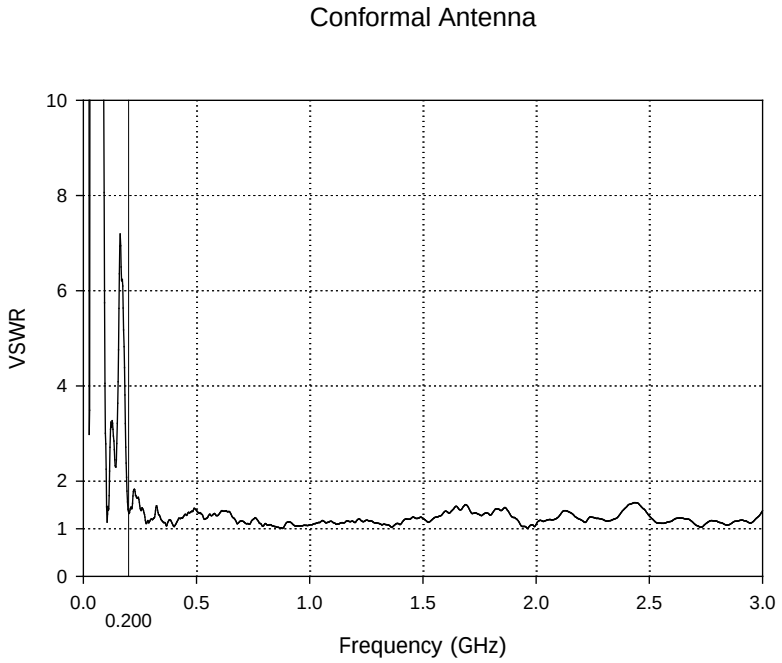

Figure 120. SWR measurement (calculated from S11) of updated conformal antenna (on the aircraft skin) placed on a non-conductive structure.

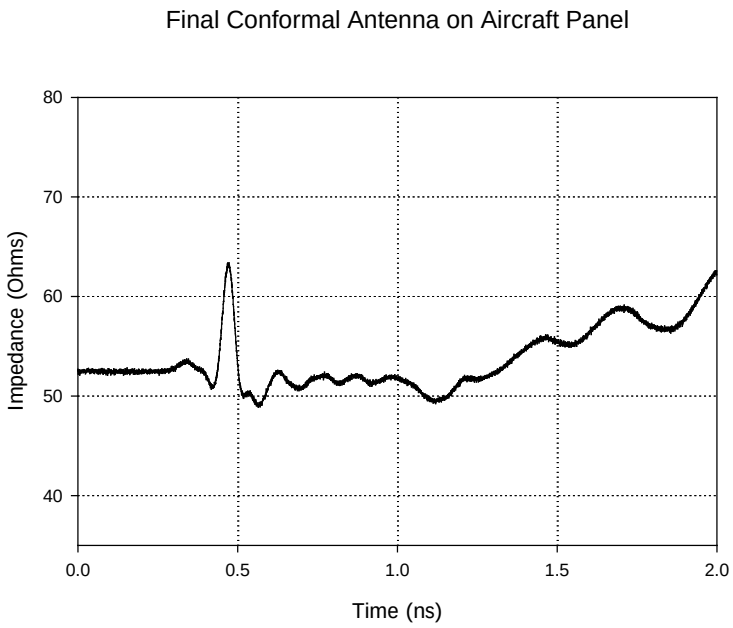

Figure 121. TDR measurement of updated conformal antenna (on the aircraft skin) placed on non-conductive structure.

Figure 122. Photo of conformal antenna placed over conductive ground plane.

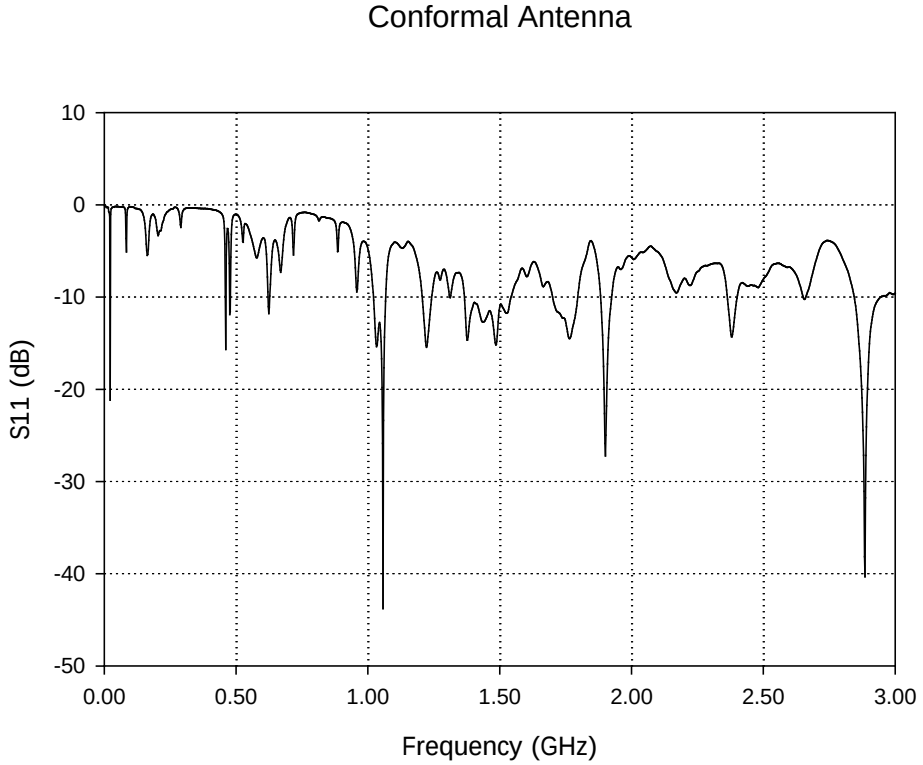

Figure 123. S11 measurement of conformal antenna on the aircraft skin place over a conductive ground plane (severely degraded)

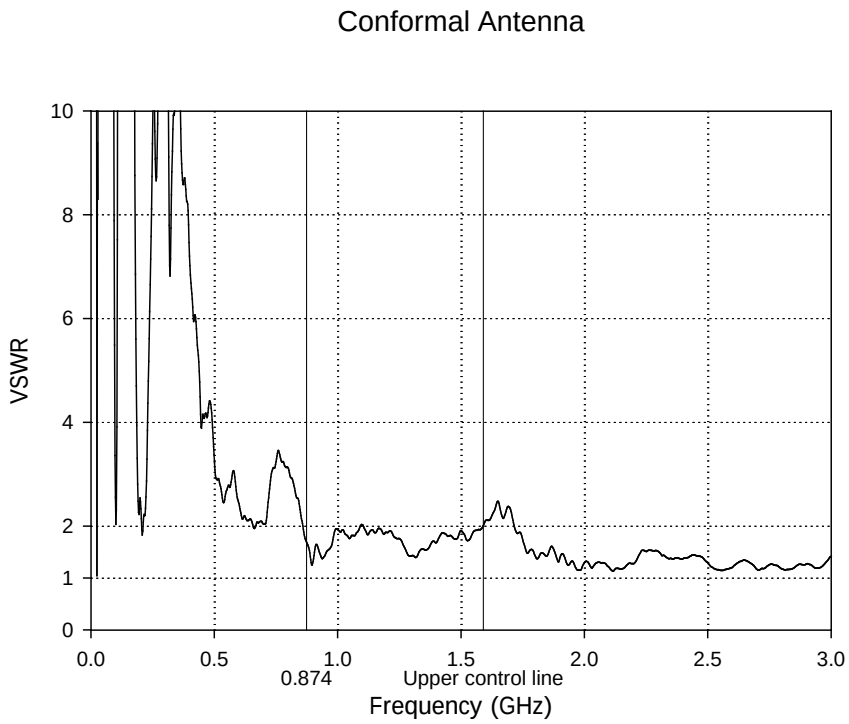

Figure 124. SWR measurement (calculated from S11) of updated conformal antenna (on the aircraft skin) placed on a conductive ground plane.

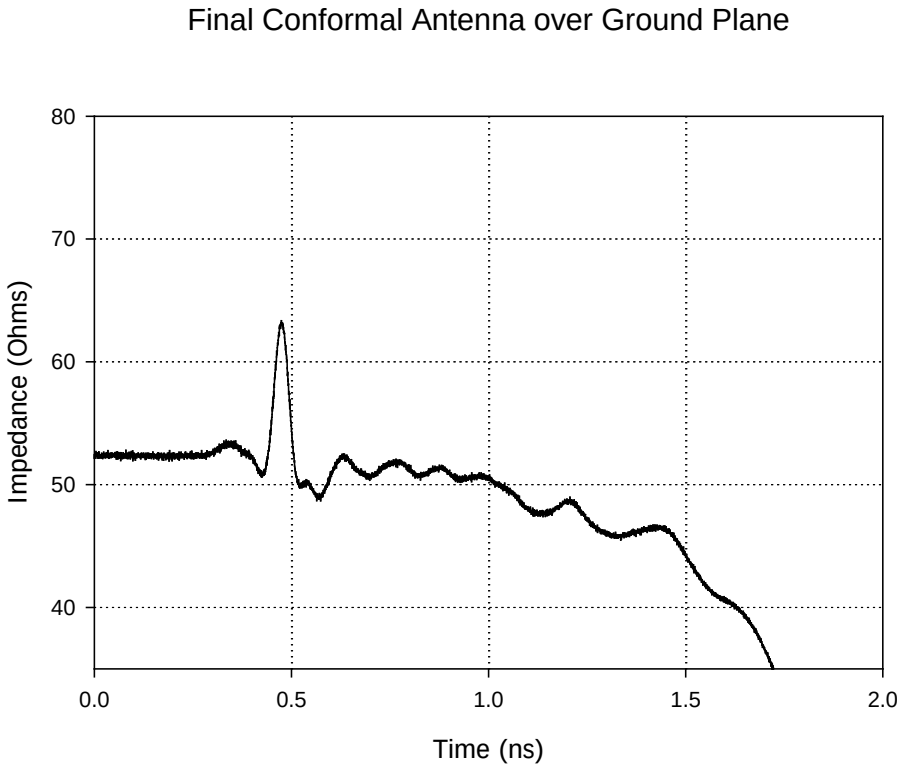

Figure 125. TDR measurement of updated conformal antenna (on the aircraft skin) placed on conductive ground plane.

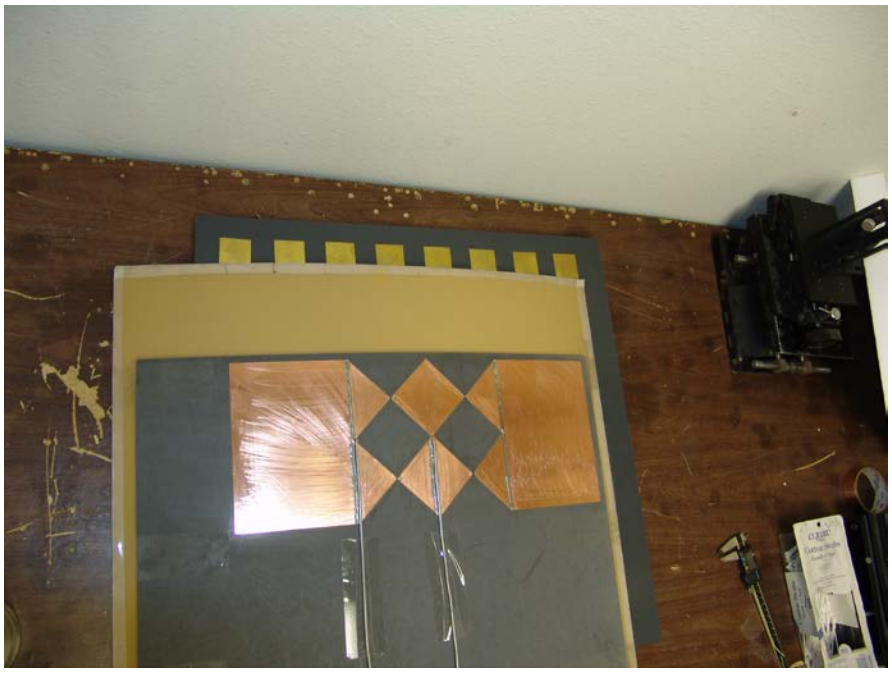

Figure 126. Photo of aircraft skin with conformal antenna placed over the EBG structure.

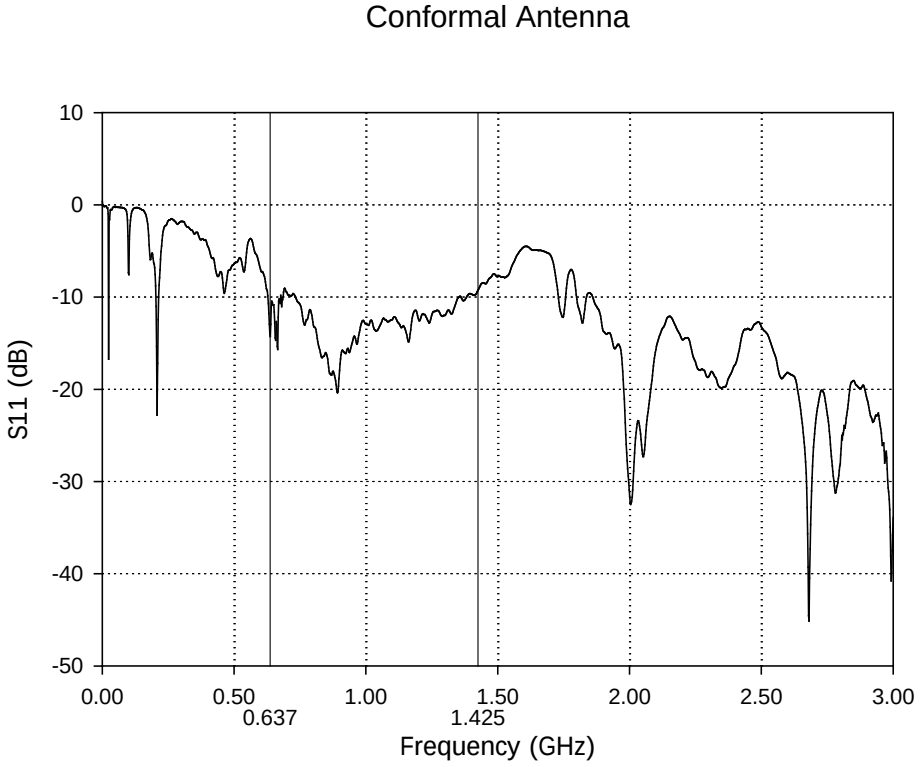

Figure 127. S11 measurement of conformal antenna on the aircraft skin place over the EBG structure.

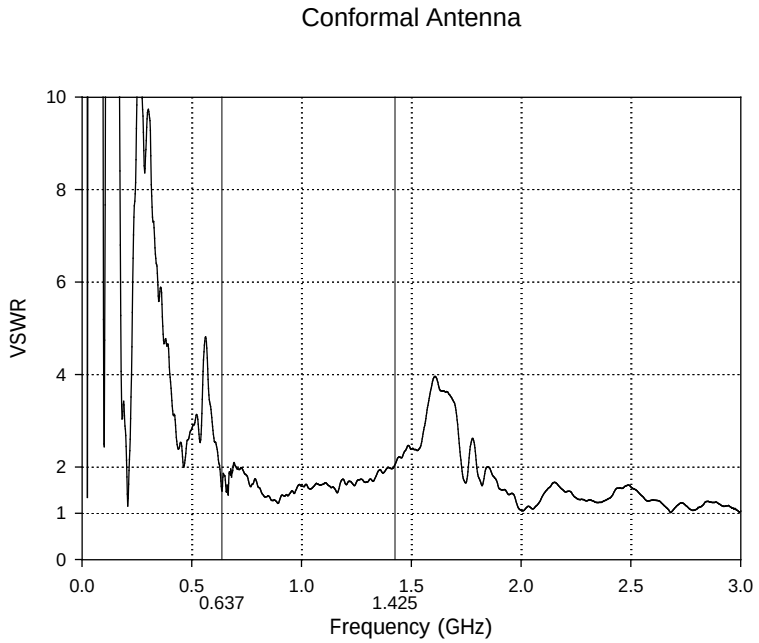

Figure 128. SWR measurement (calculated from S11) of updated conformal antenna (on the aircraft skin) placed over the EBG structure.

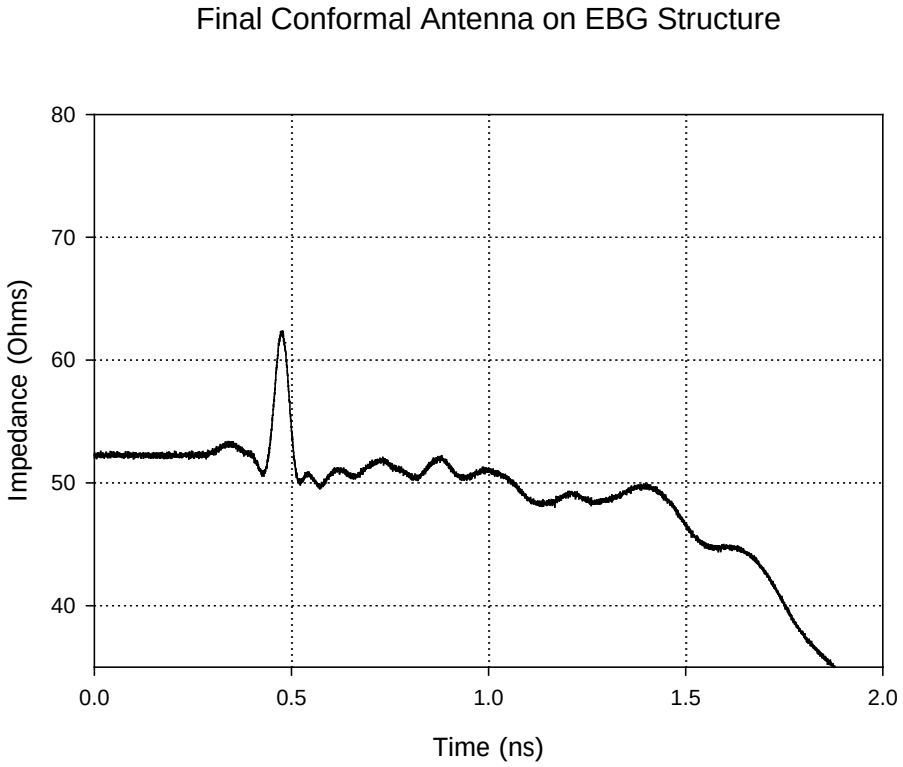

Figure 129. TDR measurement of updated conformal antenna (on the aircraft skin) placed over the EBG structure.

6.0 Conclusions

We start with the analytical basis and prototype measurement. Earlier, we had designed, built and tested a prototype 2 x 2 array of bow-tie antennas. The antennas are configured in a series-parallel configuration so that the net impedance is $Z_0 / 8 \sim 47$ Ohms. Starting with a 50 Ohm connector/cable, we split this into 2 x 100 Ohm cables and then convert each 100 Ohm line into two 200 Ohm strip lines. Each of these 200 Ohm strip line then connects to one of the four antenna elements. The performance of the array is monitored by measuring TDR and S11 (return loss). From the measured S11, we also derive the VSWR. The isolated conformal array testing indicated a very broad bandwidth of operation (transmit or receive modes). It was also established that the isolated array can be made to perform in the desired bandwidth of 200 MHz to 2 GHz. The prototype array was built on a rigid substrate of nylon material.

Low-profile conformal electrical antennas have a serious problem when they are placed near a metallic surface. We placed the prototype conformal array near perfect conducting ground planes, and saw that the performance is completely degraded and there is no bandwidth to speak of. We then analyzed, designed and fabricated an Electromagnetic Band Gap (EBG) structure to be placed between the antenna array and the metallic back plane.

The measurements demonstrate that the conformal array performs significantly better when placed over the EBG structure. A summary of the conformal array results is shown in Table 3. The antenna is determined to be operational when S11 is less than -10 db or when the VSWR is less than 2. The antenna is not operational over any significant frequency range when the antenna is placed over a conductive ground plane. When the antenna is placed over the EBG structure, good performance is obtained over a significant frequency range. The bandwidth is found to be 500 MHz for the antenna over the EBG without wings and 800 MHz for the antenna with wings.

The updated conformal array performed well when attached to the sample aircraft skin, built by Northrop Grumman Corporation. The bandwidth for the antenna on a non-conductive structure is almost 3 GHz with the low end extending to 200 MHz. When a metal conductor is placed behind the antenna, there is no bandwidth to speak of. The bandwidth is improved significantly

(637 MHz to 1.425 GHz), when the conductive plane is replaced with the EBG structure. A summary of the updated conformal antenna measurements is shown in Table 4.

TABLE 3. Summary conformal array measurements.

Conformal Antenna Configuration	Low Frequency Limit	High Frequency Limit	Bandwidth
Non-conductive Surface	622 MHz	> 3 GHz	2.4 GHz
Conductive Surface	**	**	**
EBG Structure	964 MHz	1.46 GHz	0.5 GHz
Non-conductive Surface with Wings	279 MHz	> 3 GHz	2.7 GHz
Conductive Surface with Wings	**	**	**
EBG Structure with Wings	604 MHz	1.37 GHz	0.8 GHz
** No significant operational range			

TABLE 4 . Summary of updated conformal array (installed on the curved- aircraft skin provided by Northrop Grumman Corporation) measurements.

Updated Conformal Antenna Configuration	Low Frequency Limit	High Frequency Limit	Bandwidth
Non-conductive Surface	200 MHz	> 3 GHz	2.8 GHz
Conductive Surface	**	**	**
EBG Structure	637 MHz	1.425 GHz	0.78 GHz
** No significant operational range			

References

1. D. V. Giri, K. F. Casey, M. Skipper and M. Abdalla, “Conformal Impulse Receive Antenna Arrays”, Final Report, SBIR- Phase I Govt. Contract FA9451-04-M-0081, Air Force Research Laboratory/DEHP, Kirtland Air Force Base, NM 87117, 15 February 2005.

2. G. Caille, E. Vouch, M. Martin, A. Mosig, P. Iversen, “Conformal Array Antenna for LEO Observation Platform”, European Microwave Conference, 1998.Caille et al, 1998.

3. D. V. Giri and C. E. Baum , “Early-Time Performance at Large Distances of Periodic Arrays of Flat-Plate Conical Wave Launchers”, Sensor and Simulation Note 299, 1 April 1987.